Cape Peninsula
University of Technology

Faculty of Engineering

Department of Mechanical Engineering

Smart Alignment System Research Group

Effects of Thermo-Mechanical Cycling and Aging on Quasi-Plastic Material Response exhibited by NiTi Shape Memory Alloys

By

M D Mukhawana NDipME, BTechME

Thesis submitted towards partial fulfilment of the Masters Degree in Technology: Mechanical Engineering (MTechME)

Under the supervision of

Dr. Oscar Philander (DTech, CPUT Bellville Campus)

CAPE TOWN, 2005

Declaration of Originality

The work described in this thesis was carried out in the Faculty of Engineering, Department of Mechanical Engineering (Bellville Campus) at the Cape Peninsula University of Technology. Except where otherwise acknowledged, the work presented for this degree is my own and contains no material which has been presented for a degree at this or any other university and, to the best of my knowledge and belief, contains no copy or paraphrase of work published by another person, except where duly acknowledged in the text.

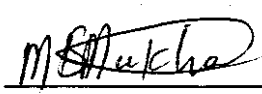

MD Mukhawana (MDipME, BTechME, PENTECH)

Cape Town, South Africa

December 2005

Acknowledgements

I would like to thank Dr O. Philander my supervisor for introducing to me this exciting research project. He not only introduced a high level of technology of Shape Memory Alloys, but he also monitored the progress of my research regularly. He also gave me his full support in terms of providing the equipment needed to complete my studies

I would like to thank the National Research Foundation (NRF) and Cape Peninsula University of Technology (CPUT) for the financial assistance that they provided to me and the project.

I would like to thank all the members of the Smart Alignment Research Group for sharing their experience on the technology of Shape Memory Alloys.

I would also thank Ms R Ziegler, Lecturer in the Mechanical Engineering Department. She often spent long hours in helping me.

I would like to give credit to Prof G. Oliver, a Lecturer in the Mechanical Engineering Department (Bellville Campus) for his assistance on the use of dilatometer.

A special word of thanks to my parents Wilson and Evelyn Mukhawana, my sisters Beatrice, Teggy and Revonia Mukhawana and my Brothers Given and Bongani Mukhawana. You have supported since the start of my academic career.

I would like to extend a word of thanks to Eric and Zukiswa Sebokedi for acting as my guardians and providing financial support during my undergraduate studies. Your support has played a very important role to my studies and my life.

Abstract

The working characteristics of a shape memory alloy element providing either sensor or actuator capability is specified by the beginning and/or completion temperatures of the actuation (i.e. austenitic start and finish temperatures and martensitic start and finish temperatures), the working actuator stroke (i.e. load induced twinned⇒de-twinned martensitic phase transformation also known as quasi-plastic deformation), and the working actuator force (provided by the temperature induced de-twinned martensite⇒austenite phase transformation). The successful design of these smart devices harnessing the shape memory effect for their operation, rely on a very good characterization of these three working characteristics of NiTi shape memory alloy before use. The design of actuators harnessing the shape memory effect exhibited by NiTi shape memory alloys requires a complete understanding of the load induced martensitic phase transformation. This material behaviour, also known as quasi-plasticity, provides the actuation stroke for these kinds of actuator systems.

This thesis presents an experimental investigation into the effects that thermo-mechanical cycling and aging temperature have on the mechanical (transformation strain,

transformation load, etc.) and thermal (transformation temperatures) properties of the quasi-plastic material response. Four batches of 3mm diameter and 340mm long NiTi shape memory alloys was subjected to aging temperatures ranging from 200 to 350^{0}C. Each batch was soaked for a period of ten hours. Upon cooling to room temperature, these aged specimens were then subjected to 10 mechanical and thermal loading cycles. Load-Displacement graphs were plotted using the data obtained from mechanical testing and the results showed some interesting material behaviours. Firstly the load-displacement graphs showed that the hardening like behaviour as discussed by Philander [4] has been erased for the first mechanical loading cycles. This suggests that aging had an effect on the orientation of the twinned martensitic phase structure. The load-displacement graphs did however show that there were still variations in the total transformation strain, i.e. different actuation strokes were achieved.

The results obtained from the mechanical and thermal loading experiments were tabulated and mathematical functions were obtained to further predict the quasi-plastic behaviour of the NiTi shape memory alloy rods subjected to mechanical and thermal loading. These functions showed similar trends for individual mechanical properties and suggest that stabilisation of these properties would be achieved after prolonged mechanical and thermal cycling. The second yield load values remained constant even after repeated mechanical and thermal loading cycles.

The thermal analyses conducted on the aged and thermo-mechanical cycled NiTi shape memory alloys using a dilatometer also showed some interesting findings. Firstly an un-aged specimen was sectioned and subjected to the thermal procedure, i.e. controlled heating and cooling and the results show that an actuator manufactured of this material, i.e. un-aged, would have a poor performance since a large temperature range would be required to operate it. The results obtained from a specimen subjected to thermo-mechanical cycling coupled with an aging temperature of 250^{0}C would produce an actuator start and completion temperature with a narrower temperature range than that of

untreated specimens. Furthermore, the overall results of the thermal analyses show that an increase in the aging temperatures will bring about slight increases in all the transformation temperatures. The results of the thermal analyses also show that increases in the aging temperature decreases slightly the volumetric expansions that occur in the material during heating. This decrease in the volumetric expansion could be the result of the increases in the initial yield load as described above.

On average the experimental investigation into the effects that thermo-mechanical cycling and aging temperature have on the quasi-plastic material response exhibited by shape memory alloys, and its effects on transformation temperature shows that these kinds of procedures have positive effects on NiTi shape memory alloy behavior. Furthermore, it suggests that these materials should never be used in critical components without a prior history of thermal and mechanical loading. For actuator design in terms of actuation stroke, actuation force, actuation starting and completion temperature, and actuator repeatability these considerations are thus critical.

Table of content

Chapter 2 Thermo-Mechanical Experimental Investigation

Chapter 3 Thermal Analysis

Chapter 4 Mathematical functions

Chapter 5 Conclusions and Recommendations

List of Figures

Chapter 1

Chapter 2

Chapter 3

Chapter 4

List of Tables

Chapter 1

Introduction

1.1 Problem Statement

Shape Memory Alloys (SMA's) are viewed as one of the most promising among the emerging 'smart' materials in that their potential applications encompass a wide range of fields such as aerospace, civil, mechanical and biomedical engineering [1]. Typically these shape memory alloys are used as actuators in the different fields of interest. SMA materials rely solely on changes in their environmental temperature to induce actuation. SMA materials consist of a low temperature martensitic phase (made up of different variants of martensite called twins) and a high temperature austenitic phase. The actuation produced by the material is derived from a crystallographic twinned↔de-twinned martensitic phase transformation (responsible for the actuation stroke) and a martensite↔austenite phase transformation (responsible for the actuation force). The

unique material behavior exhibited by SMA's can further be divided into two phenomena, i.e. the shape memory effect and the pseudo-elastic effect.

This research focuses on the use of the shape memory effect exhibited by NiTi SMA to design and manufacture actuator systems for sensor, actuator, and sensor-actuator applications. This material effect has the unique capacity to develop very large apparent plastic strain under load (tensile, compression, torsion, etc.) at low temperature. This behavior is also known as quasi-plasticity and the apparent plastic deformation is caused by the load induced martensitic phase transformation i.e, twinned⇒de-twinned martensitic phase transformation. These apparent plastic strains will remain until an increase in the temperature of material causes its martensitic phase structure to transform to austenite. Macroscopically this transformation brings about a complete recovery of the material's original geometry.

SMA's have been widely used as force-displacement actuators in the above mentioned fields due to their unique mechanical properties (fracture toughness, fatigue strength, etc.) and characteristics [2]. During design of these smarts devices harnessing the shape memory effect, it is critical to have a clear understanding of this SMA material phenomenon before use, i.e quasi-plasticity (actuation stroke), and martensite⇒austenite phase transformation (actuation force).

The Smart Alignment Systems Research Group (SASRG) located in the Department of Mechanical Engineering (Bellville Campus) at the Cape Peninsula University of Technology is currently developing a range of smart devices that will harness the shape memory effect exhibited by NiTi shape memory alloys for actuation purposes. These devices include active and passive polymeric composite surfaces and sections, reconfigurable or morphing airplane wings, prosthetic devices, linear load-displacement actuators, sensors, and sensor-actuators devices.

Most smart devices using shape memory alloys for their operation rely on the shape memory effect for actuation purposes. Tobushi et al [3] reported that the working

characteristics of a shape memory alloy element providing either sensor or actuator capability is specified by the beginning and/or completion temperatures of the actuation (i.e. austenitic start and finish temperatures and martensitic start and finish temperatures), the working actuator stroke (i.e. load induced twinned⇒de-twinned martensitic phase transformation also known as quasi-plastic deformation), and the working actuator force (provided by the temperature induced de-twinned martensite⇒austenite phase transformation). The successful design of these smart devices harnessing the shape memory effect for their operation, rely on a very good characterization of these three working characteristics of NiTi shape memory alloy before use.

Recently Philander [4] performed an experimental investigation into the quasi-plastic behavior of NiTi shape memory alloys. The experimental investigation was performed to determine the effect that different displacement rates have on geometric and mechanical properties of 1, 2 and 3mm diameter NiTi shape memory alloys wires specimens of varying lengths. He found that Quasi-plastic material response displays three distinct regions when plotted graphically on a load-displacement graph, i.e., an initial elastic region (IE), a nearly horizontal region (NH), and finally another elastic region (FE) (see fig 1.1a, b and c). The elastic regions suggest that the specimen changes from its initial state to some final state through a transformation and the slopes of these elastic regions were found to be similar. The nearly horizontal regions on these graphs thus determine the location of the transformation behavior from one elastic state to the other (see fig. 1.1a).

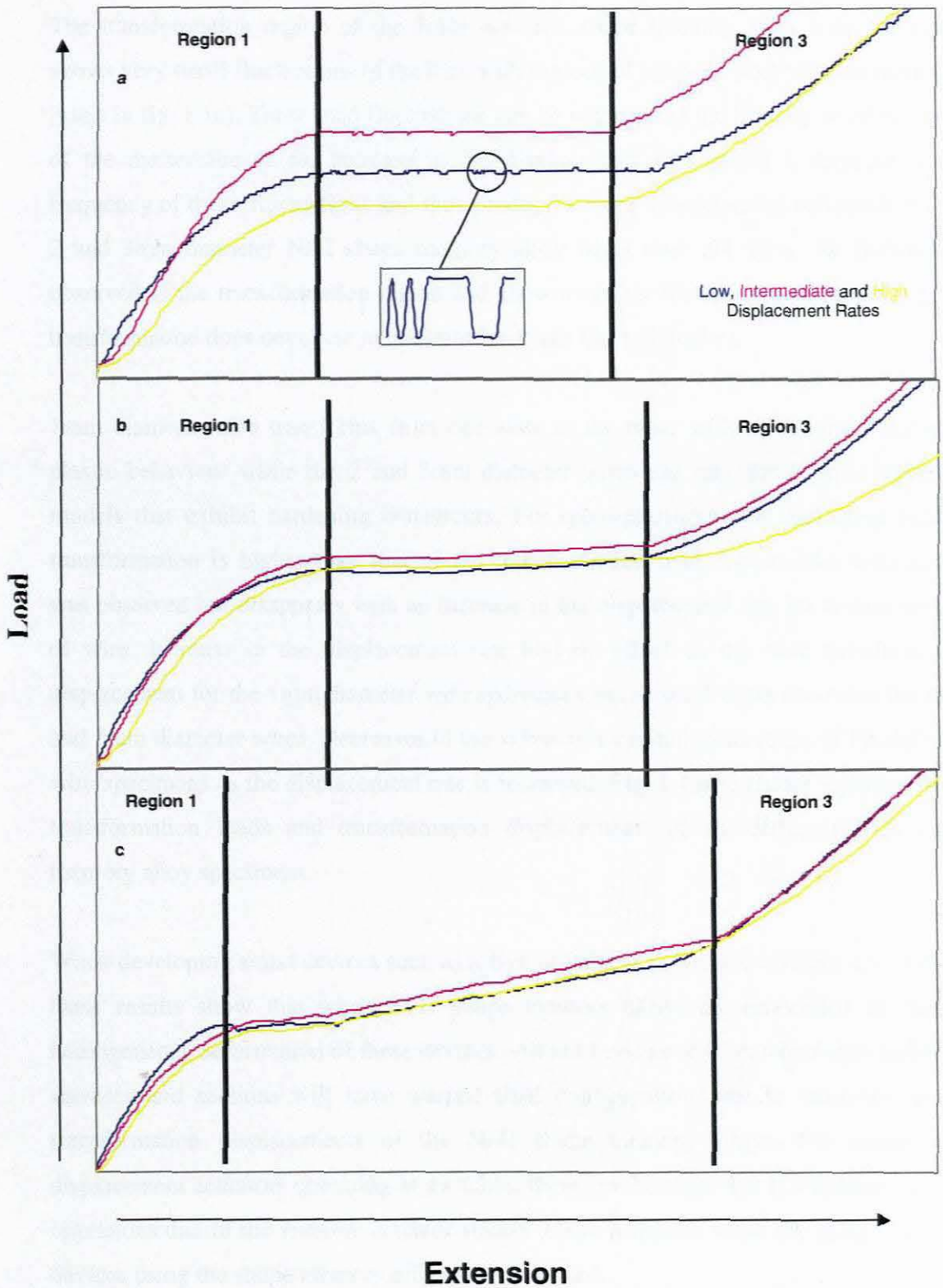

Figure 1.1: Load – Extension behaviour for NiTi Shape memory alloy wires of (a) 1mm, (b) 2mm and (c) 3mm diameters at Low, Intermediate and High Displacement Rates

The transformation region of the 1mm diameter shape memory alloy wire specimens shows very small fluctuations of the load with regions of constant load between them (see insert in fig. 1.1a). These load fluctuations can be regarded as the flipping or de-twinning of the martensitic twins. Increase in the displacement rate causes a decrease in the frequency of these fluctuations and thus produce a more homogeneous deformation. The 2 and 3mm diameter NiTi shape memory alloy wires does not show the fluctuations observed in the transformation region and show a steeper transformation region, i.e. the transformation does not occur at constant load (see fig. 1.1b and c).

1mm diameter wire transforms from one state to the other with a seemingly perfectly plastic behaviour while the 2 and 3mm diameter wires can take the form of plasticity models that exhibit hardening behaviours. For quasi-plasticity, the nucleation load of transformation is higher than that of the transformation load. Lüders-like deformation was observed but disappears with an increase in the displacement rate for certain lengths of wire. Increase in the displacement rate had no effect on the total transformation displacement for the 1mm diameter wire specimens but showed slight decreases for the 2 and 3mm diameter wires. Decreases in the value of the initial yield stress of the different wire specimens as the displacement rate is increased. Fig. 1.1 also shows variation in the transformation loads and transformation displacements of the different NiTi shape memory alloy specimens.

When developing smart devices such as active or passive polymeric surfaces and sections these results show that when NiTi shape memory alloys are embedded in them a homogeneous deformation of these devices will not be achieved, i.e. when activated these surfaces and sections will have warped final configurations due to variations in the transformation displacements of the NiTi shape memory alloys. For linear load-displacement actuators operating as switches, these results show that it will have variable operations due to the variable actuator stroke. These problems make the design of smart devices using the shape memory effect a difficult task.

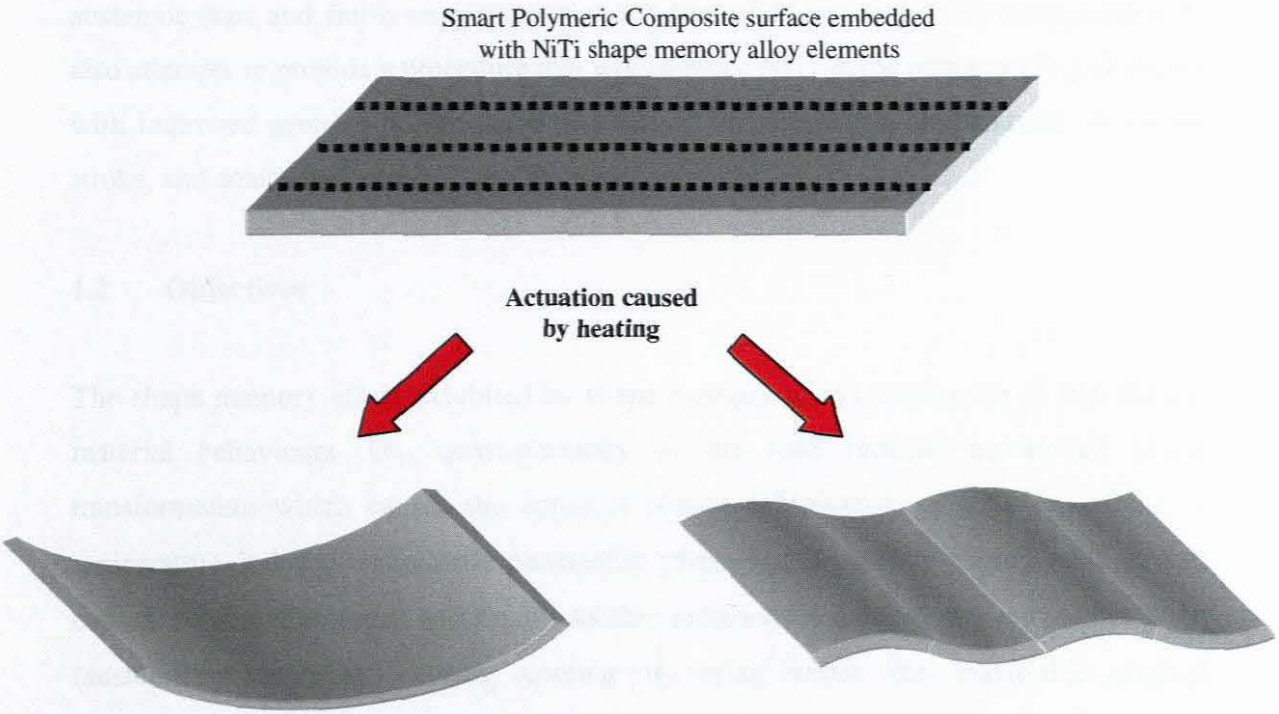

Figure 1.2: Comparison of Smart Polymeric Composite surface deformation with Homogeneous and Non-Homogeneous NiTi shape memory alloy actuator stroke

Researchers such as Shaw [5] and Tobushi et al [3] found that when they applied thermo-mechanical cycling to the shape memory alloys before use in smart devices the materials performed much more efficiently. Their investigations were however focused on the characterization of the high temperature pseudo-elastic behavior exhibited by shape memory alloys.

The research presented in this thesis describes an experimental investigation into the effects that thermo-mechanical cycling and aging temperatures have on the quasi-plastic material response exhibited by NiTi shape memory alloys undergoing the shape memory effect. Furthermore, this study also investigates the effect that these mechanical and thermal loadings have on NiTi shape memory alloy transformation temperatures, i.e.

austenitic start and finish temperatures and martensitic start and finish temperatures. It also attempts to provide a procedure that will produce NiTi shape memory alloy elements with improved actuator performance in terms of transformation temperatures, actuation stroke, and actuation force.

1.2 Objectives

The shape memory effect exhibited by shape memory alloys consist out of two unique material behaviours, i.e., quasi-plasticity or the load induced martensitic phase transformation which causes the apparent plastic deformation or actuation stroke, a temperature induced martensitic⇒austenitic phase transformation during heating that causes the actuation force, and finally another temperature induced phase transformation (austenitic⇒martensitic) during cooling to bring about the material's original configuration.

In 2004, Philander [4] discussed quasi-plasticity observed in the shape memory effect of NiTi shape memory alloys and found that untreated specimens have variability in terms of transformation strains (actuation stroke), and transformation loads (initial and final). If these untreated specimens are used in actuator systems it means that the actuator will have variable performance and therefore will not operate efficiently. Shaw [5] and Mayers et al [6] suggested that the variability observed in SMA material behavior could be alleviated if the material specimens are subjected to thermo-mechanical cycling before use. Liu and Gaven [7] performed an experimental investigation into the effects of annealing/aging on transformation temperatures and found that annealing/aging increased the transformation temperatures.

The main objectives of this study are to determine experimentally the effects that thermo-mechanical cycling and aging have on:

- ***Total Transformation Displacement*** – load induced martensitic phase transformation causing the apparent plastic deformation. This strain is further

divided into three, i.e. initial elastic, transformation, and final elastic displacement.

- ***Transformation/Initial Yield load*** – load at which the load induced martensitic transformation begins,
- ***Final Yield load*** – load at which the load induced martensitic transformation ends. The Initial and Final Yield loads represent the ***working load*** of a SMA actuator.
- ***Transformation Temperatures*** – Temperatures at which forward and reverse transformations occur. These are the temperatures signify the beginning and completion of actuation for a SMA element. These include austenitic start and finish temperatures and martensitic start and finish temperatures.

The results obtained from these experiments will then be used to develop mathematical functions to describe these mechanical and thermal properties in terms of aging temperature and number of thermo-mechanical cycles. These functions will typically assume the following forms:

- $transformation\ strian(T_{aging}) = f(C_{1,2\ldots,n}, N)$
- $initial\ yield\ load(T_{aging}) = f(C_{1,2\ldots,n}, N)$
- $second\ yield\ load(T_{aging}) = f(C_{1,2\ldots,n}, N)$
- $A_s = f(C_{1,2\ldots,n}, T_{aging})$
- $A_f = f(C_{1,2\ldots,n}, T_{aging})$
- $M_s = f(C_{1,2\ldots,n}, T_{aging})$
- $M_f = f(C_{1,2\ldots,n}, T_{aging})$

Where C_n represents a n^{th} mathematical constant, N is the number of thermo-mechanical cycles, and T_{aging} is the aging temperature.

1.2.1 Measures of displacement

This section will examine the effect of the thermo-mechanical cycling and aging on the initial elastic displacement (from a- b at figure 1.1) and transformation displacement (from b-c at figure 1.1). This will be presented by means of force-displacement graphs under axial load using tensile test machine. The data of each cycle will be captured and the load-displacement graph for each cycle will be presented. All the graphs will be analyzed in order to determine the effect that these mechanical and thermal loading cycles have on the displacement measures.

Shape Memory alloy specimens will be aged in a temperature controlled furnace. The temperatures were selected so as not to induce permanent memory change. After aging the specimens will be loaded mechanically in a tensile testing machine. Again load-displacement data will be presented graphically and discussions on the effect that aging has on displacement measures will be presented.

1.2.2 Working stress

This section will examine the effect of the thermo-mechanical cycling and aging on the initial yield load (figure 1.3 at point b) and second yield load (figure 1.3 at point c). The data presented in 1.2.1, i.e. load-displacement graphs for each cycle, will be analysed and discussed.

1.2.3 Transformation temperatures

As mentioned above, one of the working characteristics of a shape memory alloy element is the beginning and/or completion temperatures of the actuation. Upon completion of the tasks described in 1.2.1 and 1.2.2, the specimens will be prepared for thermal analyses. A dilatometer will be used for this investigation. This instrument determines all temperatures of transformation i.e. austenite start, austenite finish, martensite starts and martensite finish temperature, and provides data in the form of temperature-displacement graphs. These graphs will be compared and analysed to determine the effect that thermo-mechanical cycling and aging have on the thermal working characteristics of shape memory alloy elements.

1.3 Background

The first reported steps towards the discovery of the shape memory effect were taken in the 1930s. In 1932, a scientist by the name of Olander discovered the *pseudoelastic* behavior of the gold-cadmium (Au-Cd) alloy. Mihalzcs [2] reported that a few years later in 1938, two researchers, Greninger and Mooradian, observed the formation and disappearance of a martensitic phase by changing the temperature of a copper-zinc (Cu-Zn) alloy. After that, the basic phenomenon of the shape memory effect, which is governed by the thermoelastic behavior of the martensite phase, was documented by two scientists named Kurdjumov and Khandros in 1949. Finally in 1967, a researcher named Buehler and his co-workers at the U.S. Naval Ordinance Laboratory discovered this shape memory effect in an alloy of nickel and titanium (Ni-Ti). Buehler was working with metals (namely high nickel-bearing alloys) for gas turbine components and accidentally left a small ingot of a Ni-Ti alloy on his desk in direct sunlight. He left for lunch and upon returning, noticed that the alloy had changed its shape. Now known as Nitinol (derived from **Ni-Ti** Naval **O**rdinance **L**aboratories), the name has become the general title for nickel-titanium SMAs . Since that time, intensive investigations have been made to explain the mechanics of SMAs' basic behavior. Starting in the 1970s, commercial products involving SMAs began to appear. For the most part, the early devices functioned as fasteners such as couplings for piping systems and connectors for electrical systems [2]

1.3.1 General Discussion

Shape Memory Alloys (SMA) have unique behaviours in that they can remember their original shape after deformation. These unique behaviours are termed the shape memory effect and the pseudo-elastic effect. These phenomena are now discussed both microscopically and macroscopically.

Shape Memory Alloys (SMA) exhibit a crystallographically reversible martensitic transformation. At high temperatures a load free SMA exists as a high-symmetry, usually cubic, austenitic phase termed the parent or memory phase. Upon cooling to below the martensite finish temperature, the austenite transforms to a monoclinic thermoelastic martensite phase whose structure has many variants typically in the form of sheared platelets (see Fig 1.4). Due to the self-accommodating nature of the martensitic phase, the deformation on transformation from austenite to martensite is zero. The transformation temperatures are dependent on the alloy type, composition and also on the thermo-mechanical treatments previously applied. The heating and cooling transformations do not overlap and the transformation is said to exhibit hysteresis (see Fig 1.5). The magnitude of the hysteresis also varies with the alloy type and is typically in the range of 10-50°C.

The ***shape memory effect (SME)*** consists out of a load induced martensitic phase transformation, and a temperature induced martensitic⇒austenitic phase transformation (see Fig 1.6). The interfacial strength between platelets in the martensite phase is low and thus slips very readily. If a load is applied at low temperature, the martensite deforms by a slipping mechanism termed de-twinning (see Figs 1.5 & 1.6) that transforms the different variants to a variant that can accommodate the maximum elongation in the direction of the applied force. This de-twinning occurs when a certain transformation load is achieved and should continue at this transformation load, i.e. constant load-temperature transformation.

The austenite phase has only one possible orientation, thus when heated, all the possible deformed structures of the martensite phase must revert to this one orientation of the austenite memory phase and the material recovers its original shape.

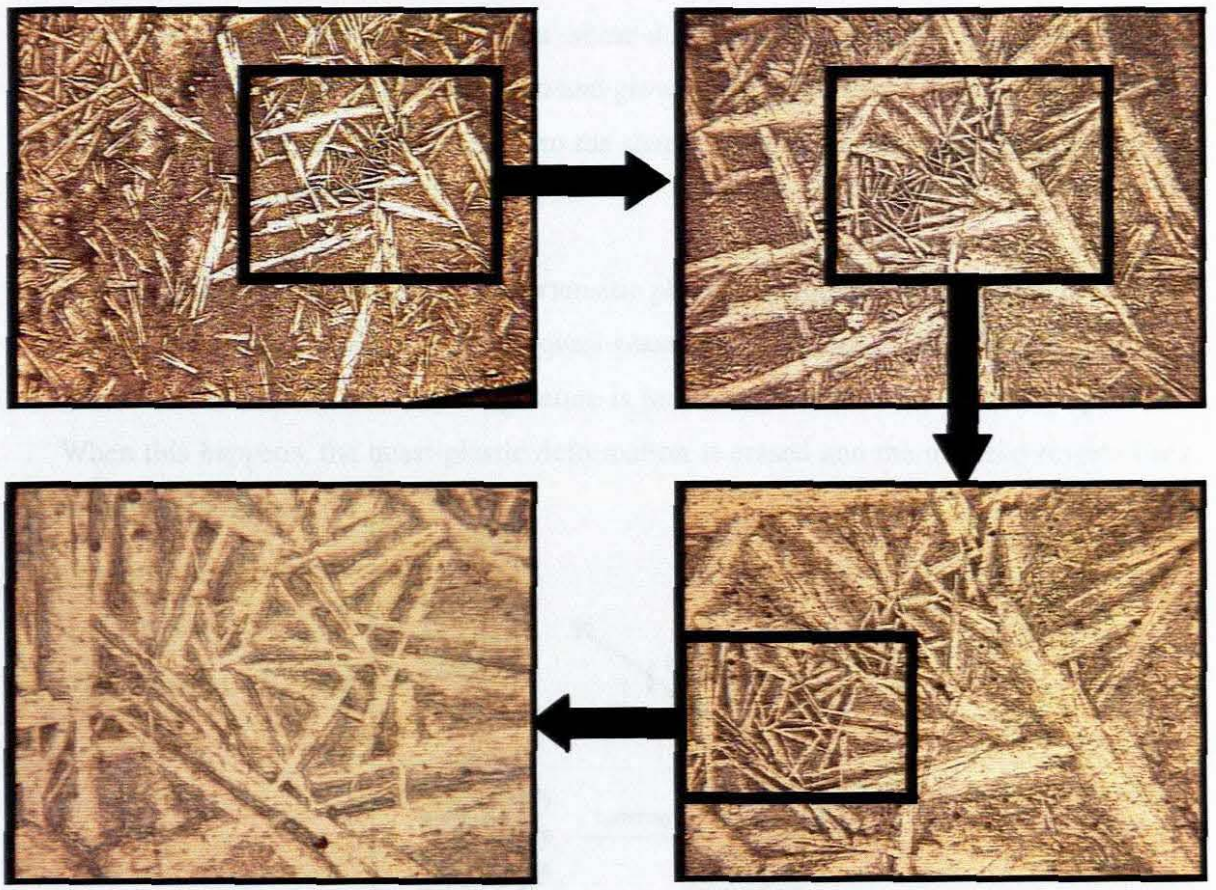

Figure 1.3: Microscopic view of twinned martensite showing its different variants.

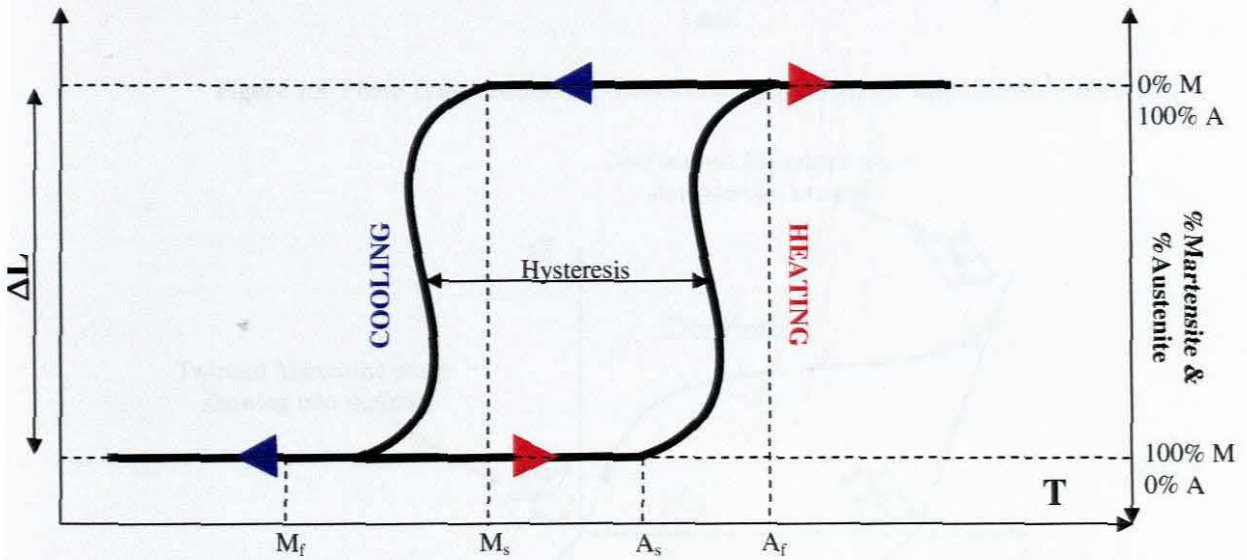

Figure 1.4: Thermal Hysteresis Loop exhibited by Shape Memory Alloys showing transformation temperatures

The martensitic transformation is a shear-dominant diffusionless solid-state phase transformation occurring by nucleation and growth of the martensitic phase from a parent austenitic phase. The heat transferred to the shape memory alloy is the power driving the molecular rearrangement of the alloy.

Macroscopically, the load induced martensitic phase transformation resembles permanent plastic deformation and is termed quasi-plastic deformation. This deformation will remain in the material until its temperature is increased to its austenitic start temperature. When this happens, the quasi-plastic deformation is erased and the material reverts back to its original shape

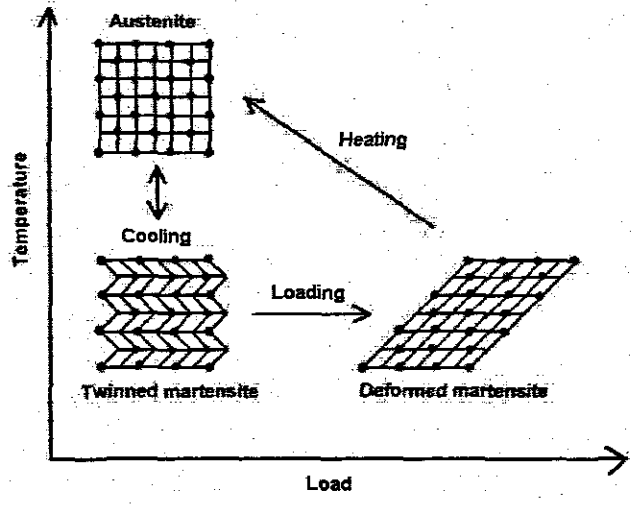

Figure 1.5: Phase Transformation of SMA's occurring during the shape memory effect [8]

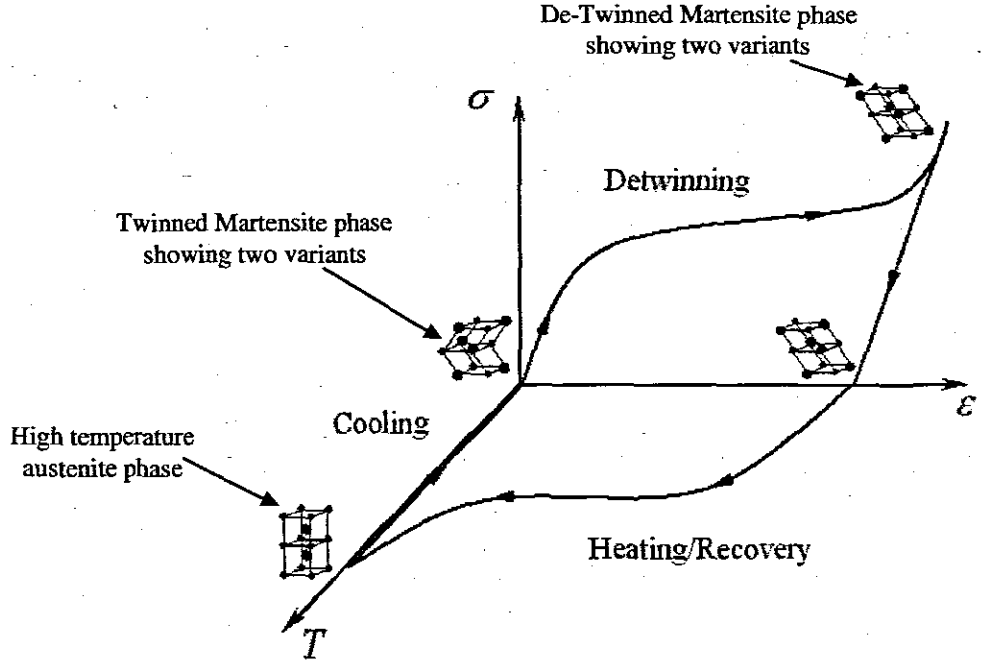

Figure 1.6: Schematic of the shape memory effect behavior of SMAs [9]

Pseudo-elasticity (PE) occurs at elevated temperatures, i.e. temperatures exceeding the material's austenite finish temperature. The pseudo-elastic effect is attributed to a reversible stress-induced martensitic transformation. The interfacial strength of the austenite phase is high in this state. If loaded to a given high temperature transformation load, the austenite phase will transform to a de-twinned martensitic structure. Again this phase transformation occurs at this constant load and upon removal of this load the reverse transformation to austenite occurs. The loading and unloading paths differ and it is said that pseudo-elasticity has a hysteretic behavior.

Macroscopically the material behaves initially in an elastic manner. When the transformation load is reached the deformation resembles that of plastic deformation. At any stage during this high temperature loading path, if the load is released the material will transform back to its original configuration.

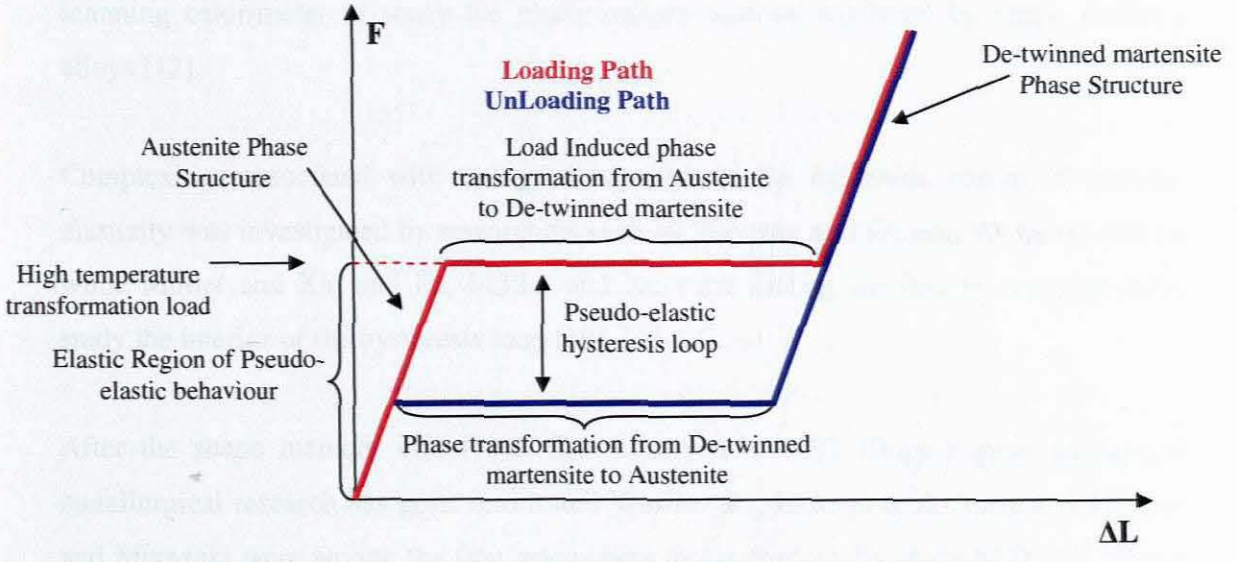

Figure 1.7: Schematic of the pseudo-elastic behavior of SMAs

1.4 Review of the related literature

The research presented in this thesis focuses on an experimental investigation into the effects that thermo-mechanical cycling and aging has on the quasi-plastic material behaviour of the shape memory effect and transformation temperatures of shape memory alloys. The literature however shows that most of the experimental investigations into sma behaviour was conducted to study the pseudo-elastic behaviour.

Otsuka et al., Delaey et al., Perkins, Schetky, and Funakubo [10], [5], [11] were among the first researchers to report that the remarkable behaviour of shape memory alloys is caused by interplay of a high temperature austenite phase and a low temperature martensite phase. Furthermore, Wasilewski et al., Khachin et al. and Miyazaki et al. [12] demonstrated that the transformation temperature and other properties of shape memory alloys could be altered by small changes in the composition of the alloy and by various thermo-mechanical heat treatments. Daniels, and Pope and Judd used a differential scanning calorimeter to study the phase transformations exhibited by shape memory alloys [12].

Complexities associated with energy dissipation of the hysteretic nature of pseudo-elasticity was investigated by researchers such as Wayman and Deurig, Wayman, and Fu while Müller and Xu, and Fu, Müller and Xu were among the first to experimentally study the interior of the hysteresis loop [10], [13-14].

After the shape memory effect was first observed in NiTi alloys a great amount of metallurgical research has gone into it and Wasilewski, Jackson et al., Ling and Kaplow and Miyazaki were among the first researchers to experimentally study NiTi [12]. These experiments looked at the effects of temperature, strain range and mechanical cycling on NiTi alloys.

By far the most detail and beneficial experimental investigations into the unstable transformation and inhomogeneous macroscopic deformation of shape memory alloys, is the works by Shaw and Kyriakides [12, 15-16]. A brief summary of their findings will thus be given below:

- Experimental observation show that stress-induced martensitic transformation in certain polycrystalline NiTi shape memory alloy can lead to strain localization and propagation phenomena when uniaxially loaded in tension;
- The Number of nucleation events and kinetics of transformation fronts were found to be sensitive to the nature of ambient media and imposed loading rate due to release / absorption of latent heat and the material's inherent temperature sensitivity of transformation stress;
- Nucleation stress is higher than the transformation stress;
- During unstable transformation, deformation is distinctly inhomogeneous;
- Each nucleation spawns two transition fronts and active deformation of the transition fronts is limited to the neighbourhood of these fronts;
- As a result, latent heat is released in discrete local regions rather than distributed over the entire length of the specimen (suggest strong thermo-mechanical coupling);
- Higher nucleation stress and displacement rates results in multiple fronts;
- Coexisting fronts travel at the same speed;
- The front speed is proportional to the rate of the applied end displacement;
- The front speed in inversely proportional to the number of active fronts;
- More proportions of fronts implies lower front speed and reduced local rate of heating;
- Distinct instability and Lüders-like deformation occurs under isothermal conditions;
- Within an insulating media and higher loading rates the material cause self-heating, which leads to higher force-displacement response and multiple transformation fronts; and
- As the number of fronts increase the deformation appears to become homogeneous.

Gall and Sehitoglu performed experiments on one-dimensional shape memory alloy bars loaded in tension and compression. Their results showed that the shape memory alloys phase transformations is influenced by the texture of the specimen [17].

Sittner et al. performed experimental analyses to study the three-dimensional constitutive behaviour of shape memory alloys. They investigated the stabilization of transformation behaviour in stress-induced martensitic transformation in NiTi alloy hollow bar. The loading cycles were for combined Tension and Torsion. The specimen was then loaded either in tension or torsion. The results revealed strain anisotropy, which implies the existence of other strain components [18].

Gall *et al* [19] studied the effects that tension and compression loading has on recoverable strain of single crystal NiTi shape memory alloy specimens. They found different levels of recoverable strain for the two loading states and concluded that tensile loading produced more recoverable strain than compression loading (see Fig 1.10). Furthermore they reported that the orientation of the crystal structure also has an effect on the amount of recoverable strain produced during loading.

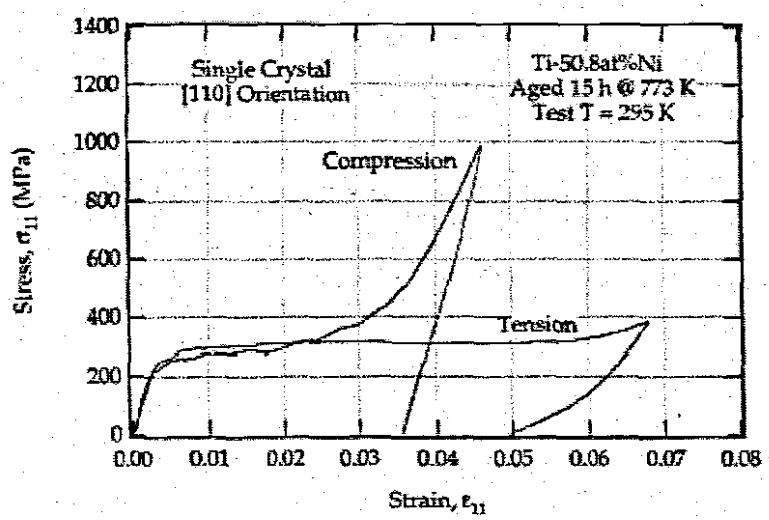

Figure 1.8: the difference in the recoverable strain levels for the [110] orientation loaded under tension versus compression [8]

Liu and Galvin [7] they reported that the stress-strain behaviour of SMAs can be influenced by various internal and external parameters like testing temperature, annealing treatment after cold deformation, grain size and others and discovered the stability effect was attributed to the change in the accommodation morphology of martensite variants from a self-accommodating state for the thermal martensite to an orientated state for stress-induced Martensite.

Liu and Gavin [7] investigated the effect of annealing/aging temperature on the transformation temperature. They chose 726 K, 776K and 1026K as their annealing temperatures for different specimens and used a Differential Scanning Calorimeter to observe the effects on transformation temperatures. Their results showed that an increase in the annealing/aging temperature will bring about an increase in the A_s and A_f temperatures (see Fig 1.11).

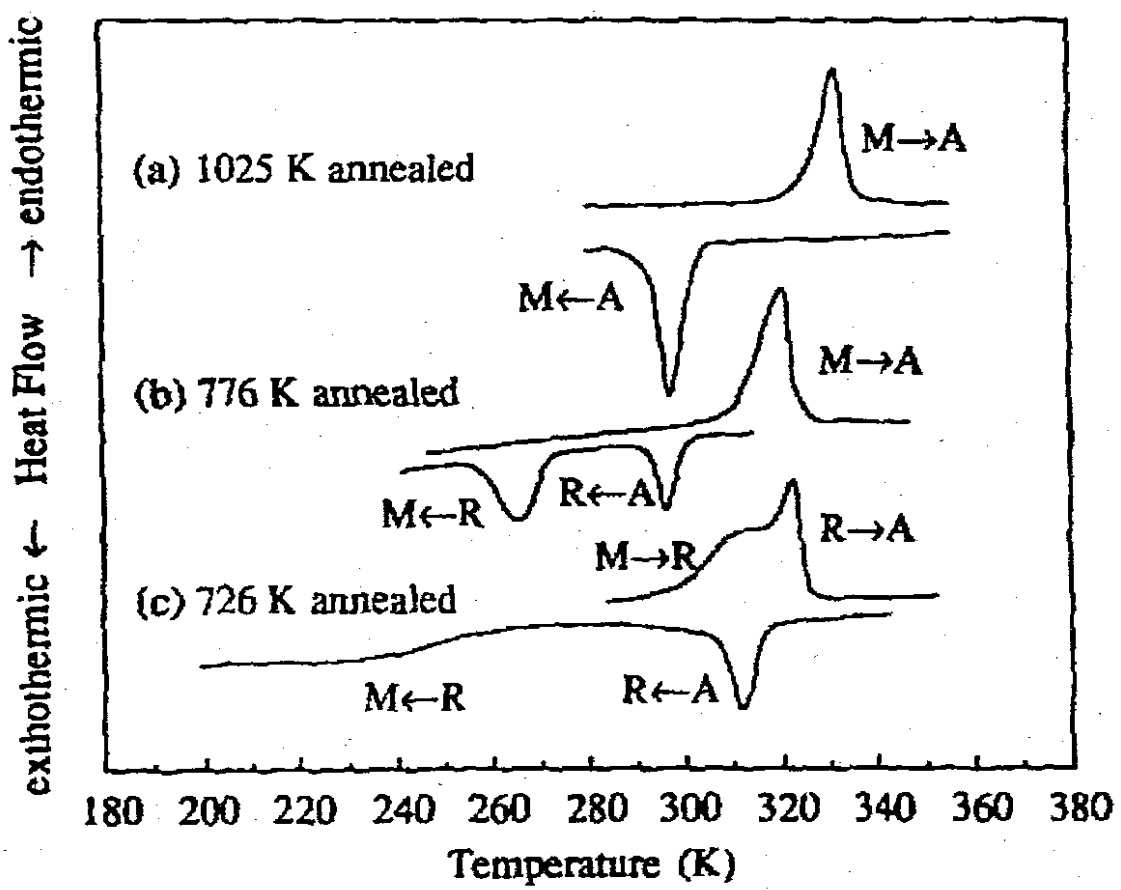

Figure 1.9: Effect of annealing on transformation temperatures. [13]

1.5 Scope of the thesis

Chapter 2 presents the experimental investigation into the effects that thermo-mechanical cycling and aging temperature has on the mechanical working characteristics (i.e. initial elastic displacement, transformation displacement, initial and second yield loads) of NiTi shape memory alloy material specimens. Chapter 3 then describes the experimental investigation into the effects that the thermo-mechanical cycling and aging temperature has on the thermal working characteristic of NiTi shape memory alloy material specimens. Chapter 4 now uses the experimental results obtained in Chapters 2 and 3 to develop mathematical functions to further predict the behavior of NiTi shape memory alloy material specimens. Finally Chapter 5 presents conclusions and recommendation on the work that was presented in this thesis.

Chapter 2

Thermo-Mechanical Experimental Investigation

Shape memory alloys (SMAs) have been used in a variety of applications due to their unique memory abilities at both low and high temperatures. At a low temperature the material is in a twinned martensitic state and it can easily deform plastically also known as quasi-plasticity. This plastic strain can be recovered completely by heating. This material behavior is called the shape memory effect (SME). The plastic deformation observed during SME is due to a de-twinning of the twinned martensitic

phase structure. When the material is heated to some elevated temperature the phase structure changes to austenite. When a load is applied to the material, it will deform plastically when some yielding/transformation load is reached. This plastic strain however is recovered by simply releasing the load. This material behavior is known as psuedo-elasticity (PE). At high temperatures the austenitic to de-twinned martensitic phase transformation governs the psuedo-elastic material response.

Researchers like Van Hambeeck [19] used these unique materials, i.e., shape memory alloys, to manufacture smart devices and structures for engineering applications. These researchers describe the nature of these material behaviors exhibited by shape memory alloys to be complex, and in order to use them in engineering design an understanding of their thermo-mechanical histories are required. Philander [4] mentioned some of these complexities as non-homogeneous transformation regions, variability in initial and final yield points and measures of strains, to name a few.

Other researchers like Mayers, *et al* [6] suggested that to alleviate some of these complexities, shape memory alloys should be subjected to thermo-mechanical cycling. This chapter investigates experimentally the effect that cycling and aging has on the quasi-plastic material behavior exhibited by SMA's during the shape memory effect.

2.1. Experimental Investigation

This section discusses the experimental investigation that was conducted on NiTi shape memory alloys. The main focus here is to study the effects that thermo-mechanical cycling and "aging" have on the variability of initial and final yield points and measures of strains observed during the quasi-plastic material response exhibited by NiTi shape memory alloys. Furthermore is also discusses the extent to which these mechanical and thermal loading cycles influence shape memory alloy actuator working characteristics in terms of actuation stroke, actuation force, and transformation temperatures.

Here aging refers to soaking of the sma material specimens at different temperatures for a period of time. It was anticipated that this aging treatment would have positive influences on the quasi-plastic material response. All experiments were conducted at the Strength of Materials Laboratory of the Department of Mechanical Engineering (Bellville Campus) at the Cape Peninsula University of Technology.

2.1.1 Materials Tested

Commercially available NiTi shape memory alloy wires of 3mm nominal diameter were used in these experiments. The material was obtained from the supplier Johnson Matthey, based in the United Sates of America and Table 2.1 shows its properties. Before testing, measurements were taken to determine the actual diameter of the NiTi shape memory alloy material specimens. This was done because nominal and actual diameters often vary due to manufacturing tolerances or batch variations. Specimens were taken from the wire reel and a vernier caliper was used to take measurements along the length of the specimens. A total of 50 diameter measurements were taken and it was found that the maximum and minimum diameters were 3.040 and 2.970mm respectively with an average diameter of 2.995mm. The standard deviation was determined as 0.018.

Table 2.1: Shape memory alloy material data

Diameter (mm)	Chemical Composition					Temper	Surface	Active A_f (^{0}C)
	Ni	Ti	C	O	Total All Others			
3	55.32	Bal	≤ 0.05	≤ 0.05	≤ 0.30	Straight Annealed	Oxide	73
All Others Are: Al, Co, Cr, Cu, Fe, Mn, Mo, Nb, Si, W								
Materials obtained from Johnson Matthey, 1070 COMMERCIAL ST., SUITE 110, SAN JOSE, CA 95112								

2.1.2 Experimental Set-ups Aging

Thirty-two lengths of 340mm and 3mm diameter wire were considered for testing. These specimens were divided into four groups, each group consisting of eight specimens. Each group was "aged" in a furnace at different temperatures, i.e., 200, 250, 300, and 350^{0}C, with a soaking time of ten hours each. The furnace used for the aging experiments is digitally controlled and thermocouples built into the system measures and control the test chamber's environmental temperature. During soaking periods the temperature varied by ±3^{0}C. These temperatures for aging were chosen so as not to induce memory changes or training of the specimens (memory changes usually occurs above 450^{0}C). After 10 hours the furnace was switched off and the specimens were cooled to room temperature inside the furnace. The specimens were ready for thermo-mechanical cycling.

2.1.3 Experimental Set-ups for Thermo-Mechanical Cycling

The aged specimens were placed in a furnace and heated to a temperature of 100^{0}C. The specimens were held at this temperature for a sufficient amount of time and this ensured that all specimens were transformed to their austenitic state. All specimens were then removed from the furnace and allowed to cool to room temperature in still air, ensuring that at the beginning of thermo-mechanical cycling they were all in their twinned martensitic states. A Hounsfield Tensile Tester was used for tensile experiments and specimens were clamped in such a way that the effective gauge lengths were 300mm. This implies that 20mm on each side of the specimen was clamped in the testing grips. A digital vernier caliper was used to measure the gauge length before every loading cycle and the accuracy of this length was ±0.2mm.

Loads were measured with a 5kN load cells. A digital encoder built into the tensile tester measured the crosshead displacement. Each specimen was subjected to a displacement rate of 5mm/min, which gave eight data sheets per aged group. The tensile testing machine was programmed to stop when a load of 500N was achieved. This value was taken from experiments that Philander [4] conducted and ensured that

the shape memory alloy specimens were exposed to all displacement ranges, i.e. initial, transformation, and final. The specimens were never fractured and after unloading they were placed back into the furnace and heated to restore their original geometric properties.

The specimens of each aged group were now thermo-mechanically cycled 9 times in this fashion. The overall performances of the wires are shown in table 2.2. The table presents the mechanical properties that influence shape memory actuator stroke, i.e., initial elastic displacement, initial yield/transformation load, transformation displacement, and second yield load.

2.2 Qualitative Discussion of the results

Philander [4] suggested that the load-displacement behavior of the quasi-plastic material response be represented by three distinct regions (See Figure 2.1). For discussion purposes he called them respectively the initial elastic region, a nearly horizontal region, and finally elastic region. Since regions 1 and 3 shows elastic behavior (which implies elastic properties), unloading from these regions will remove the strains obtained here. These two elastic regions suggest that the specimen changes from its initial state to some final state. Furthermore it is seen that the slopes of these elastic curves are similar thus implying equal elastic constants. The nearly horizontal regions on these graphs thus determine the location of the transformation behavior from one elastic state to the other. It also has the largest value of displacement compared to the other two regions. The beginning and the end of transformation usually has a distinct point, these are the yield points. (See Figure. 2.1)

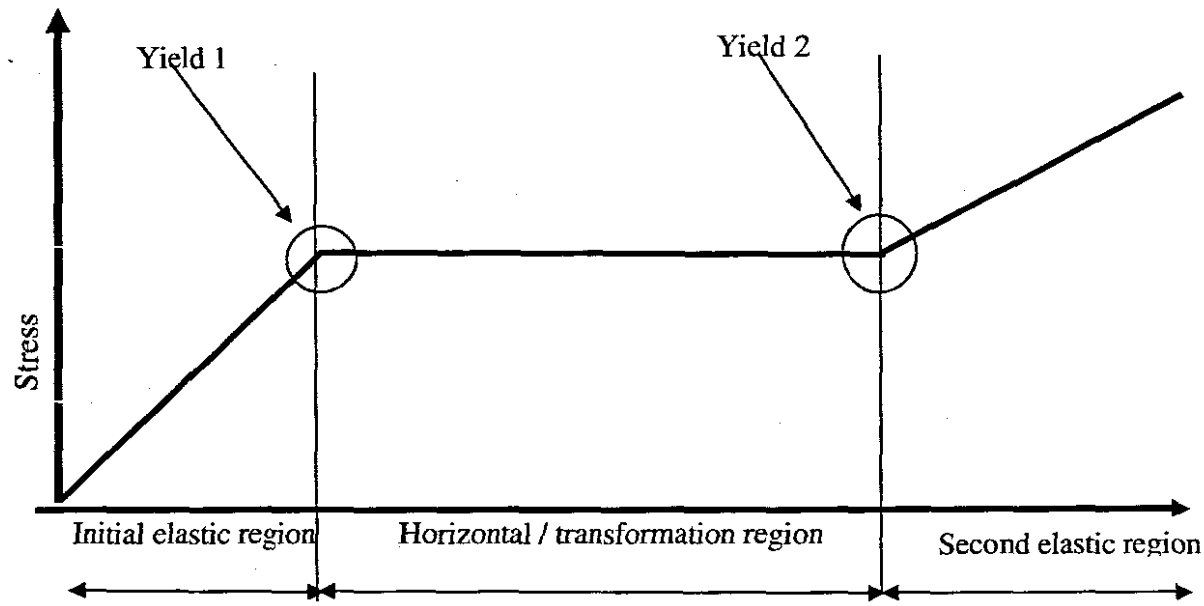

Figure 2.1 Quasi-plasticity Diagram

2.3 Quantitative Discussion of the results

Experiments were performed to find the effect of thermo-mechanical cycling and aging on mechanical properties i.e. initial and second yield/transformation load, initial and transformation displacement of the NiTi shape memory alloy wire specimens. The section below discusses the graphs for each aging temperature and all cycling. This section is referred from Appendix A and it has been summarized at table 2.2. One specimen in each aged group was used to measure its actual diameter to determine what effect the thermo-mechanical cycling and aging had on the diameteral properties of the NiTi shape memory alloy wire specimens. This data is presented in Table 2.3. The data indicates that an increase in the aging temperature coupled with 10 TM cycles decreases the variance range from 0.13mm to 0.02mm. It further shows that an aging temperature of 300^0C coupled with 10 TM cycles brings the actual and nominal diameters in closer agreement.

All the results discussed in this section is presented graphically in Appendix A. Appendix B shows yield points for each graph and the average for each cycle. Table 2.2 is the summary of Appendix B.

200 degC aging temperature

First cycle. The results of each specimen are presented graphically as load-displacement curves. All NiTi shape memory alloy material specimens displayed the quasi-plastic material response and all but one curve followed the same loading path. This curve had a shorter transformation compared to the other seven specimens. The graph also shows that a nearly horizontal transformation region was achieved for all the specimens. This indicated that the phase transformation from twinned to de-twinned martensite occurred at an almost constant load. The average initial and second yield loads were found to be 292 and 307N respectively with an average variance of 15N.

Second cycle. The curves presented on this graph are also in close agreement. One curve however showed slight differences in its initial elastic region compared to the others but links up with the other curves after yielding. The average initial and second yield loads were found to be 280 and 340N respectively with an average variance of 60N.

Third cycle. The curves presented on this graph are in close agreement for all regions. The average initial and second yield loads were found to be 269 and 335N respectively with an average variance of 66N. Although the curves are in close agreement to each other, the hardening like behavior as described by Philander [4] is starting to appear.

Forth cycle. During this cycle all the curves had similar initial elastic paths and were parallel to each other along the transformation region. All but one of the curves followed the same path during the final elastic region. This curve had a slightly longer transformation displacement.

Fifth cycle. The curves plotted on this graph do not lie on top of each other. All curves display similar second yield loads but show they all have different

transformation displacements. This maximum difference in transformation displacement amounts to 1.2mm.

Sixth cycle. The curves plotted on this graph are fairly close to each other except for two curves. These two curves show different paths during the initial elastic region. During the transformation region the curves are relatively far apart and all but one curve follows a similar final elastic loading path. This curve showed an early yielding point.

Seventh cycle. The curves plotted on this graph are more homogeneous at all regions. All but one curve showed an average initial yield load of 245N. The curve that showed a different path had an initial yield load of 315N.

Eighth cycle. The curves plotted on this graph are in close agreement to each other in the initial elastic region. The curves however move further apart during the transformation region. Most of the curves show closer agreement in the final elastic region except for two curves. One of these curves yielded before the other curves with a transformation displacement of 2.1 mm and other curve yielded last with a transformation displacement of 2.8mm.

Ninth cycle. The curves plotted on this graph show close agreement during the initial elastic region except for one curve. During the transformation region most of the curves are close to each other except for two curves, which followed a loading below the other curves. During the final elastic region the curves were separated from each other.

Tenth cycle. The curves plotted on this graph showed close agreement to each other. The curves showed an average initial yield load of 242N except for one curve, which showed an initial yield load of 300N. During the transformation region the curves are close to each other except for two curves, which followed loading paths just below the rest of the other curves.

250 degC aging temperature

First cycle. The curves plotted on this graph are in close agreement to each other during the initial elastic region except for one, which showed a greater initial elastic displacement. When the transformation region was reached however this curve joined the other curves. Here all the curves followed paths parallel to each other. In the final elastic region the curves are separated from each other but remained parallel to each other. It was observed that average initial yield load amounts to 302N while the second yield load amounts to328N showing a variance of 26N.

Second cycle. The curves plotted on this graph are in closer agreement to that shown in the curves of the first cycle for all regions. Here one curve shows a different loading path during the initial elastic region. The average initial and second yield loads are calculated to be 323 and 356N respectively with a variance of 33N.

Third cycle. The curves plotted on this graph also show closer agreement to each other in all regions. The average initial and second yield loads are calculated to be 305 and 341N respectively with a variance of 36N.

Fourth cycle. The curves plotted on this graph are separated but parallel to each other in the initial elastic region. The curves are closer to each other along the transformation region but separate from each other during the final elastic region.

Fifth cycle. The curves plotted on this graph are close to each other during the initial elastic region. During transformation region the curves are separated but parallel to each other. The curves are separated during the final elastic region.

Sixth cycle. The curves plotted on this graph are in close agreement to each other in all regions. The average initial and second yield loads amounts to 291 and 351N respectively with a variance of 60N.

Seventh cycle. The curves plotted on this graph are in closer agreement to each other for all regions and shows better agreement to the previous six cycles.

Eighth cycle. The curves plotted on this graph are slightly separated during the initial elastic region. The transformation region shows that the curves are on top of each other. The final elastic region shows slight separations of the curves.

Nine cycle. The curves plotted on this graph show close agreement to each other for all regions except for one. This curve shows differences in the initial and final elastic regions and has a greater transformation displacement compared to the other curves. The average initial and second yield loads amounts to 276 and 341N respectively with a variance of 65N.

Tenth cycle. The curves plotted on this graph show close agreement to each other during the initial elastic region except for one curve, which has a longer initial elastic displacement. During the transformation region the curves are close to each other and during the final elastic region the curves are close to each except for two curves. These two curves are slightly separated from the other curves. During the transformation region one curve shows a sudden step downwards but then returns to join the other curves.

300 degC aging temperature

First cycle. The curves plotted on this graph show close agreement to each other during the initial elastic region except for two curves that are slightly separated from the other curves. During the transformation region the curves lie on top of each other except for two curves. One of these curves follows a path that is slightly below the other curves and shows a slightly greater transformation displacement compared to the other curves. The other curve shows a slightly shorter transformation displacement than the other curves. The average initial and second yield loads amounts to 337 and 347N respectively with a variance of 10N.

Second cycle. The curves plotted on this graph show close agreement for all regions except for one curve, which has a longer initial elastic displacement and a shorter transformation displacement compared to the other curves. The average initial and second yield loads amounts to 288 and 347N respectively with a variance of 59N.

Third cycle. The curves plotted on this graph show a very close agreement (on top of each other) to each other during the initial elastic region. During the transformation region, the curves are close to each other. The final elastic region shows separation but are however parallel to each other.

Fourth cycle. The curves plotted on this graph are separated during the initial elastic region. The curves do however move closer to each other during the transformation and final elastic regions.

Fifth cycle. The curves plotted on this graph show close agreement to each other during the initial elastic and transformation regions except for one curve, which is separated from the other curves during the initial elastic region. During the final elastic region the curves are separated but parallel to each other. The average initial and second yield loads amounts to 274 and 348N respectively with a variance of 74N.

Sixth cycle. The curves plotted on this graph are separated but parallel to each other during the initial elastic region. The curves move closer to each other along the transformation region. The curves are separated but parallel to each other during the final elastic region.

Seventh cycle. The curves plotted on this graph show a very close agreement to each other for all regions and show better agreement to the six previous cycles. The graphs are more homogeneous than the previous cycles.

Eighth cycle. The curves plotted on this graph show very close agreement to each other and all curves are on top of each other. The average initial and second yield loads amounts to 245 and 340N respectively with a variance of 95N.

Ninth cycle. The curves plotted on this graph show very close agreement to each other and all curves are on top of each other. The average initial and second yield loads amounts to 255 and 338N respectively with a variance of 83N.

Tenth cycle. The curves plotted on this graph show very close agreement to each other during the initial elastic and transformation regions except for two curves, which are separated from the other curves during the initial elastic region. During the final elastic region the curves are close to each other except for two curves.

350 degC aging temperature

First cycle. The curves plotted on this graph show very close agreement to each other during the initial elastic and transformation regions. During the final elastic region the curves are separated. The average initial and second yield loads amounts to 326 and 342N respectively with a variance of 16N.

Second cycle. The curves plotted on this graph show close agreement to each other for all regions except for one. This curve showed a slightly greater transformation displacement. The average initial and second yield loads amounts to 321 and 348N respectively with a variance of 27N.

Third cycle. The curves plotted on this graph show close agreement to each other during the initial elastic region except for one curve, which is slightly separated from the other curves. During the transformation region however all the curves show closer agreement to each other. During the final elastic region the curves are close to each other except for two curves. One of these show a shorter transformation displacement while the other shows a greater transformation displacement as compared to the rest of the curves.

Fourth cycle. The curves plotted on this graph show close agreement to each other during the initial elastic and transformation regions except for one curve, which follows a path slightly below the other curves during the transformation region. During the final elastic region the curves are separated but parallel to each other.

Fifth cycle. The curves plotted on this graph are on top of each other during the initial elastic and transformation regions. During the final elastic region the curves are separated but parallel to each other.

Sixth cycle. The curves plotted on this graph show close agreement to each other during the initial elastic and transformation regions except for one curve, which had a slightly greater initial elastic displacement. This curve however joins the other curves during the transformation region. During the final elastic region the curves are separated but parallel to each other.

Seventh cycle. The curves plotted on this graph show close agreement to each other during the initial elastic and transformation regions except for two curves, which have slightly smaller amounts of transformation displacements compared to the other curves. The average initial and second yield loads amounts to 275 and 336N respectively with a variance of 61N.

Eighth cycle. The curves plotted on this graph are all on top of each other for all regions.

Ninth cycle. The curves plotted on this graph show close agreement to each other during the initial elastic and transformation regions. During the final elastic region the curves are close to each other except for two curves, which have slightly shorter transformation displacements as compared to the other curves. The average initial and second yield loads amounts to 269 and 343N respectively with a variance of 74N.

Tenth Cycle. The curves plotted on this graph show close agreement to each other during the initial elastic and transformation regions except for one curve, which have a slightly greater initial elastic displacement. During the final elastic region the curves are separated from each other.

Table 2.2: Summary of TM and Aging Results

Aging Temperature = 200 degC										
No cycle	**1**	**2**	**3**	**4**	**5**	**6**	**7**	**8**	**9**	**10**
Ave. Initial Yield Force	292	280	269	256	267	267	245	254	251	242
Ave. Second Yield Force	307	340	335	334	341	344	338	322	340	331
Ave. Transformation disp.	1.8	1.8	1.95	1.9	1.85	2.2	2	2	2.05	2
Ave. Initial Elastic disp.	0.6	0.6	0.55	0.5	0.55	0.5	0.5	0.5	0.55	0.55

Aging Temperature = 250 degC										
No cycle	**1**	**2**	**3**	**4**	**5**	**6**	**7**	**8**	**9**	**10**
Ave. Initial Yield Force	302	323	305	298	300	291	278	277	276	266
Ave. Second Yield Force	328	356	341	345	351	351	347	344	341	338
Ave. Transformation disp.	1.85	1.93	2	2.05	2.1	2.15	2.1	2.15	2.13	2.18
Ave. Initial Elastic disp.	0.6	0.65	0.6	0.55	0.6	0.55	0.5	0.55	0.52	0.52

Aging Temperature = 300 degC										
No cycle	**1**	**2**	**3**	**4**	**5**	**6**	**7**	**8**	**9**	**10**
Ave. Initial Yield Force	337	288	294	290	274	263	251	245	255	247
Ave. Second Yield Force	347	347	340	344	348	341	339	340	338	339
Ave. Transformation disp.	1.83	2.05	2.05	1.9	2.1	2.1	2.1	2.05	2.1	2.15
Ave. Initial Elastic disp.	0.65	0.55	0.55	0.6	0.55	0.5	0.52	0.55	5	0.55

Aging Temperature = 350 degC										
No cycle	**1**	**2**	**3**	**4**	**5**	**6**	**7**	**8**	**9**	**10**
Ave. Initial Yield Force	326	321	319	306	290	287	275	270	269	278
Ave. Second Yield Force	342	348	337	332	341	335	336	337	343	348
Ave. Transformation disp.	1.85	1.9	2.05	2	2.1	2.15	2.15	2.1	2.2	2.2
Ave. Initial Elastic disp.	0.66	0.6	0.5	0.66	0.55	0.5	0.5	0.55	0.5	0.55

Table 2.3: Summary of Diameter Measurements

	TM Cycled and Aged Specimens			
	Measured Diameters after 10 TM Cycles			
	200^0C	250^0C	300^0C	350^0C
	2.980	3.000	3.000	3.000
	2.990	2.990	2.990	3.000
	3.000	3.000	2.980	2.990
	2.990	3.000	2.980	2.980
	3.000	2.980	2.990	2.980
	3.000	2.990	2.990	3.000
	3.000	3.010	2.990	2.990
	2.990	2.990	3.000	2.990
	2.970	2.980	2.980	3.000
	2.990	2.990	2.990	2.990
	3.000	2.990	3.000	2.980
	3.000	2.990	2.990	2.990
	2.990	2.980	3.000	2.970
	3.000	3.000	2.990	2.970
	3.100	2.990	3.000	2.980
	2.990	3.000	3.000	3.000
	3.000	2.980	2.990	2.990
Average	**2.999**	**2.992**	**2.992**	**2.988**
Maximum	**3.100**	**3.010**	**3.000**	**3.000**
Minimum	**2.970**	**2.980**	**2.980**	**2.970**
STDEV	**0.027**	**0.009**	**0.007**	**0.010**
Variance	**0.130**	**0.030**	**0.020**	**0.030**

Table 2.4: Summary of Statistical Results for TM and Aging Results

Aging Temperature = 200 degC for 10 cycles					
No cycle	**Average**	**Max**	**Min**	**stdev**	**Variances range**
Initial Yield Force	262.24	292.00	241.75	15.85	50.25
Second Yield Force	333.07	344.13	307.00	11.15	37.13
Transformation disp.	1.96	2.20	1.80	0.12	0.40
Initial Elastic disp.	0.54	0.60	0.50	0.04	0.10

Aging Temperature = 250 degC for 10 cycles					
No cycle	**Average**	**Max**	**Min**	**stdev**	**Variances range**
Initial Yield Force	291.43	322.63	265.75	17.17	56.88
Second Yield Force	344.16	356.25	328.00	7.94	28.25
Transformation disp.	2.06	2.18	1.85	0.11	0.33
Initial Elastic disp.	0.56	0.65	0.50	0.05	0.15

Aging Temperature = 300 degC for 10 cycles					
No cycle	**Average**	**Max**	**Min**	**stdev**	**Variances range**
Initial Yield Force	294.03	337.00	245.25	28.64	91.75
Second Yield Force	342.50	347.75	338.00	3.80	9.75
Transformation disp.	2.04	2.15	1.83	0.10	0.32
Initial Elastic disp.	1.00	5.00	0.50	1.41	4.50

Aging Temperature = 350 degC for 10 cycles					
No cycle	**Average**	**Max**	**Min**	**stdev**	**Variances range**
Initial Yield Force	294.03	326.00	268.88	22.09	57.13
Second Yield Force	339.98	348.00	332.13	5.32	15.88
Transformation disp.	2.07	2.20	1.85	0.12	0.35
Initial Elastic disp.	0.56	0.66	0.50	0.06	0.16

2.4. Summary of experimental findings

The experimental investigation was performed to determine the effect that thermo-mechanical cycling and aging have on the quasi-plastic material behavior exhibited by SMA's during the shape memory effect. All load-displacement graphs are shown in appendix A. A summary of these findings will follow.

- Quasi-plastic material response displays three distinct regions when plotted graphically, i.e., an initial elastic region, a nearly horizontal region, and final elastic region. See figure 2.2

- Elastic regions suggest that the specimen changes from twinned martensitic states to de-twinned martensitic state through a transformation and the slopes of these elastic regions are similar.

- The nearly horizontal regions on these graphs thus determine the location of the transformation behavior from one elastic state to the other.

- Figure. 2.3 show the load-displacement results of the first thermo-mechanical cycle of NiTi Shape memory alloys aged at 200^0C. It is clear to see that aging erased the hardening-like behavior that was observed by Philander [4] (See figure. 2.2). Appendix A also shows that the initial yield loads look similar for all the aged specimens at +-320N. Philander [4] observed a variance in the first and second yield load of up to 60N. The first cycle for each aged group showed a reduction in this variance to 10-15N.

- The graph figure 2.4- 2.7 compare the initial and second yield loads for each aging temperature specimen, it shows that initial yield load decline and the second yield load is stays constant as the numbers of cycles increased.

- As the number of cycles increased, the transformation displacement is increased for all aging temperature. All are inclined at the same gradient. The results show that, the lower the aging temperature the produces shorter transformation displacement. On the other hand, if the aging temperature is increased, the transformation displacement also increases. (See figure 2.8)

- The results show increased on transformation displacement as the aging temperature increased, these results are important during designing of the force-displacement actuators. (See figure 2.8)

- The initial elastic displacement declined as the number of cycle increased. It was observed that these initial elastic displacements for all aging temperature

are converged. Furthermore it shows variability initial displacement elastic at the first cycles, but as the cycle increased the strains are converged. This shows that thermo-mechanical cycling reduce variability of initial displacement. (See figure 2.9)

- Figure 2.10 shows that the initial yield load declined as the number cycle increased.

- It has been observed that the lower aging temperature, there is lower initial yield load and higher aging temperature is appearing on the top of other graphs. It has been suggested that aging is increasing initial yield load. (See figure 2.10)

- Second yield load stays constant as the number of cycle increased (See figure 2.11)

- The second yield loads are converged as the cycle increased. The results shows the variability yield points at the firsts cycles, it shows thermo-mechanical cycle does alleviate some of these inconsistent yield points. (See figure 2.11)

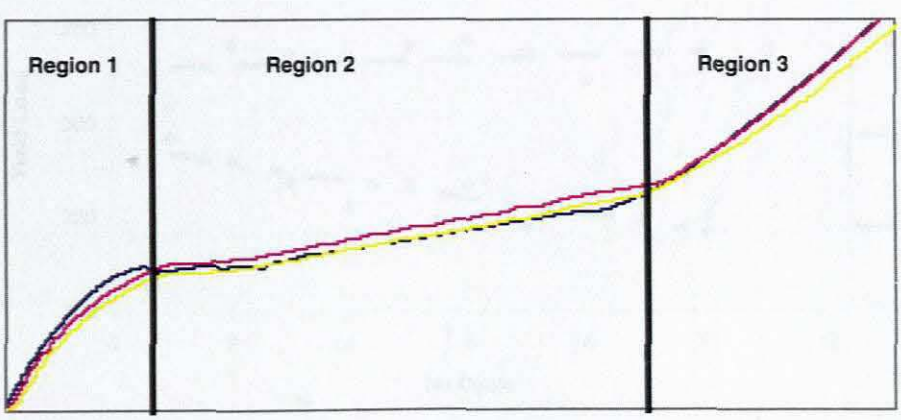

Figure 2.2: Quasi-plastic behavior of untreated 3mm diameter NiTi shape memory alloy wires. [4]

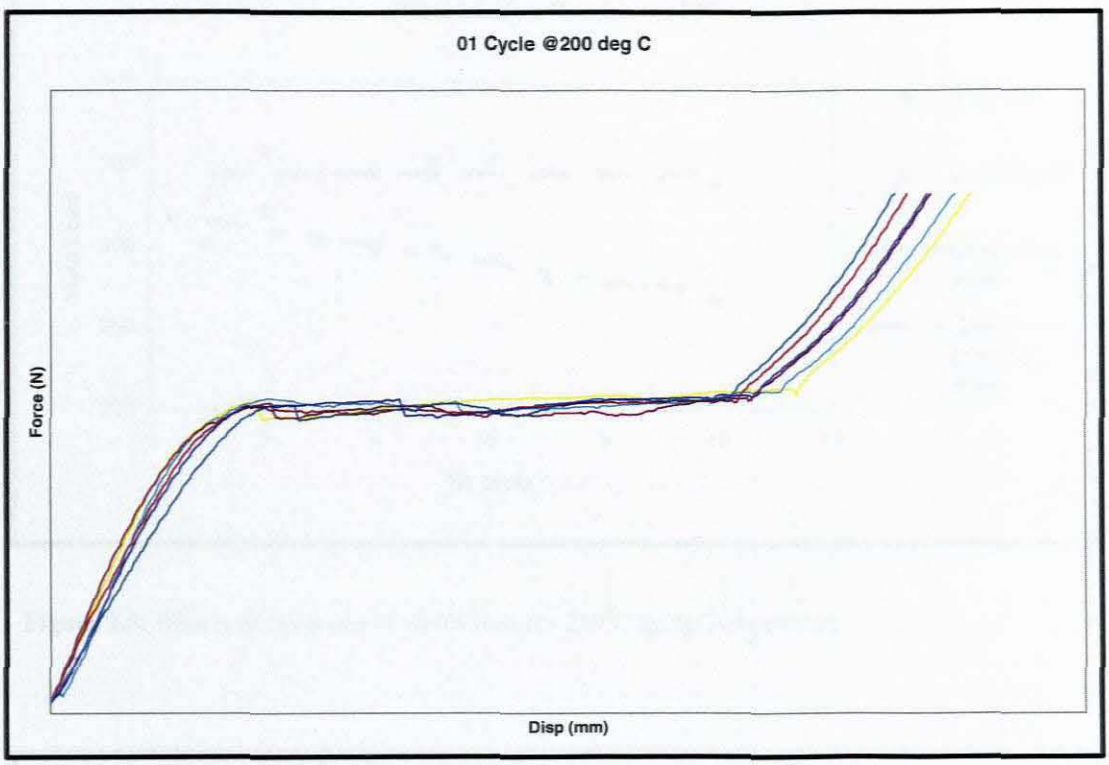

Figure 2.3 Quasi-plastic behaviors of aged 3mm diameter NiTi shape memory alloy wires.

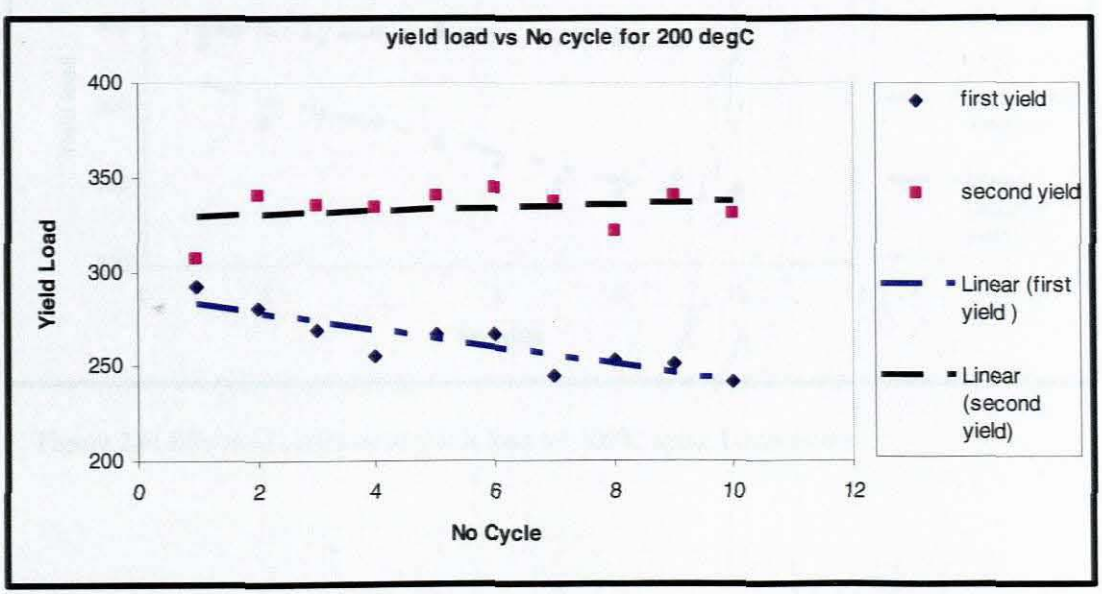

Figure 2.4: Effects of cycles on yields load for 200°C aging Temperature

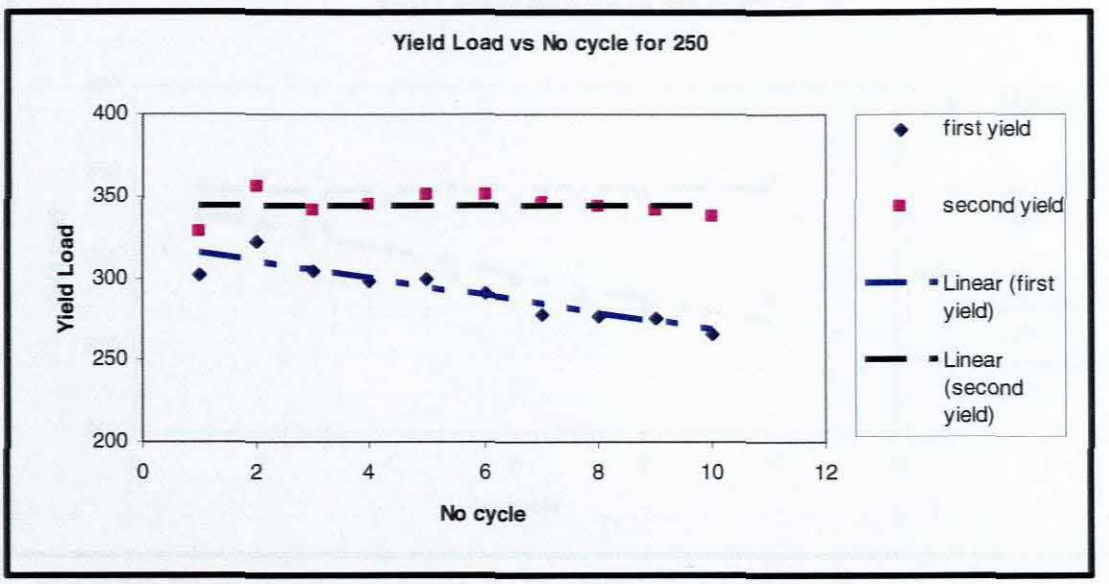

Figure 2.5: Effects of cycles on of yields load for 250°C aging Temperature

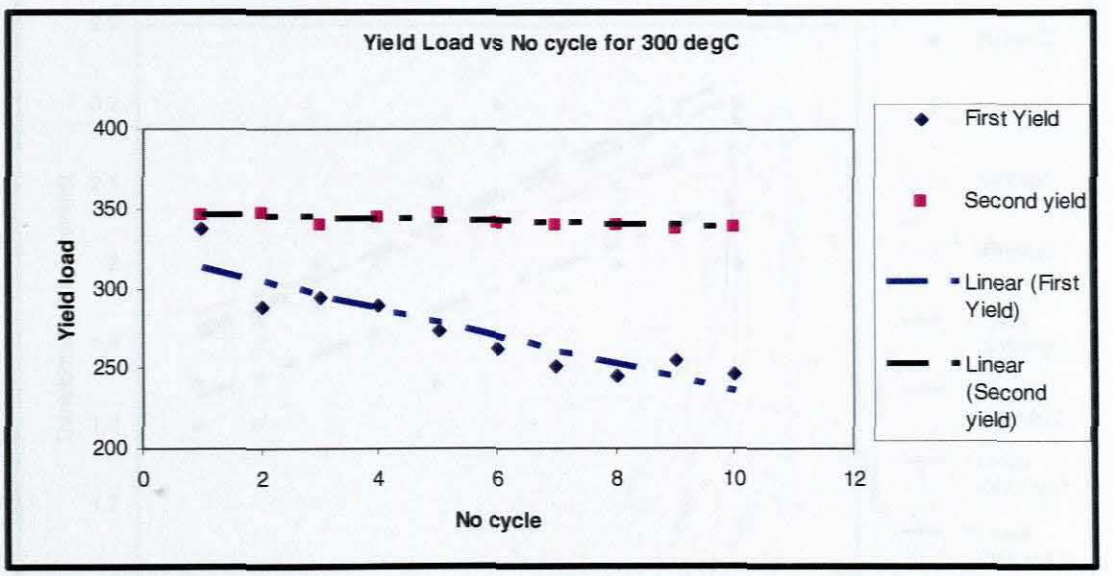

Figure 2.6: Effects of cycles on of yields load for 300°C aging Temperature

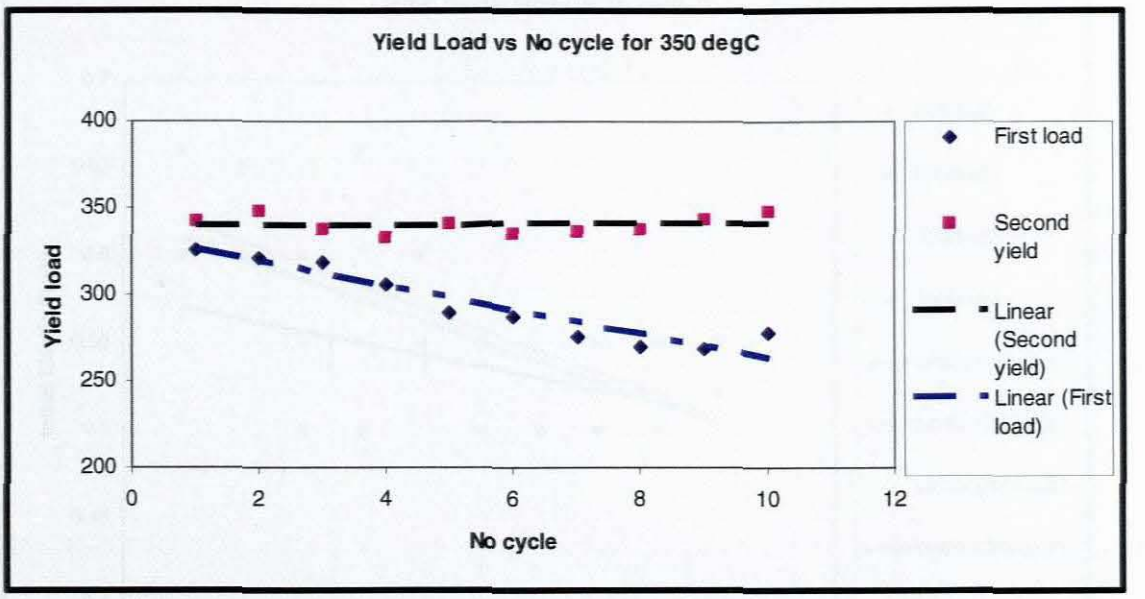

Figure 2.7: Effects of cycles on of yields load for 350°C aging Temperature

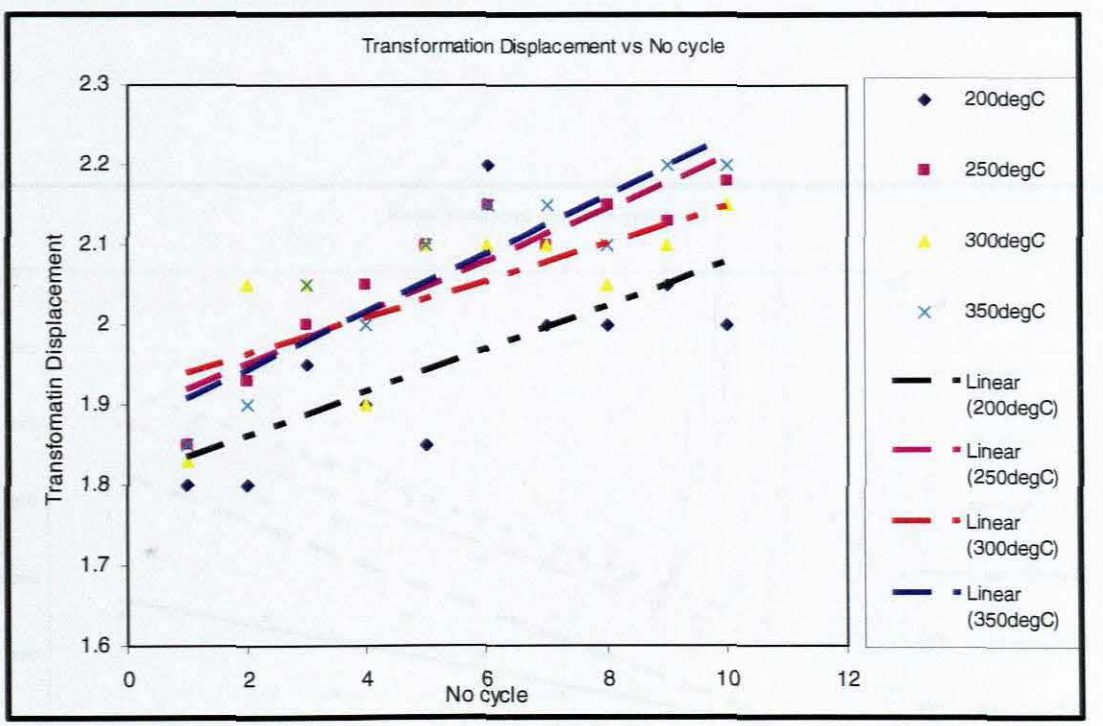

Figure 2.8: Transformation Displacement vs number cycle

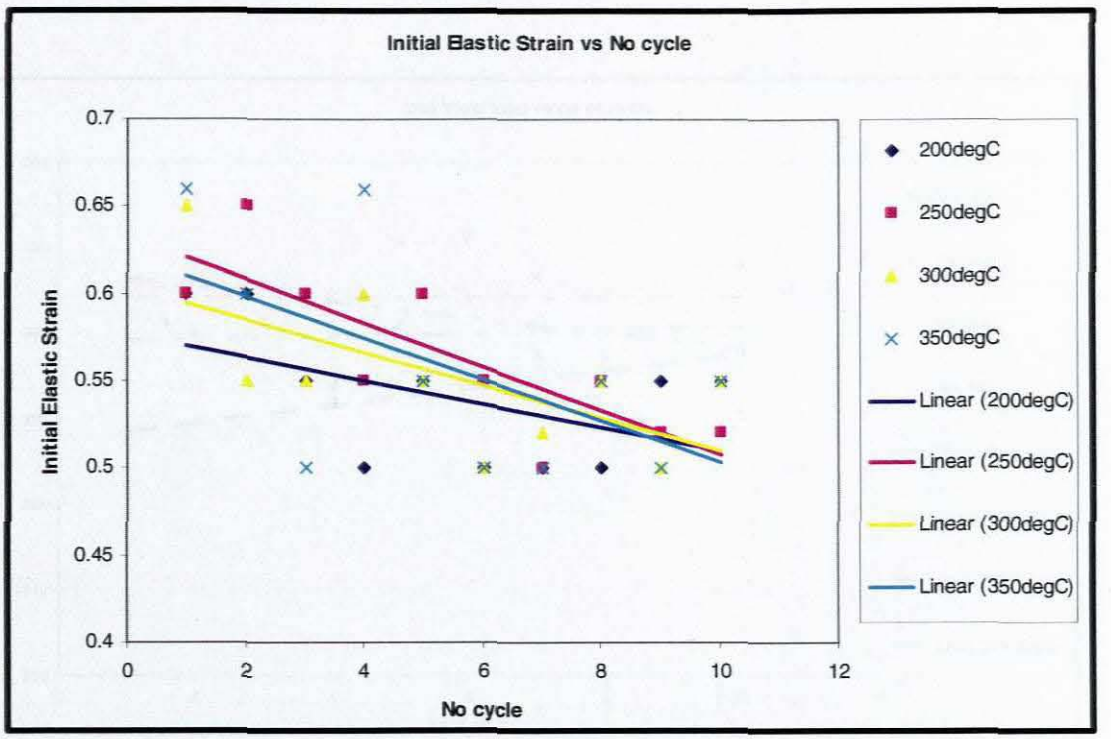

Figure 2.9: *initial elastic strain vs number cycle*

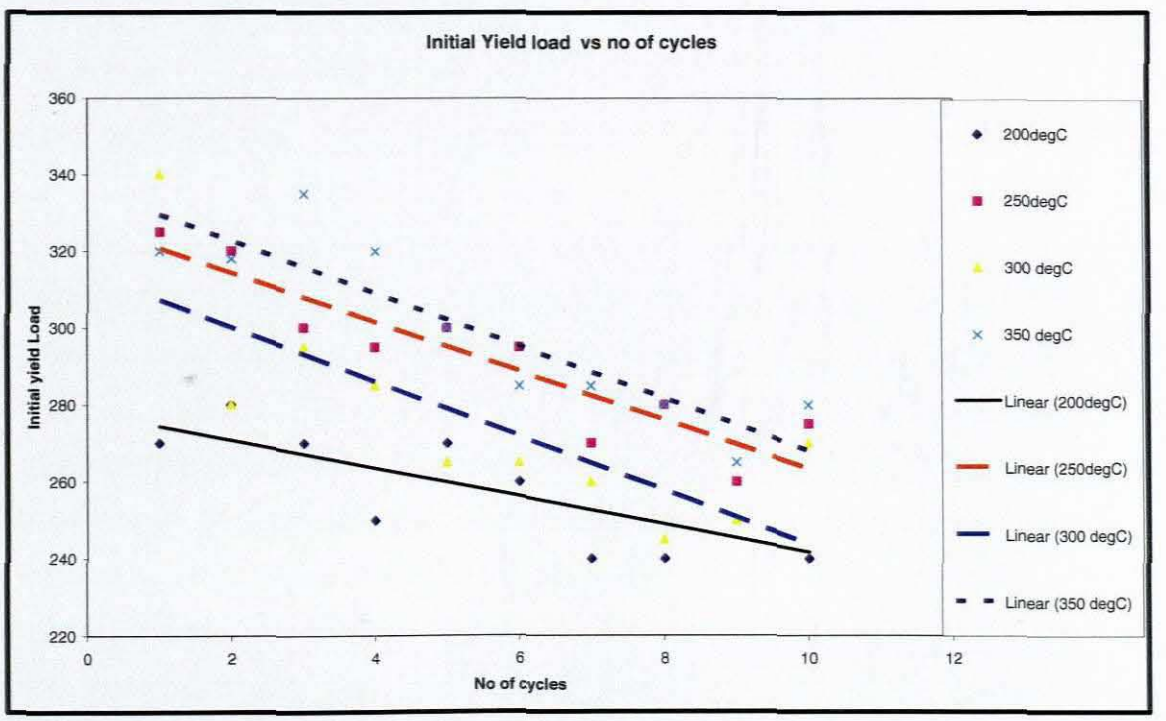

Figure 2.10: Comparing Initial Yield loads vs Number cycle

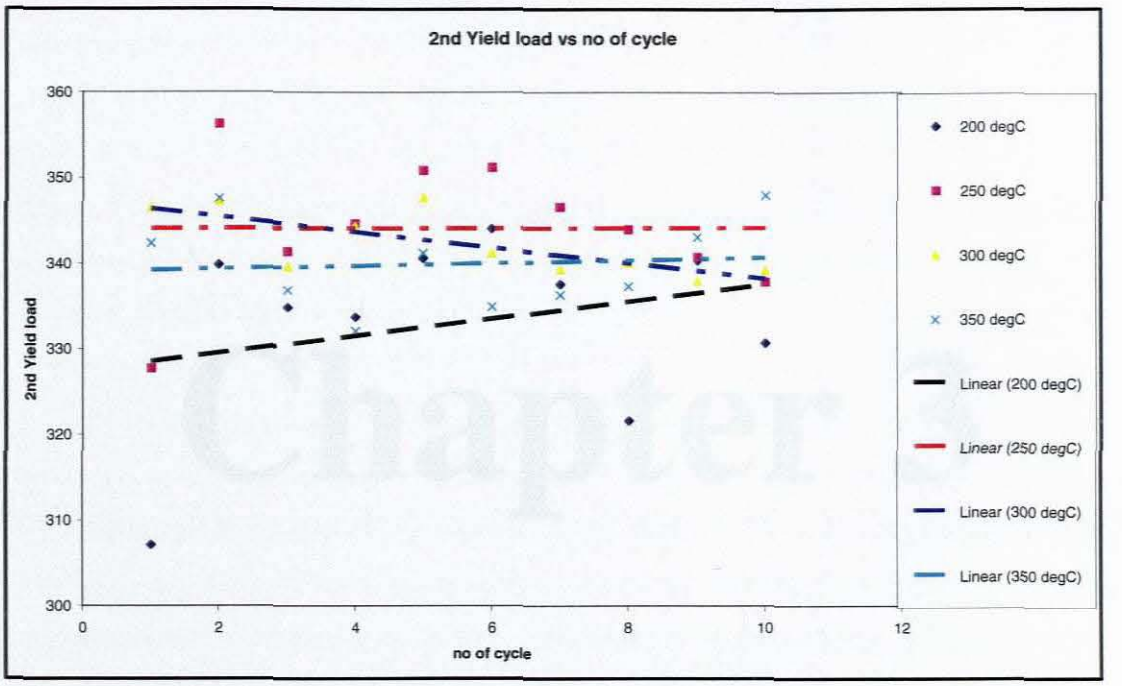

Figure 2.11: Comparing Second Yield loads vs Number cycle

Chapter 3

Thermal analysis

3.1 Introduction

A NiTi shape memory metal alloy can exist in two different temperature-dependent crystal structures called the martensite phase at lower temperature and austenite/parent phase at higher temperature. Several properties of these two phases are notably different. When martensite NiTi is heated, it begins to transform into austenite. The temperature at which this transformation starts is called austenite start temperature (A_s). The temperature at which all the martensite has transformed to austenite is called the austenite finish temperature (A_f). When the austenite phase is cooled, it transforms back into the martensite phase. The temperature at which this transformation starts is called martensite start temperature (M_s). The temperature at which all the austenite has transformed to martensite is called the martensite finish temperature (M_f) (See figure 3.1) [2]. It said that the difference between the transition temperatures upon heating and cooling is called the

transformation hysteresis. Mihialcz [2] defined hysteresis as the difference between the temperature at which the material is 50% transformed to austenite upon heating and 50% transformed to martensite upon cooling. This difference can be of the order of 20-30 °C. Several methods have been reported for determining SMA transformation temperatures. These include differential scanning calorimetry (DSC), the electrical resistance method and the applied constant loading method using a Dilatometer. The DSC is reported to be the most popular and convenient method [20].

In applications such as actuators, sensors, and actuator-sensor systems, SMA's are typically used as working elements that performs cyclic motions. As mentioned previously the thermal working characteristics of SMA elements are specified by their beginning and completion temperatures, i.e. A_s, A_f, M_s and M_f [3]. Chapter 2 investigated and discussed the effects that thermo-mechanical cycling and aging temperature had no transformation loads and displacements. This section will investigate experimentally, the effect of thermo-mechanical cycling and aging temperature on transformation temperatures A_s, A_f, M_s and M_f.

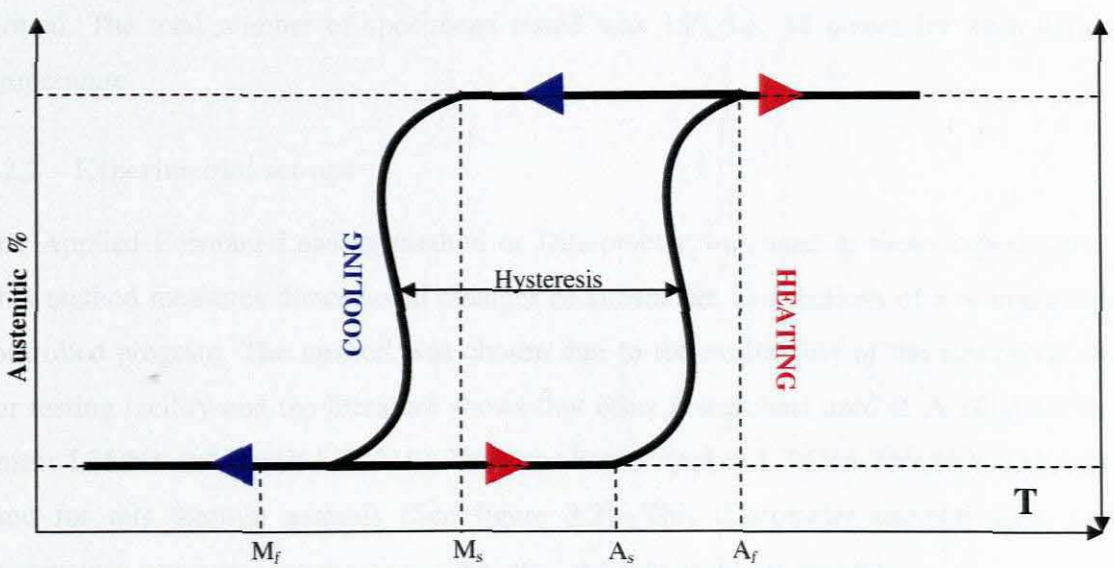

Figure 3.1: Martensitic Transformation base on Mihialcz [2]

specimens to determine its temperature during the heating and cooling cycles. Carbon dioxide is used to cool the specimen.

In order to ensure that the specimens are in their martensitic phase, the specimen was cooled to 10°C. When the temperature in the test section is maintained at this temperature, the furnace was turned on. The temperature was now gradually increased to 120°C. During this period the specimen transforms from it Martensite to Austenite phase. The specimen was now held constant at 120°C for 10 minutes. After this the furnace switches off automatically and the specimen cools to room temperature. In order to speed up this process, the furnace was removed from the test section. If the room temperature was greater than 10°C, carbon dioxide was again applied to cool the specimen to its starting temperature. A data logger built into the system was used to capture temperature (increases/decreases), change in length and time.

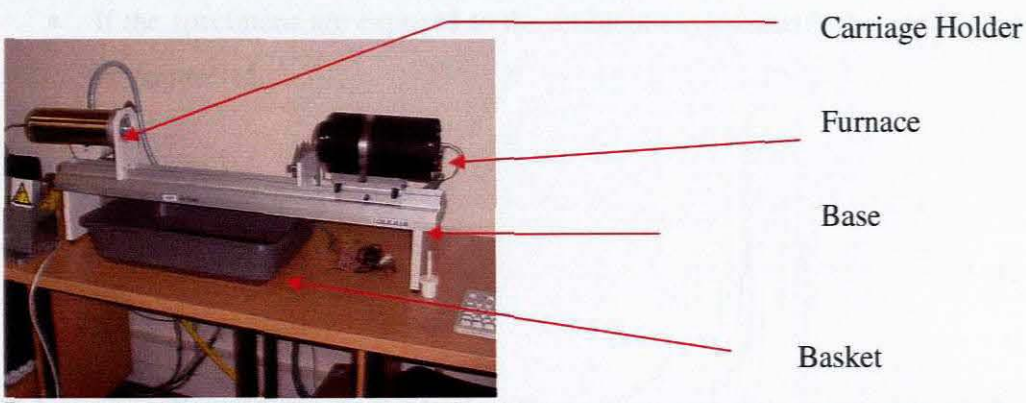

Figure 3.2: Dilatometer used during Experiments

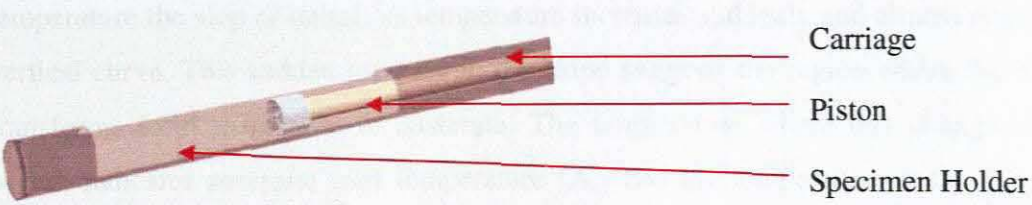

Figure 3.3: Carriage [36]

3.2.3 Constraints to remember when performing the dilatometry experiments.

- Fluctuations in the room temperature may corrupt the experimental data. Whenever this happened carbon dioxide had to be used to merge the experimental starting and ending temperature.
- A bolt cutter was used to cut the specimens. This however causes sharp edges on the ends of the specimens. This meant that the specimens had to be ground flat since its edges have to be perpendicular to the carriage piston of the dilatometer.
- The dilatometer is a very sensitive piece of equipment and while in use it should be touched since slight movements could alter the experimental results.
- When the test section is exposed to the ambient environment of the testing room (during cooling) the furnace should be moved in such a way as to not disturb the test section.
- If the specimens are exposed to the ambient environment, the cooling rate cannot be controlled.

3.3 Discussion of results

3.3.1 Qualitative Discussion

This section discusses qualitatively the effects that aging temperature has on the thermal working characteristics of NiTi shape memory alloy wire specimens. The graphical data obtained suggests that the material undergoes expansion during heating cycles. At a given temperature the slop of deltaL vs temperature increases suddenly and almost resembles a vertical curve. This sudden increase in the slope suggests the region where the material transforms from martensite to austenite. The temperature where this change in slope occurs indicates austenite start temperature (A_s) and the temperature at the top of this slope indicates the austenite finish temperature (A_f). (See Fig 3.4)

During cooling a similar path is followed. This cooling path is not on top of the heating path and shows the thermal hysteric behavior of the material. The cooling path also shows a steep downward slope and is almost parallel to the heating slope. This downward slope indicates the transformation from austenite to martensite. The temperature at which this downward slope begins is thus the martensite start temperature (M_s) and the temperature at the end of the downward slope is the martensite finish temperature (M_f). (See figure 3.4).

The volumetric expansion and contraction due to heating and cooling respectively of the NiTi shape memory alloy specimens are ascribed to the microstructural changes that occur during martensite⇒austenite and austenite⇒martensite phase transformation. (See Fig 3.4)

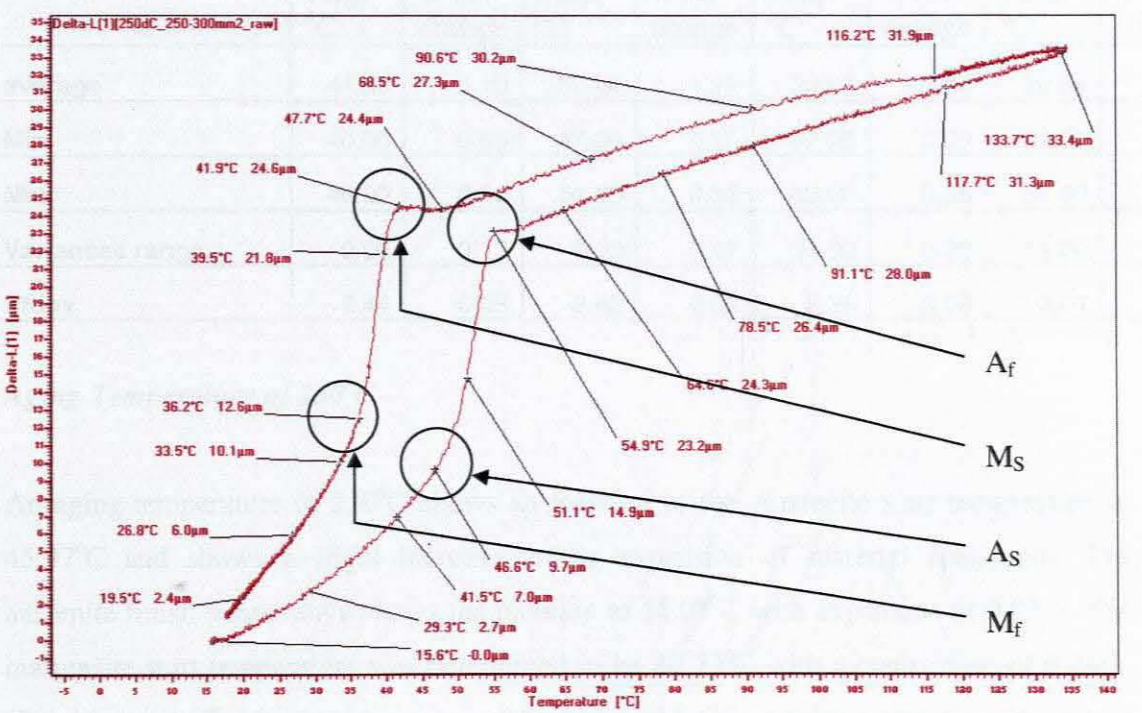

Figure 3.4: Dilatometer results

3.3.2 Quantitative Discussion.

Aging Temperature of 200^{0}C

For an aging temperature 200°C, the average values for Austenite start temperature was measured to be 44.65 °C and the expansion is 0.1% while the austenite finish temperature was measured to be 52.43 °C and the expansion is 0.22%. The martensite starts temperature was measured to be 39.63 and the contraction was 0.23%. The martensite finish temperature is 32.54 °C and the contractoin was 0.11%. (Table 3.1)

Table 3.1. Transformation Temperatures and percentage on expansion of 200°C aged

200°C aged	A_s		A_f		M_s		M_f	
	Temp. °C	% vol change	Temp. °C	% vol change	Temp. °C	% vol change	Temp. °C	% vol change
average	44.65	0.10	52.04	0.22	39.63	0.23	32.54	0.11
Min	40.00	0.05	47.00	0.15	32.00	0.09	22.00	0.06
Max	49.00	0.18	56.00	0.32	43.00	0.35	37.00	0.24
Variances range	9.00	0.13	9.00	0.17	11.00	0.26	15.00	0.18
Stdev	2.44	0.03	2.82	0.05	2.28	0.06	3.01	0.04

Aging Temperature of 250^{0}C

An aging temperature of 250°C shows an increase of the Austenite start temperature to 45.97°C and shows a slight increase in the expansion of material specimens. The austenite finish temperature shows the increase to 54.07°C with expansion of 0.25%. The martensite start temperature was determined to be 40.72°C with a contraction of 0.24%. The martensite finish temperature was found to be 34.1°C and the contraction was found to similar for specimens aged at 200°C with a value of 0.11%. (See Table 3.2)

Table 3.2 Transformation Temperatures and percentage on expansion of 250°C aged

250°C aged	A_s		A_f		M_s		M_f	
	Temp. °C	% vol change	Temp. °C	% vol change	Temp. °C	% vol change	Temp °C.	% vol change
average	45.72	0.11	53.48	0.25	40.72	0.24	34.10	0.11
Min	43	0.06	49	0.14	36	0.17	27	0.07
Max	47	0.17	56	0.81	44	0.36	38	0.2
Variances range	4.00	0.11	7.00	0.67	8.00	0.19	11.00	0.13
Stdev	1.16	0.03	1.74	0.12	1.93	0.05	2.40	0.03

Aging Temperature of 300°C

For an aging temperature of 300°C, the austenite start temperature shows a slight decrease as compared to the 250°C aging temperature. It was calculated to be 45.76°C with a drop in the expansion of 0.09%. The austenite finish temperature was calculated to be 52.92 °C with an expansion of 0.21%. The martensite starts temperature was calculated to be 40.54°C with a contraction of 0.22%. The martensite finish temperature was calculated as 34.92 °C with a contraction of 0.10%. (See Table 3.3)

Table 3.3 Transformation Temperatures and percentage on expansion of 300°C aged

300°C aged	A_s		A_f		M_s		M_f	
	Temp. °C	% vol change	Temp. °C	% vol change	Temp. °C	% vol change	Temp. °C	% vol change
average	45.76	0.09	53.04	0.21	40.54	0.22	34.92	0.10
Min	41.00	0.06	46.00	0.16	37.00	0.16	32.00	0.07
Max	49.00	0.16	59.00	0.31	45.00	0.30	41.00	0.18
Variances range	8.00	0.10	13.00	0.15	8.00	0.14	9.00	0.11
Stdev	2.31	0.02	3.16	0.04	2.17	0.04	2.36	0.02

Aging Temperature of 350^{0}C

For an aging temperature of 350°C, all the transformation temperatures were found to be higher than the 300°C aged specimens. The expansion and contraction values remained constant however. (See Table 3.4)

Table 3.4 Transformation Temperatures and percentage on expansion of 350°C aged

	A_s		A_f		M_s		M_f	
	Temp. °C	% vol change	Temp. °C	% vol change	Temp. °C	% vol change	Temp. °C	% vol change
average	46.07	0.10	54.74	0.24	42.11	0.25	35.78	0.12
min	33.00	0.04	49.00	0.18	36.00	0.18	30.00	0.08
max	49.00	0.16	58.00	0.31	47.00	0.32	41.00	0.20
Variances range	16.00	0.11	9.00	0.13	11.00	0.14	11.00	0.12
Stdev	3.17792	0.02883	2.3421	0.02968	3.085	0.03305	3.54264	0.0299

Table 3.5 Transformation Temperatures and percentage on expansion of no aged

	A_s		A_f		M_s		M_f	
	Temp. °C	% vol change	Temp. °C	% vol change	Temp. °C	% vol change	Temp. °C	% vol change
average	45.88	0.10	53.68	0.22	42.00	0.23	35.36	0.11
Min	40.00	0.04	48.00	0.12	35.00	0.12	31.00	0.03
Max	51.00	0.15	60.00	0.31	47.00	0.32	40.00	0.17
Variances range	11.00	0.11	12.00	0.19	12.00	0.20	9.00	0.14
Stdev	2.8624	0.03127	3.90512	0.05328	3.82971	0.05664	3.06703	0.04107

Un-Aged Specimens

For un-aged specimens, the austenite start temperature was calculated to be 46.07°C with an expansion of 0.1%. The austenite finish temperature was calculated to be 54.74°C and an expansion of 0.24% was obtained. The martensite start temperature was calculated to be 40.11°C with a contraction of 0.25%. The martensite finish temperature was calculated as 35.78°C with a contraction of 0.12%. (See Table 3.5).

3.3.3 Summary of experimental findings

The experimental investigation was performed to determine the effect that aging have on the austenite start, the austenite finish, the martensite starts and the martensite finish temperatures. The summary of results are given in point form.

- For specimen aged at 200°C the results showed that certain specimens taken from the same length of material had variations in the austenitic start temperature and the austenite finish temperature of up to 9^0C. The martensite start temperatures had a variation of about 11^0C and martensite finish temperatures had a variation of about 15^0C (See Table 3.1)

- For specimen aged at 250°C, the results showed that certain specimens taken from the same length of material had variations in the austenitic start temperature of up to 4^0C. For the austenite finish temperature this variation was about 7^0C. The martensite start and finish temperatures had a variation of about 8^0C and 11^0C respectively (See Table 3.2).

- 300°C aging temperature showed that certain specimens taken from the same length of material had variations in the austenitic start temperature of up to 8^0C. For the austenite finish temperature this variation was about 13^0C. The martensite start and finish temperatures had a variation of about 8^0C and 9°C respectively (See Table 3.3).

- 350°C aging temperature showed that certain specimens taken from the same length of material had variations in the austenitic start temperature of up to 11^0C. For the austenite finish temperature this variation was about 12^0C. The martensite start and finish temperatures had a variation of about 9^0C (See Table 3.4)

- The results of no aging specimen showed that certain specimens taken from the same length of material had variations in the austenitic start temperature of up to 16^0C. For the austenite finish temperature this variation was about 9^0C. The martensite start and finish temperatures had a variation of about 11^0C (See Appendix C)

- The austenite start temperature slightly increased as the aging temperature increased. (See figure 3.5)

- The austenite finish temperature shows every little increase as the aging temperature is increased. (See figure 3.5)

- The martensite starts temperature shows an increase as the aging temperature is increased (See figure 3.5).

- The martensite finish temperature increases as the aging temperature is increased. (See figure 3.5)

- It has been observed that the expansion of material is decreased as the aging temperature increases. (See figure 3.6)

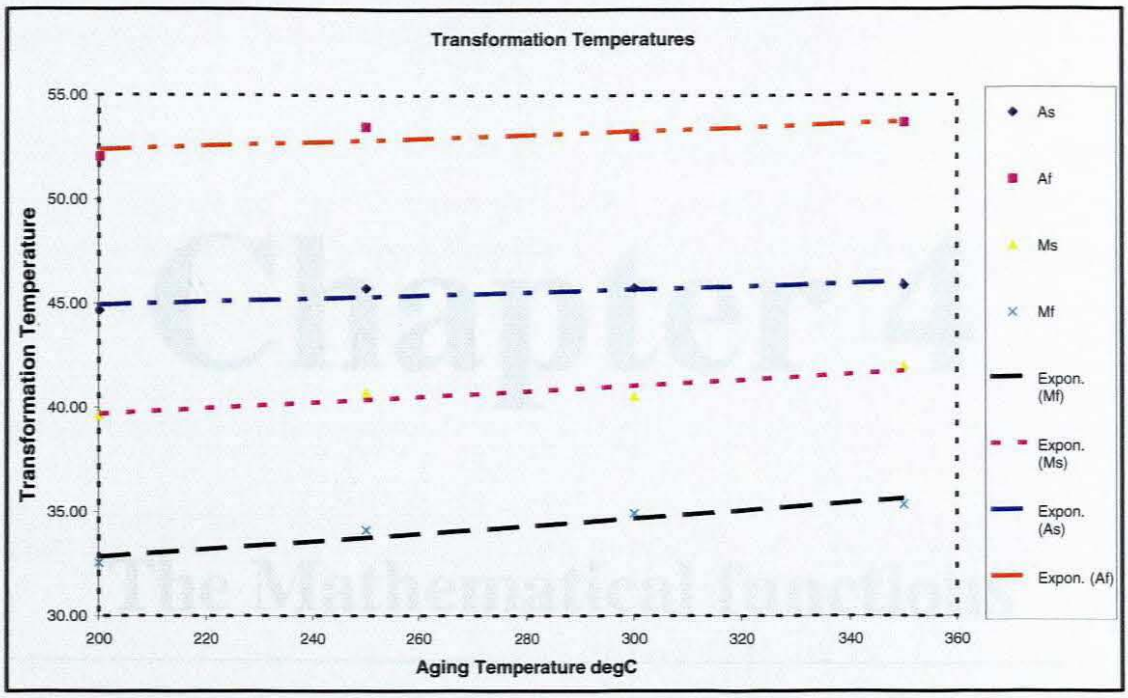

Figure 3.5: Summary of effect of aging temperature on transformation temperature.

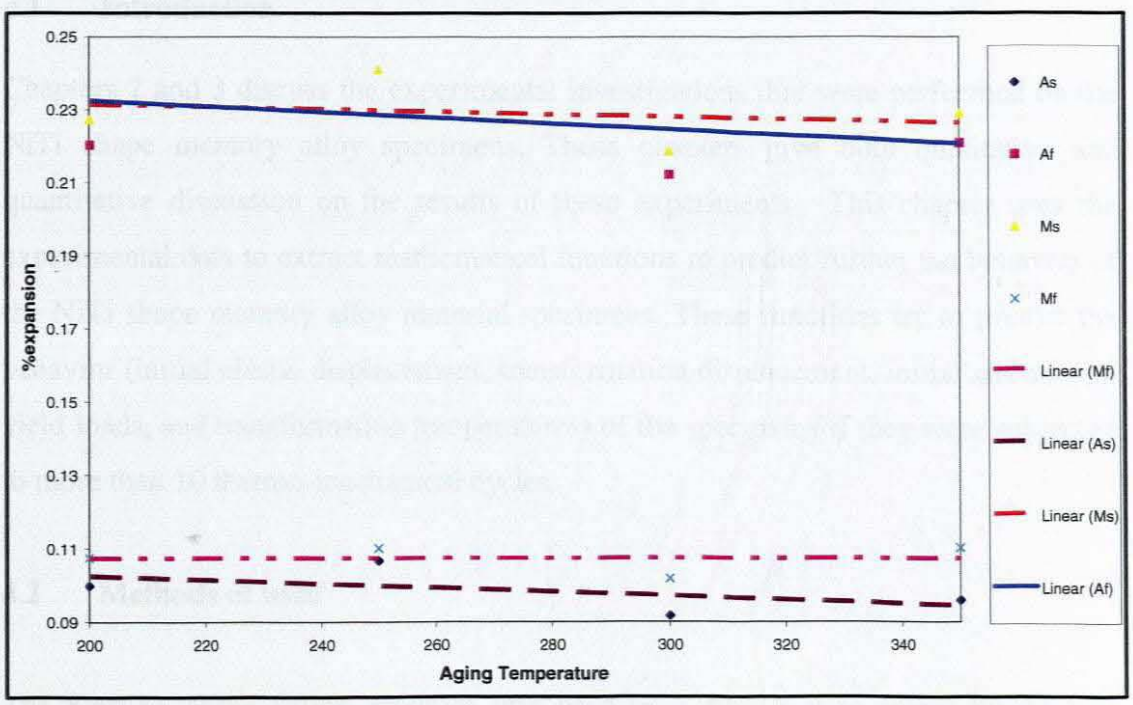

Figure 3.6: Summary of effect of aging temperature on transformation expansion of materials.

Chapter 4

The Mathematical functions

4.1 Introduction

Chapters 2 and 3 discuss the experimental investigations that were performed on the NiTi shape memory alloy specimens. These chapters give both qualitative and quantitative discussion on the results of these experiments. This chapter uses the experimental data to extract mathematical functions to predict further the behavior of the NiTi shape memory alloy material specimens. These functions try to predict the behavior (initial elastic displacement, transformation displacement, initial and second yield loads, and transformation temperatures) of the specimens if they were subjected to more than 10 thermo-mechanical cycles.

4.2 Methods of used

The Kurv++ curve fitting program was used as a first tool to select the best-fit function for the different experimental data. The WFIT&PLOT program was then used to determine coefficients for the initial functions obtained from Kurv++ that would produce fits of a higher quality. WFIT uses marquard's algorithm to find values of coefficients that make a function fit a set of data points in a least squares sense. The function can be non linear with respect to the coefficients. The algorithm

requires an initial estimate of the value of each coefficient; it then uses an iterative process to find new values of coefficients that give a better fit.

The curves presented here are predictions of what would happen to the working characteristic of the NiTi shape memory alloy elements that was subjected to 20 thermo-mechanical cycles. These function curves are plotted with the experimental data points obtained from Chapters 2 and 3.

4.3 Results and discussion.

4.3.1 Initial elastic displacement

For NiTi shape memory alloy material specimens aged at 200^0C, the initial elastic displacement was very small and the data obtained could not be used to extract an adequate function. For this reason a function could not be extrapolated for the initial elastic displacement of 200^0C aged specimens.

Function (1) below shows the initial elastic displacement of 250^0C aged NiTi shape memory alloy material specimens as a function of 10 thermo-mechanical cycles. The experimental results were used as input for the WFIT&PLOT program and a 0.97 coefficient of determination was achieved after a number of iterations.

$$\delta_{1\text{-}250}(N) = 0.46445 + \frac{0.56831}{N} - \frac{0.4317}{N^2} \quad \text{.....(1)}$$

This function was plotted (See Fig 4.1) and the curve represents a prediction of how the initial elastic displacement would behave if the NiTi shape memory alloy material specimens were thermo-mechanically cycled for 20 cycles. The graph of Fig 4.1 shows the experimental data points for 10 thermo-mechanical cycles with the function embedded in it. The function curve shows that the initial elastic displacement would attain some form of stability if the NiTi shape memory alloy material specimens are thermo-mechanically cycled for more than 20 cycles. Liu and Galvin [7] reported a "stability effect" of shape memory alloys and ascribed it to the

change in the accommodation morphology of martensite variants from a self-accommodating state for the thermal martensite to an orientated state for stress-induced Martensite. It is clear that this "stability effect" would be achieved at approximately 0.5mm for the initial elastic displacement of 250^0C aged specimens.

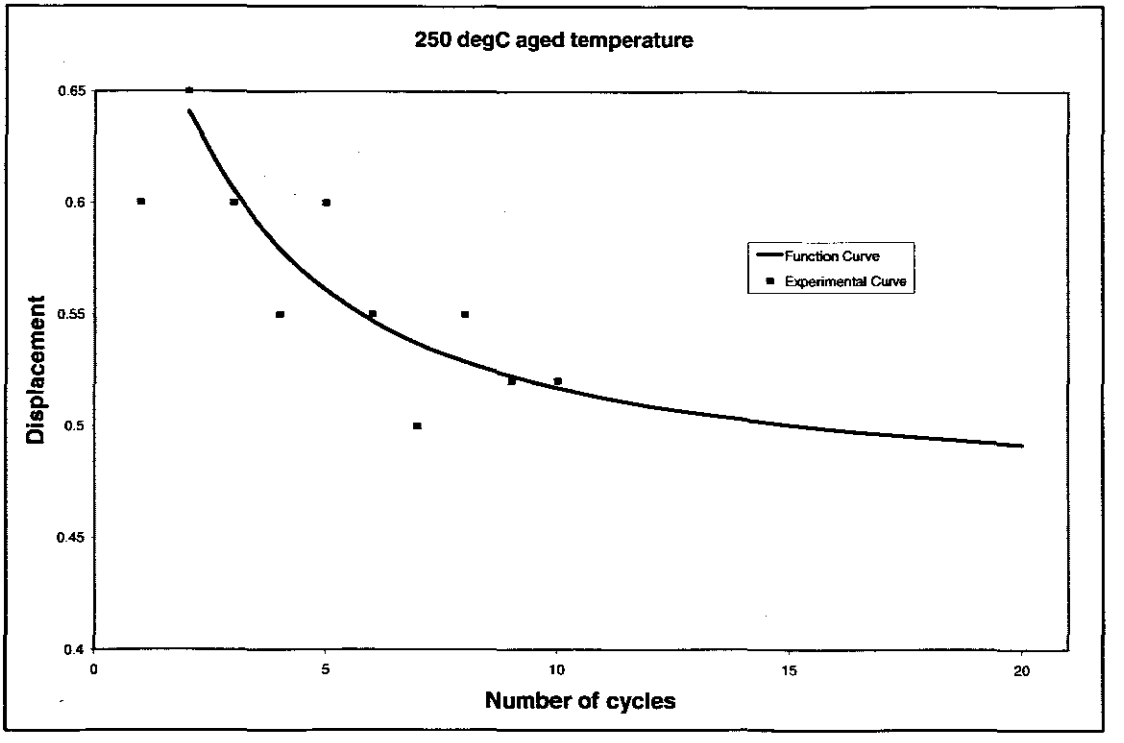

Figure 4.1: Behavior of initial displacement as the number of cycles increases for a 250°C aging temperature

Function (2) below shows the initial elastic displacement of 250^0C aged NiTi shape memory alloy material specimens as a function of 10 thermo-mechanical cycles. The experimental results were used as input for the WFIT&PLOT program and a 0.83 coefficient of determination was achieved after a number of iterations. The prediction curve shown in Fig 4.2 has similar tendencies to that shown in Fig 4.1 and also shows some stability of the initial elastic displacement for 300^0C aged specimens would be achieved at approximately 0.53mm

$$\delta_{1-300}(N) = 0.52326 + \frac{0.06927}{N} + \frac{0.054519}{N^2} \quad \text{.....(2)}$$

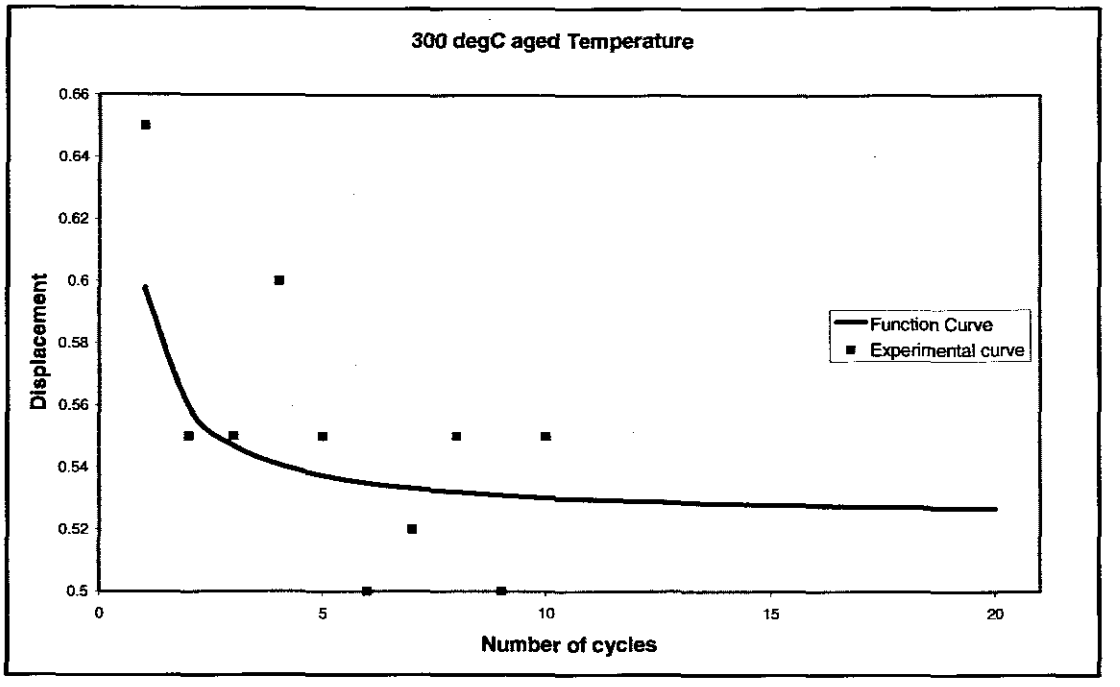

Figure 4.2: Behavior of initial displacement as the number of cycles increases for a 300°C aging temperature

Function (3) below shows the initial elastic displacement of 350^{0}C aged NiTi shape memory alloy material specimens as a function of 10 thermo-mechanical cycles. The experimental results were used as input for the WFIT&PLOT program and a 0.82 coefficient of determination was achieved after a number of iterations. This function curve (see Fig 4.3) has a similar appearance to function curve shown in Fig 4.1.

$$\delta_{1-350}(N) = 0.4231071 + \frac{0.7479732}{N} - \frac{0.510954}{N^2} \quad \text{.....(3)}$$

Fig 4.3 shows the prediction curve of function (3) embedded in the experimental data points for 10 thermo-mechanical cycles and also shows the "stability effect".

The plots of Figs 4.1-4.3 shows a decrease in the initial elastic displacement of 250, 300, and 350^{0}C aged NiTi shape memory alloy material specimens. These three

curves show that some measure of stability in terms of a fixed initial elastic displacement would be achieved after repeated thermo-mechanical cycling, i.e. in excess of 20 thermo-mechanical cycles.

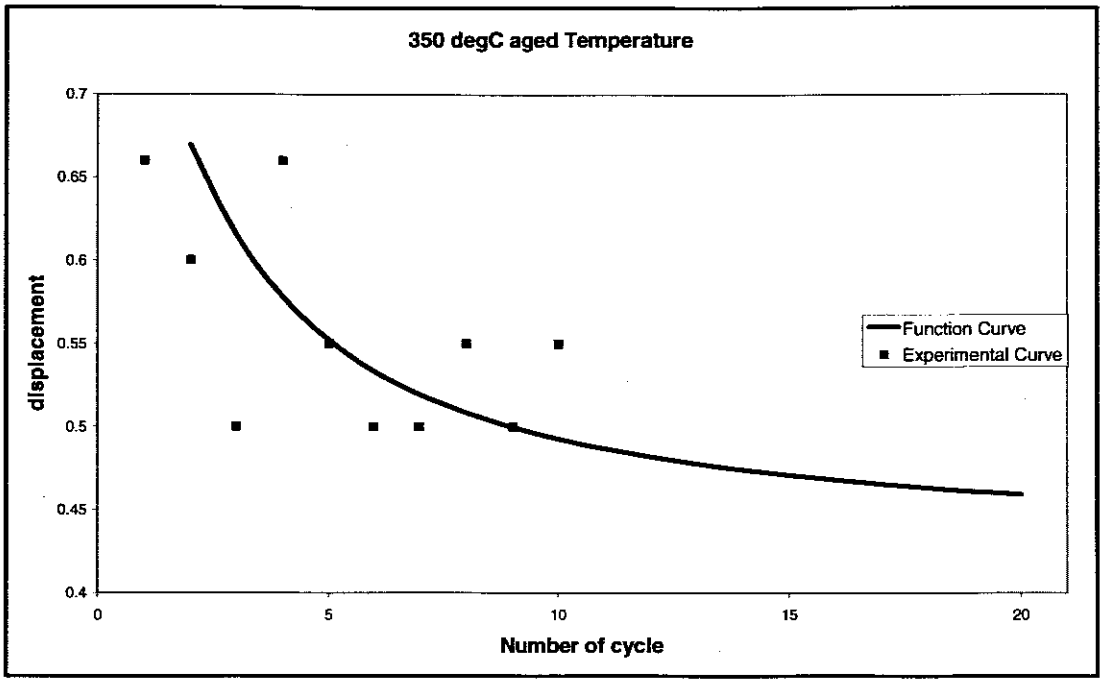

Figure 4.3: Behavior of initial displacement as the number of cycles increases for a 350°C aging temperature

4.3.2 Transformation displacement

Function (4) below shows the transformation displacement of 200^{0}C aged NiTi shape memory alloy material specimens as a function of 10 thermo-mechanical cycles. The experimental results were used as input for the WFIT&PLOT program and a 0.82 coefficient of determination was achieved after a number of iterations. The experimental data suggested that an increase in the transformation displacement was achieved if thermo-mechanical cycling was achieved to the specimens. The curve of function (4) (see Fig 4.4) shows a similar tendency.

$$\delta_{t-200}(N) = 1.8794e^{0.017337N} \quad \text{.....(4)}$$

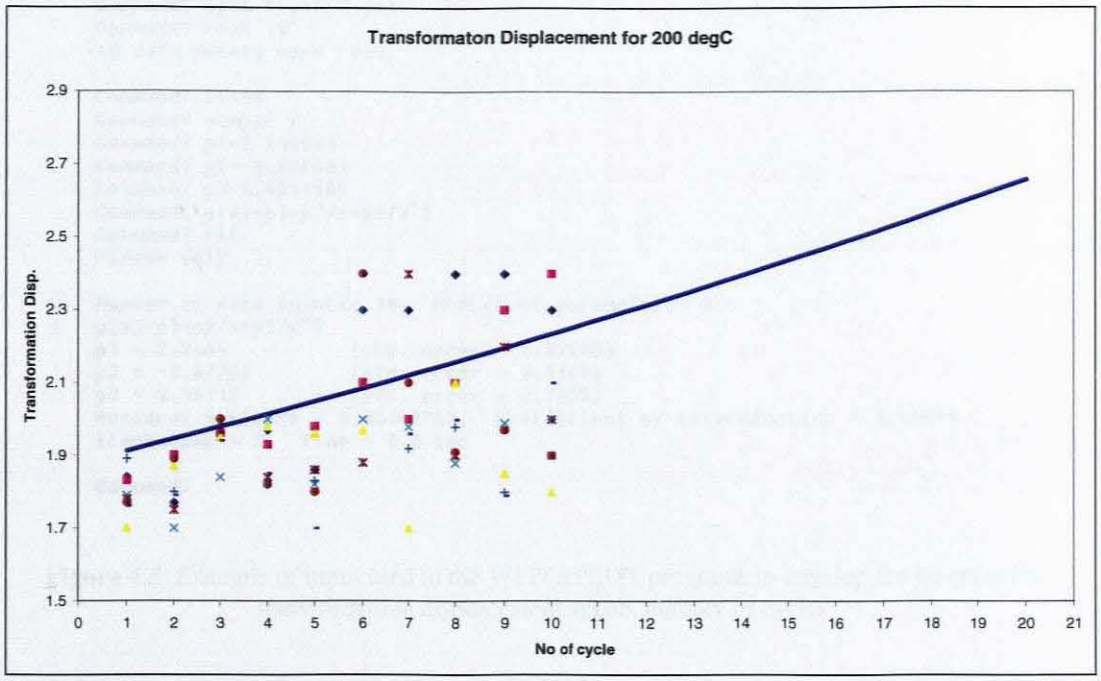

Figure 4.4: Behavior of transformation displacement as the number of cycles increases for a 200°C aging temperature.

Function (5) below shows the transformation displacement of 250^{0}C aged NiTi shape memory alloy material specimens as a function of 10 thermo-mechanical cycles. The experimental results were used as input for the WFIT&PLOT program and a 0.96 coefficient of determination was achieved after a number of iterations.

$$\delta_{t-250}(N) = 2.2465 - \frac{0.87766}{N} - \frac{0.48112}{N^2} \quad \text{.....(5)}$$

Fig 4.5 shows typical input and output for the WFIT&PLOT program. Fig 4.6 shows the prediction curve of function (5) for 20 thermo-mechanical cycles embedded in the experimental data. This prediction curve however shows that the "stability effect" would also be achieved after repeated thermo-mechanical cycles. A stability value for the transformation displacement of 250^{0}C aged specimens would be achieved at approximately 2.2mm.

```
I:\DATFIL~1\WFIT.EXE

Type HELP for command information.

Command? open tran250.dat
Command? read 10
10 data points were read.

Command? close
Command? numpar 3
Command? p1=2.246501
Command? p2=-0.877661
Command? p3=0.4811189
Command? y(x)=p1+p2/x+p3/x^2
Command? fit
Please wait ...

Number of data points: 10,  Number of parameters: 3
y(x)=p1+p2/x+p3/x^2
p1 = 2.2465          (std. error = 0.02003)
p2 = -0.87766        (std. error = 0.1179)
p3 = 0.48112         (std. error = 0.1069)
Residual Variance = 0.00048762,  Coefficient of Determination = 0.96694
Iterations = 2,  Time = 0.0 sec

Command?
```

Figure 4.5: Example of input used in the WFIT&PLOT programs to develop the function for transformation displacement versus number of cycles

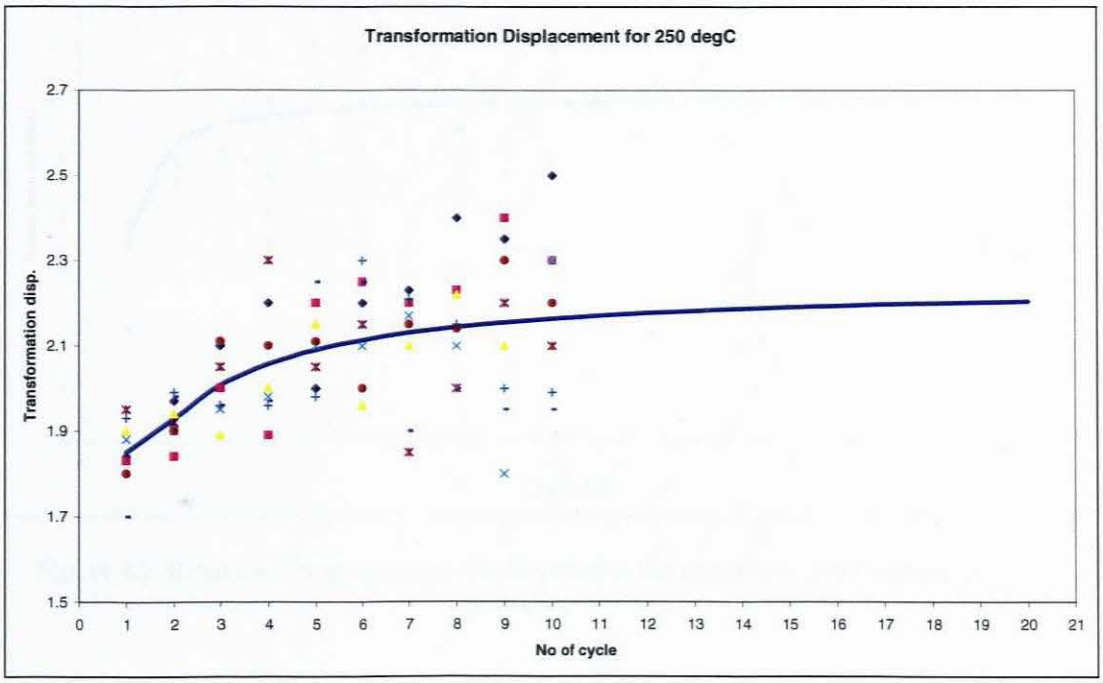

Figure 4.6: Behavior of transformation displacement as the number of cycles increases for a 250°C aging temperature.

Function (6) below shows the transformation displacement of 300^{0}C aged NiTi shape memory alloy material specimens as a function of 10 thermo-mechanical cycles. The experimental results were used as input for the WFIT&PLOT program and a 0.83 coefficient of determination was achieved after a number of iterations.

When plotted, function (6) has similar behavior to that of function (5). (See Fig 4.7) Fig 4.7 also shows that stability of the transformation displacement would be achieved. This stability would be obtained at approximately 2.1mm.

$$\delta_{t-300}(N) = 2.1133 - \frac{0.12513}{N} - \frac{0.12588}{N^2} \quad \text{.....(6)}$$

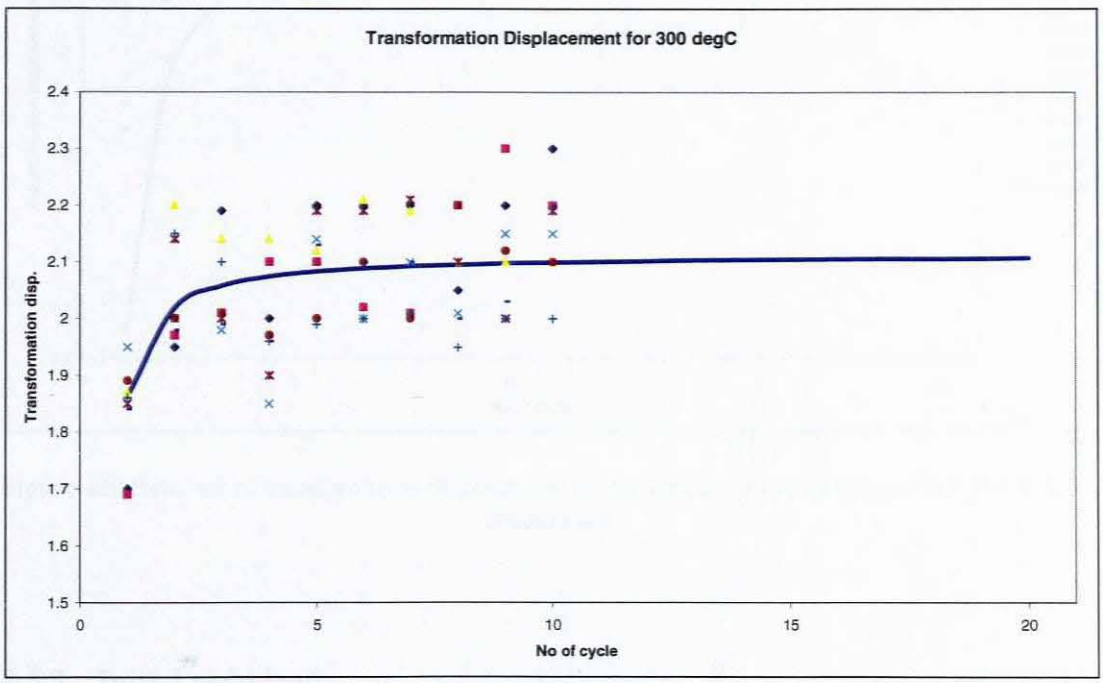

Figure 4.7: Behavior of transformation displacement as the number of cycles increase for 300°C aging temperature

Function (7) below shows the transformation displacement of 350^{0}C aged NiTi shape memory alloy material specimens as a function of 10 thermo-mechanical cycles. The experimental results were used as input for the WFIT&PLOT program and a 0.91 coefficient of determination was achieved after a number of iterations.

When plotted, function (7) shows similar behaviors to that of functions (5) and (6). (See Fig 4.8) Stability for 350^{0}C aged specimens would be achieved at approximately 2.3mm.

$$\delta_{t-350}(N) = 2.2825 - \frac{1.0544}{N} - \frac{0.62173}{N^2} \quad \text{.....(7)}$$

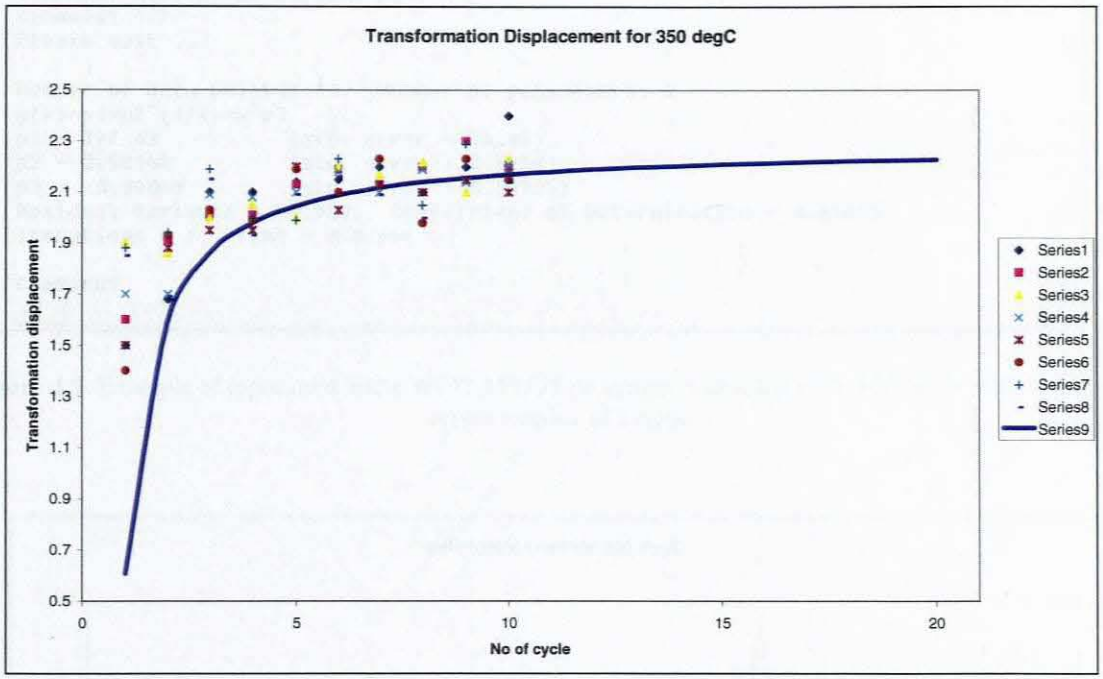

Figure 4.8: Behavior of transformation displacement as the number of cycles increase for 350°C aging temperature

4.3.3 Initial yield load

Function (8) below shows the initial yield load of 200^{0}C aged NiTi shape memory alloy material specimens as a function of 10 thermo-mechanical cycles. The experimental results were used as input for the WFIT&PLOT program and a 0.84 coefficient of determination was achieved after 7 iterations. (See Fig 4.9) The prediction curve of function (8) (see Fig 4.10) shows that repeated thermo-mechanical cycling would reduce the initial yield load to approximately 200N (or even less).

$$f_{y1-200}(N) = 297.43 * 0.98148^{\frac{1}{N}} * N^{-0.08048} \quad \text{.....(8)}$$

```
Command? open init200.dat
Command? read 12
10 data points were read.

Command? close
Command? numpar 3
Command? p1=298.05
Command? p2=0.9961865
Command? p3=-0.59093
Command? y(x)=p1*p2^(1/x)*x^p3
Command? fit
Please wait ...

Number of data points: 10,  Number of parameters: 3
y(x)=p1*p2^(1/x)*x^p3
p1 = 297.43          (std. error = 24.85)
p2 = 0.98148         (std. error = 0.0939)
p3 = -0.08048        (std. error = 0.03725)
Residual Variance = 48.989,  Coefficient of Determination = 0.84637
Iterations = 7,  Time = 0.0 sec

Command?
```

Figure 4.9: Example of input used in the WFIT&PLOT programs to develop the function for initial yield load versus number of cycles

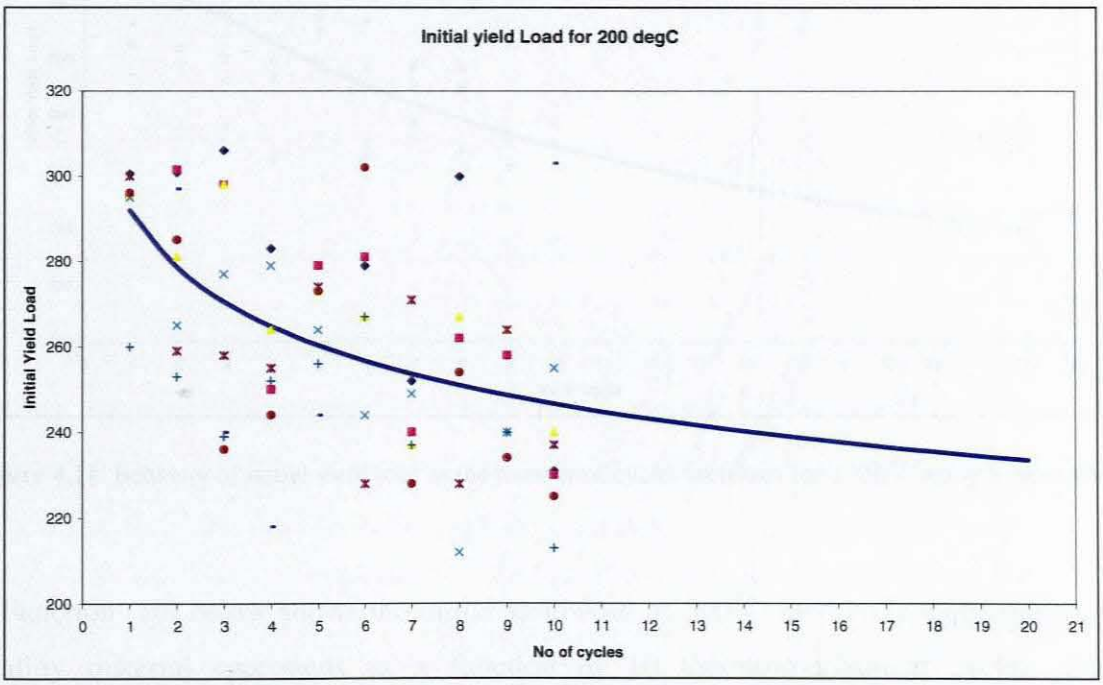

Figure 4.10: Behavior of initial yield load as the number of cycles increases for a 200°C aging temperature

Function (9) below shows the initial yield load of 250^{0}C aged NiTi shape memory alloy material specimens as a function of 10 thermo-mechanical cycles. The experimental results were used as input for the WFIT&PLOT program and a 0.94 coefficient of determination was achieved after several iterations. The prediction curve of function (9) (see Fig 4.11) shows similar behavior to that of the prediction curve of function (8), i.e. a decrease in the initial yield load as the number of thermo-mechanical cycles is increased. Stability of the initial yield load for 250^{0}C aged specimens would be achieved at approximately 250N (or even less).

$$f_{y1-250}(N) = 375.48 * 0.86584^{\frac{1}{N}} * N^{-0.13985} \quad \text{.....(9)}$$

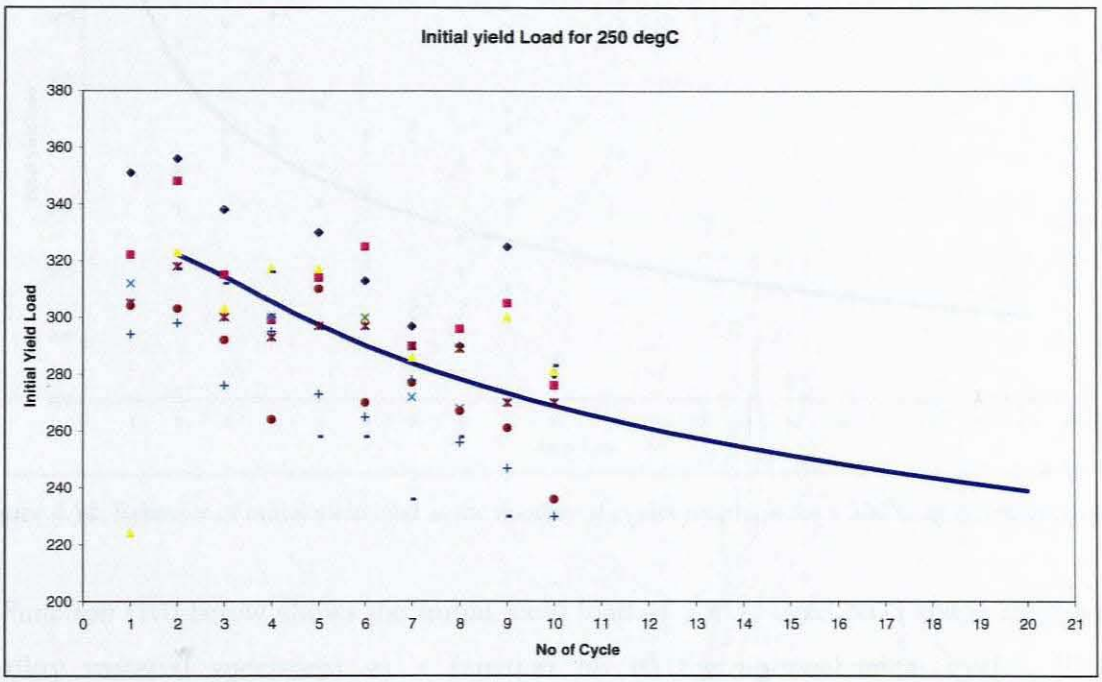

Figure 4.11: Behavior of initial yield load as the number of cycles increases for a 250°C aging temperature

Function (10) below shows the initial yield load of 300^{0}C aged NiTi shape memory alloy material specimens as a function of 10 thermo-mechanical cycles. The experimental results were used as input for the WFIT&PLOT program and a 0.92 coefficient of determination was achieved after several iterations. The form of this function is different to the functions obtained for 200 and 250°C aging temperatures.

This plotted prediction function (See Fig 4.12) does however show similar behaviors to the other graphs, i.e. Figs 4.10, and 4.11, showing a decrease in the initial yield load as the number of thermo-mechanical cycles is increased. Stability would be achieved at approximately 250N (or even less).

$$f_{y1-250}(N) = 327.71 * 1.0188^{\frac{1}{N}} * N^{-0.12395} \quad \text{.....(10)}$$

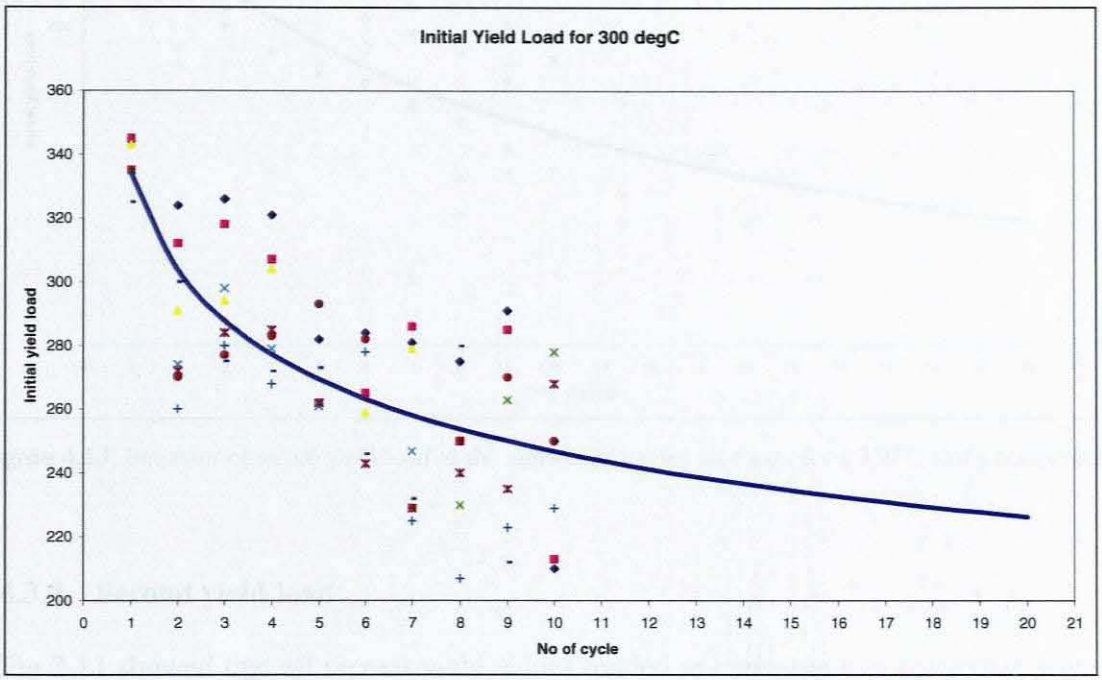

Figure 4.12: Behavior of initial yield load as the number of cycles increases for a 300°C aging temperature

Function (10) below shows the initial yield load of 350°C aged NiTi shape memory alloy material specimens as a function of 10 thermo-mechanical cycles. The experimental results were used as input for the WFIT&PLOT program and a 0.94 coefficient of determination was achieved after several iterations. The form of this function is different to the functions obtained for functions (8), (9), and (10). This plotted prediction function (See Fig 4.13) does however show similar behaviors to the other graphs, i.e. Figs 4.10, 4.11, and 4.12, showing a decrease in the initial yield load as the number of thermo-mechanical cycles is increased. Here stability would be achieved at approximately 250N.

$$f_{y1-350}(N) = 408.55 * 0.79853^{\frac{1}{N}} * N^{-0.17557} \quad \text{.....(11)}$$

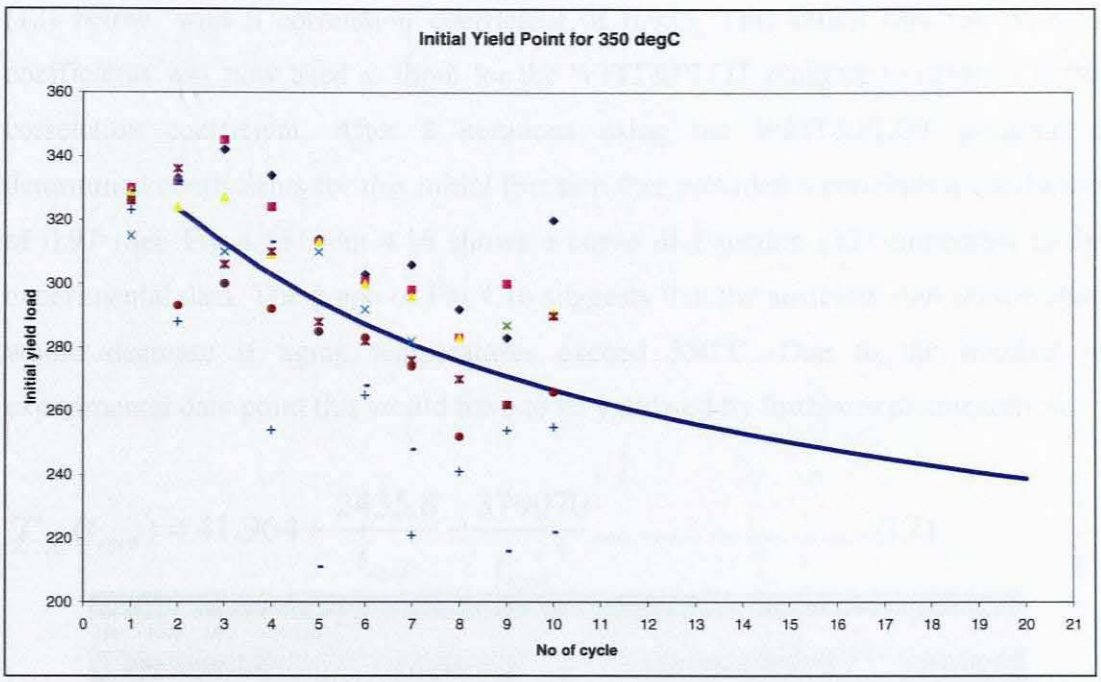

Figure 4.13: Behavior of initial yield load as the number of cycles increases for a 350°C aging temperature

4.3.4. Second yield load

Fig 2.11 showed that all second yield values tended to converge to a particular point. This shows that the "stability effect" for the second yield load would also be achieved at a value of approximately 340N (See Fig 2.11).

4.3.5 Transformation temperatures

Chapter 3 discussed the effect that thermo-mechanical cycling and aging temperature have on the thermal working characteristics of NiTi shape memory alloy material specimens. One of the important findings of this section was that aging increases all the transformation temperatures. This section uses the experimental data obtained in Chapter 3 to develop mathematical functions that could predict further the effects of thermo-mechanical cycling and aging temperature on these thermal working characteristics.

Fig 4.14 shows the typical input data required for the Kurv++ curve fitting program. The input presented in Fig 4.14 is that of Austenite start temperature versus aging temperature. The results of the initial curve fitting present a function, i.e. function (12) below, with a correlation coefficient of 0.935. This initial function with its coefficients was now used as input for the WFIT&PLOT program to obtain a better correlation coefficient. After 2 iterations using the WFIT&PLOT program it determined coefficients for this initial function that provided a correlation coefficient of 0.97 (See Fig 4.15). Fig 4.16 shows a curve of Function (12) embedded in the experimental data. The graph of Fig 4.16 suggests that the austenite start temperature would decrease if aging temperatures exceed 350^0C. Due to the number of experimental data point this would have to be validated by further experimentation.

$$T_{As}(t_{eged}) = 41.964 + \frac{2435.8}{t_{eged}} - \frac{379070}{t_{eged}^{2}} \quad \text{.....(12)}$$

Curve Fitting

File Edit Help Calculator

Data Display/Editor
i:\datfil~1\as.dat

X	Y
200	44.65
250	45.72
300	45.76
350	45.88

Fit to 25 Equations =>
Tabular Comparison
Graphical Comparison
Forecast
Fit to 3 Polynomials

Equations	a	b	c	Correlation Coefficient
Y=a+b*X	43.451	.00746	.	0.5616482
Y=b*X	.	.1591937	.	0.
Y=1/(a+b*X)	.0229807	-.000003	.	0.557795
Y=a+b*X+c/X	58.08827	-.019515	-1900.94	0.8911205
Y=a+b/X	47.63947	-562.715	.	0.7500355
Y=X/(a*X+b)	.0209359	.2748027	.	0.747072
Y=a+b/X+c/X^2	41.96433	2435.793	-379069.	0.9348092
Y=a+b*X+c*X^2	36.5635	.05971	-.000095	0.8119649
Y=a*X+b*X^2	.3327332	-.000584	.	0.8038452
Y=a*X^b	35.14671	.046141	.	0.6589915
Y=a*b^X	43.48376	1.000164	.	0.5597151
Y=a*b^(1/X)	47.69995	.000004	.	0.74855
Y=a*X^(b*X)	43.78600	.0000248	.	0.5441597
Y=a*X^(b/X)	48.18059	-2.71556	.	0.7299882
Y=a*e^(b*X)	43.48376	.0001648	.	0.5597151
Y=a*e^(b/X)	47.69995	-12.4348	.	0.74855
Y=a+b*lnX	33.81749	2.088333	.	0.6607212
Y=1/(a+b*lnX)	.0276841	-.001019	.	0.6572721
Y=a*b^X*X^c	10.24468	.9989883	.3162105	0.8672762
Y=a*b^(1/X)*X^c	.	.	.	0.
Y=a*e^((X-b)^2/c)	45.94812	314.1212	-474775.	0.811841
Y=a*e^((lnX-b)^2/c)	45.90991	5.741890	-7.25086	0.8883054
Y=a*X^b*(1-X)^c	.	.	.	0.
Y=a*(x/b)^c*e^(x/b)	.	.	.	0.
Y=1/(a*(X+b)^2+c)	.	.	.	0.

Figure 4.14: Example of input used in the Kurv++ curve fitting program to select the initial function of Austenite start temperature versus Transformation Temperature. It shows the initial function with its correlation coefficient.

```
I:\DATFIL~1\WFIT.EXE

Type HELP for command information.

Command? open as.dat
Command? read 4
4 data points were read.

Command? close
Command? numpar 3
Command? p1=41.96433
Command? p2=2435.793
Command? p3=-379869
Command? y(x)=p1+p2/x+p3/x^2
Command? fit
Please wait ...

Number of data points: 4,  Number of parameters: 3
y(x)=p1+p2/x+p3/x^2
p1 = 41.964          (std. error = 2.226)
p2 = 2435.8          (std. error = 1165)
p3 = -3.7907E+05     (std. error = 1.468E+05)
Residual Variance = 0.021359,  Coefficient of Determination = 0.97827
Iterations = 2,  Time = 0.0 sec

Command? _
```

Figure 4.15: Example of input used in the WFIT&PLOT program to further improve the correlation coefficient of the function for Austenite start temperature versus aging temperature.

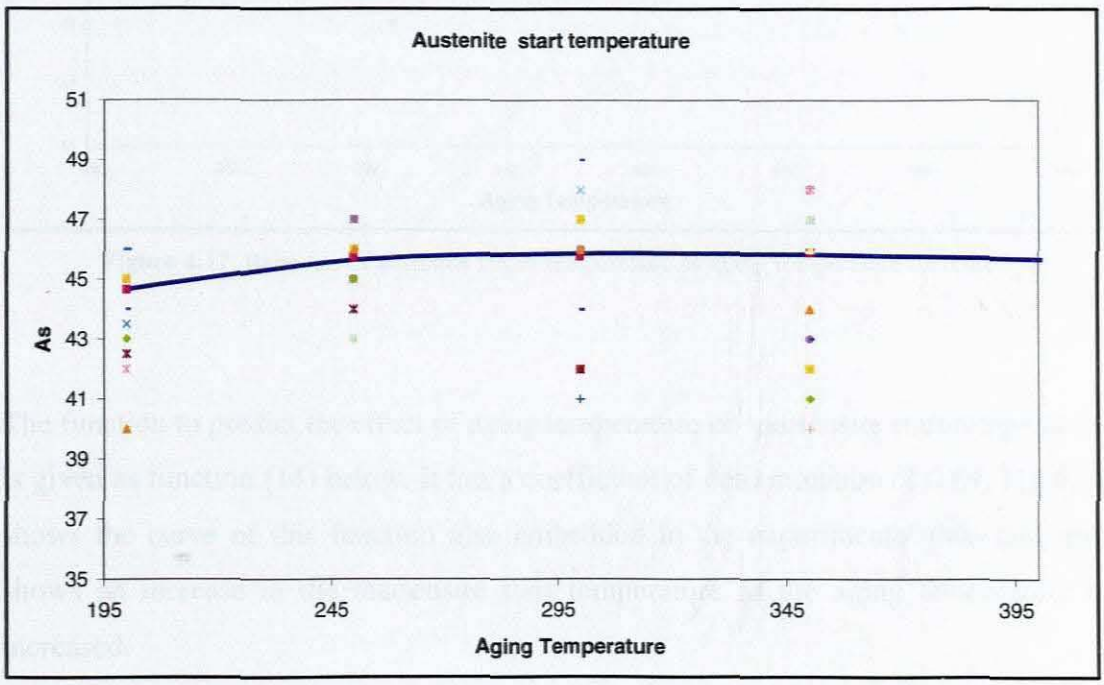

Figure 4.16: Behavior of austenite start temperature as aging temperature increased.

Function (13) was obtained in a similar fashion to that of function (12). This function represents the Austenite finish temperature versus aging temperature. This function has a coefficient of correlation 0.99. Fig 4.17 shows its curve embedded in the

experimental data. This curve shows that an increase in the aging temperature will increase the Austenite finish temperature.

$$T_{Af}(t_{eged}) = \frac{t_{eged}}{0.017955 * t_{eged} + 0.23516} \quad \text{.....(13)}$$

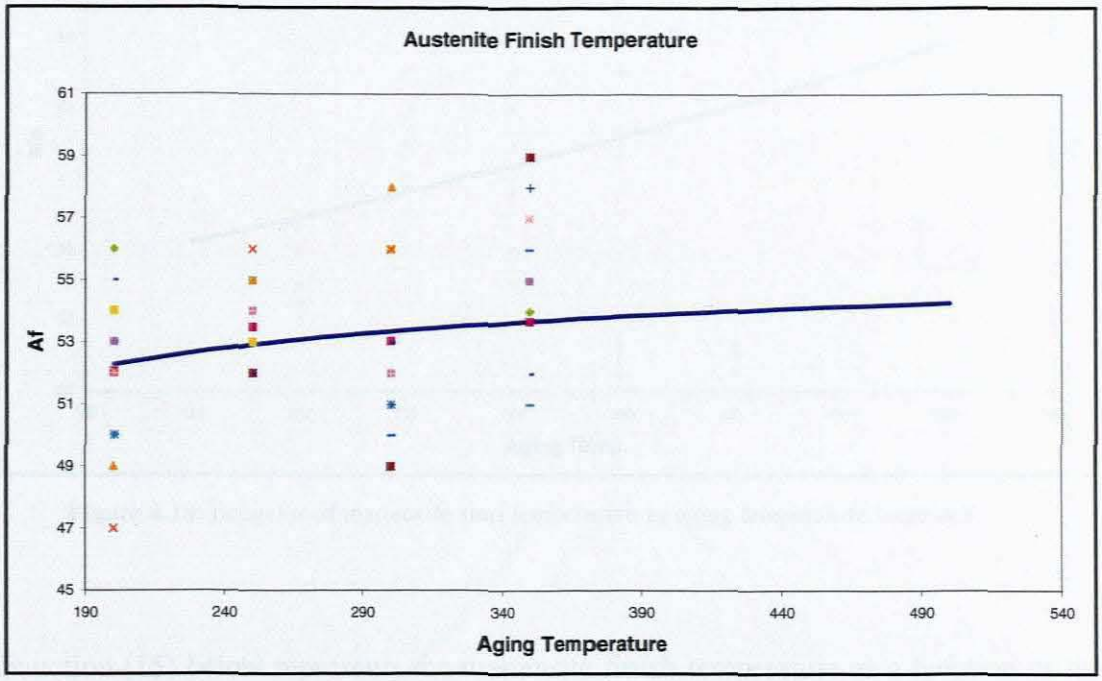

Figure 4.17: Behavior of austenite finish temperature as aging temperature increases

The function to predict the effect of aging temperature on martensite start temperature is given as function (14) below. It has a coefficient of determination of 0.84. Fig 4.18 shows the curve of this function also embedded in the experimental data and also shows an increase in the martensite start temperature as the aging temperature is increased.

$$T_{Ms}(t_{eged}) = 37.581 \times t_{eged}^{0.00005166 1 * t_{eged}} \quad \text{.....(14)}$$

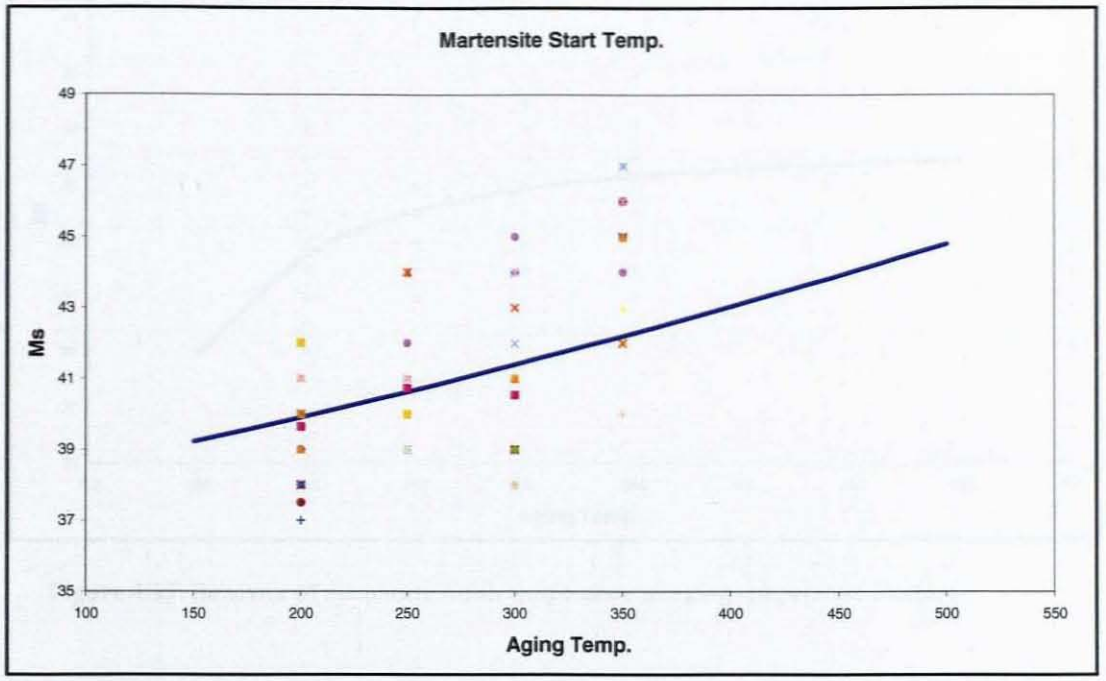

Figure 4.18: Behavior of martensite start temperature as aging temperature increases

Function (15) below represents the martensite finish temperature as a function of the aging temperature. It has a correlation coefficient of 0.99. Fig 4.19 shows this function curve embedded with the experimental data and also shows an increase in the martensite finish temperature as the aging temperature is increased.

$$T_{Mf}(t_{eged}) = 36.01193 + \frac{397.5651}{t_{eged}} - \frac{218450}{t_{eged}^{2}} \quad \text{.....(15)}$$

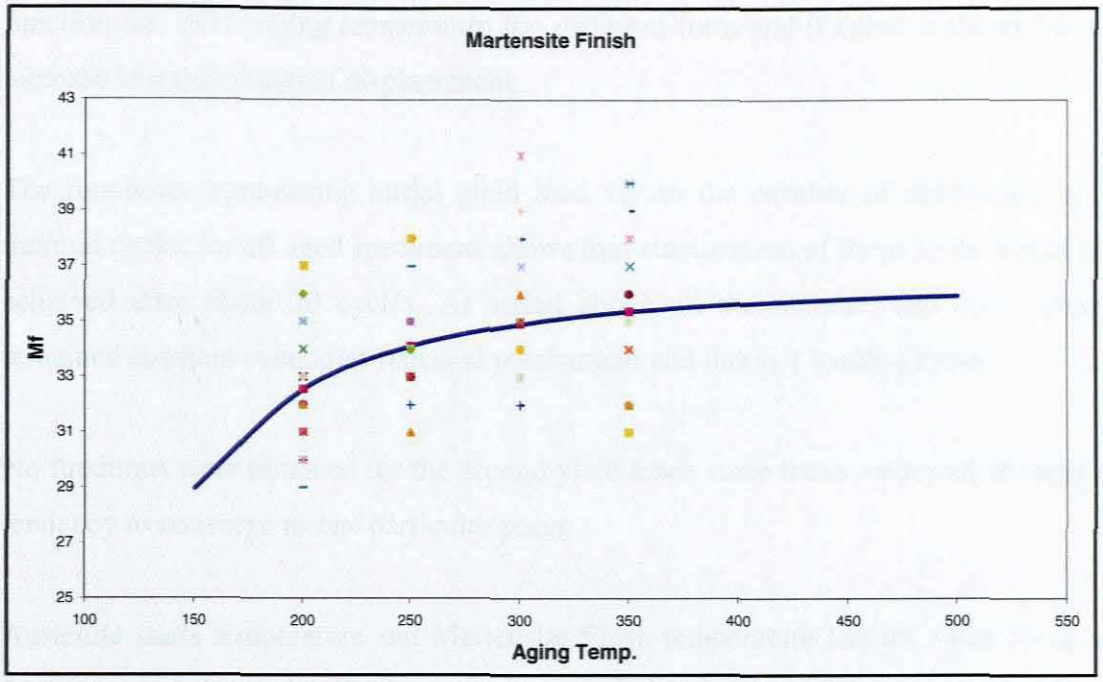

Figure 4.19: Behavior of martensite finish temperature as aging temperature increases

4.3.4 Summary of findings

The results obtained from the mechanical and thermal loading experiments were tabulated and mathematical functions were obtained to further predict the quasi-plastic behaviour of the NiTi shape memory alloy rods subjected to mechanical and thermal loading.

The functions representing initial elastic displacement versus the number of mechanical and thermal cycles for specimens aged at 250^0C, 300^0C, and 350^0C shows similar trends and a stabilisation of 0.5mm, 0.53mm and 0.45mm respectively of the initial elastic displacement after about 20 cycles was achieved. t, accept the function for 200°C whereby there is no function.

The functions representing transformation displacement versus the number of mechanical and thermal cycles for specimens aged at 250^0C, 300^0C, and 350^0C shows similar trends and a stabilisation of 2.2mm, 2.1mm and 2.2mm respectively of the transformation displacement after about 20 cycles was achieved. Whereas the

function for 200°C aging temperature has different form and it curve it shows linear increase in transformation displacement.

The functions representing initial yield load versus the number of mechanical and thermal cycles for all aged specimens shows that stabilisation of these loads would be achieved after about 20 cycles. As stated above all the second yield load values remained constant even after repeated mechanical and thermal loading cycles

No functions were obtained for the second yield loads since these values all showed a tendency to converge to one particular point.

Austenite starts temperature and Martensite finish temperature has the same form of functions and Austenite finish temperature and Martensite start temperature has a different form of functions. A_s, A_f and M_f has curve shows stability increase and M_s curve shows linear increase as the aging temperature increased.

Chapter 5

Conclusion and Recommendations

5.1 Conclusions

The design of actuators harnessing the shape memory effect exhibited by NiTi shape memory alloys requires a complete understanding of the load induced martensitic phase transformation. This material behaviour, also known as quasi-plasticity, provides the actuation stroke for these kinds of actuator systems. This thesis presented an experimental investigation into the effects that thermo-mechanical cycling and aging temperature have on the mechanical and thermal properties of the quasi-plastic material response.

Four batches of 3mm diameter and 340mm long NiTi shape memory alloys were subjected to aging temperatures ranging from 200 to 350^{0}C. Each batch was soaked for a period of ten hours. Upon cooling to room temperature, these aged specimens were subjected to 10 mechanical and thermal loading cycles. Mechanical loading was performed uniaxially with a tensile testing machine and specimens where placed in a furnace after being removed from the tensile testing machine. Thermal loading was achieved by heating the specimens in a furnace to bring about the material's original configuration and then cooled to room temperature.

Load-Displacement graphs were plotted using the data obtained from tensile testing and the results showed some interesting material behaviours. Firstly, all graphs showed the three distinct regions as discussed by Philander [4]. Secondly, a very interesting phenomenon occurred during the first and second cycles after aging. These load-displacement graphs showed that the hardening like behaviour as discussed by Philander has been erased.

This means that all the specimens transformed from twinned⇒de-twinned martensite at a constant load. Philander's [4] experimental investigations showed that this kind of behaviour only occurred in 1mm diameter NiTi shape memory alloys. This would then suggest that aging had an effect on the orientation of the twinned martensitic phase structure. If these de-twinned rods were embedded into a polymeric composite surface, and the surface was activated through some kind of externally applied heating source, the surface would be deformed. Upon cooling the rods would require a constant load provided by polymeric composite material's stiffness to recover the original shape of the surface. The load-displacement graphs did however show that there were still variations in the total transformation strain, i.e. different actuation strokes were achieved.

The third to tenth cycle for each aged temperature showed the appearance of the hardening like behaviour observed by Philander [4]. Initial mechanical loading cycles after aging at higher temperatures showed that the material's initial yield load are

increased. Repeated thermal and mechanical cycles however, lowers the values of the initial yield loads while the values of the second yield loads remained constant. Coupled to this it was observed that the initial elastic displacement decreased while the transformation displacement increased. This means an increase in the actuator stroke. The experimental investigation into the effects that thermo-mechanical cycling and aging temperature have on the quasi-plastic material response, i.e. actuation stroke of NiTi shape memory alloys, show that some of the variability of the material behaviour has been removed.

The results obtained from the mechanical and thermal loading experiments were tabulated and mathematical functions were obtained to further predict the quasi-plastic behaviour of the NiTi shape memory alloy rods subjected to mechanical and thermal loading. The functions representing initial elastic displacement versus the number of mechanical and thermal cycles for specimens aged at 250^0C, 300^0C, and 350^0C shows similar trends and a stabilisation of 0.5mm, 0.53mm and 0.45mm respectively of the initial elastic displacement after about 20 cycles was achieved.

The functions representing transformation displacement versus the number of mechanical and thermal cycles for specimens aged at 250^0C, 300^0C, and 350^0C shows similar trends and a stabilisation of 2.2mm, 2.1mm and 2.2mm respectively of the transformation displacement after about 20 cycles was achieved. The functions representing initial yield load versus the number of mechanical and thermal cycles for all aged specimens shows that stabilisation of these loads would be achieved after about 20 cycles. As stated above all the second yield load values remained constant even after repeated mechanical and thermal loading cycles.

The thermal analyses conducted on the aged and thermo-mechanical cycled NiTi shape memory alloys using a dilatometer also showed some interesting findings. Firstly an un-aged specimen was sectioned and subjected to the thermal procedure, i.e. controlled heating and cooling. The results showed that certain specimens taken from the same

length of material had variations in the austenitic start temperature of up to 16^0C. For the austenite finish temperature this variation was about 9^0C. The martensite start and finish temperatures had a variation of about 11^0C. This shows that an actuator manufactured of this material, i.e. un-treated, would have a poor performance since no clear operating temperatures would be prescribed.

Specimens sectioned from a length of NiTi shape memory alloy subjected to thermo-mechanical loading and an aging temperature of 200^0C showed a decrease in the variation of the austenite start and finish temperatures of about 9^0C. Specimens sectioned from a length of NiTi shape memory alloy subjected to thermo-mechanical loading and an aging temperature of 250^0C showed a decrease in the variation of the austenite start and finish temperatures of about 4^0C and 7^0C.

Specimens sectioned from a length of NiTi shape memory alloy subjected to thermo-mechanical loading and an aging temperature of 300^0C showed a decrease in the variation of the austenite start and finish temperatures of about 8^0C and 13^0C. Specimens sectioned from a length of NiTi shape memory alloy subjected to thermo-mechanical loading and an aging temperature of 350^0C showed a decrease in the variation of the austenite start and finish temperatures of about 11^0C and 12^0C.

These results suggest that thermo-mechanical cycling coupled with an aging temperature of 250^0C would produce an actuator start and completion temperature with a narrower temperature range than that of untreated specimens. Furthermore, the overall results of the thermal analyses show that an increase in the aging temperatures will bring about slight increases in all the transformation temperatures. The results of the thermal analyses also show that an increase in the aging temperature decreases the volumetric expansions that occur in the material during heating. This decrease in the volumetric expansion could be the result of the increases in the initial yield load as described above.

On average the experimental investigation into the effects that thermo-mechanical cycling and aging temperature have on the quasi-plastic material response exhibited by shape memory alloys, and its effects on transformation temperature shows that these kinds of procedures have positive effects on NiTi shape memory alloy behavior. Furthermore, it suggests that these materials should never be used in critical components without a prior history of thermal and mechanical loading. For actuator design in terms of actuation stroke, actuation force, actuation starting and completion temperature, and actuator repeatability these considerations are critical.

5.2 Recommendations

The findings of this research in terms of actuator design are encouraging. Based on the conclusions stated above, four critical recommendations are made.

5.2.1 It is recommended that further thermo-mechanical experimental investigations be conducted with aging temperatures below 200°C, i.e. 50, 100, 150°C. Furthermore soaking times should be increased to at least 15 to 20 hours. This is due to the results showing that there are some disadvantages brought about by aging. These include increases in the initial yield load, and increases in the transformation temperatures. These results of a study conducted at lower aging temperatures should show a decrease in the initial yield load values.

5.2.2 Cycling should be extended to at least 20 or more cycles to obtain stabilization of NiTi shape memory alloy mechanical properties, i.e. initial yield, initial elastic displacement, transformation displacement, etc., as stated in the conclusions. The study only investigated the effects that 10 thermal and mechanical loading cycles have on the quasi-plastic material response. The mathematical functions showed stabilization of mechanical properties at about 20 cycles.

5.2.3 It is also recommended that a metallurgical investigation be performed on specimens to determine what effect if any aging temperature has on the twinned martensitic phase structure. This study has observed that the aging erased the hardening-like behavior observed in the transformation region that was observed by Philander [4]. This would suggest that aging had a re-orientation effect on the twinned martensitic structure that is formed during cooling to room temperature. Furthermore, results obtained from the thermal analyses show that increases in the aging temperature decreases the volumetric expansion of shape memory alloy material specimens.

5.2.4 A further study into the effects that intermediate and high temperature mechanical cycling have on this material response should also be conducted as this study only focused on the effects that low temperature mechanical cycling has on the quasi-plastic material response exhibited by shape memory alloys.

5.2.5 The experimental investigation into the effects that thermo-mechanical cycling and aging temperature have on the thermal working characteristics (presented in Chapter 3) of NiTi shape memory alloys showed that specimens taken from the same wire reel has variance ranges for the transformation temperatures that may present difficulties when the materials are used in smart applications. Examples of these are: 16^0C for the austenite start temperature of specimens cycled and aged at 350^0C; 13^0C for the austenite finish temperature of specimens cycled and aged at 300^0C; and 15^0C for the martensite finish temperature of specimens cycled and aged at 200^0C. One reason for these differences could be ascribed to the sensitive nature of the measuring equipment. Slight changes in the environmental temperature could corrupt the results. It is recommended that a further investigation into these discrepancies be conducted.

Reference list

1. Prahlad, H. & Chopra, I. 2003. Development of a Strain-rate Dependent Model for Uniaxial Loading of SMA Wires. *Journal of Intelligent Material systems and Structure*, 14: (429-441).

2. Mihialcz, I. 2001. Fundamental Characteristics and Design Method for Nickel-Titanium Shape Memory Alloys. *Hungary: Periodica polytechnica ser. mech. Eng*, 45 (1): (75–86).

3. Tobushi, H; Yamada, S; Hachisuka, T; Ikai, A. and Tanaka, K. 1996. Thermo-mechanical Properties due to Martenistic and R-phase transformations of TiNi Shape Memory Alloy Subjected to Cyclic loadings", *Smart Materials and Structures*, 5(6): 788-795.

4. Philander, O. 2004. Experimental and Microscopic Observation of Shape Memory Alloys. (*Article under review for publication in the journal of smarts materials and structure*).

5. Shaw, J.A. 2000. Simulations of Localized Thermo-mechanical Behaviour in a NiTi Shape Memory Alloy. *International Journal of plasticity*, 16: (541-562).

6. Mayer, A.G; Scherngell, H. & Kneissl, A.L. Investigation of Degradation Effect in Shape Memory Alloys, *Internal publication of the Institute of Physical Metallurgy and Materials Testing at the University of Leoben.*

7. Liu, Y. & Galvin, S.P. 1997. Criteria for pseudo elasticity in near-equiatomic NiTi shape Memory Alloys. *Acta Material*, 45 (11):(4431-4439).

8. SMA/MEMS Research. 2001 *Shape Memory Alloys*. (Online) http://www.cs.ualberta.ca/~database /MEMS/sma_mems/sma.html (20/02/05).

9. Taxes A and M smarts Lab. *Detailed Introduction to Shape Memory Alloys*. **(Online)** http://smart.tamu.edu/overview/smaintro/detailed/detailed.html (25/02/05).

10. Auricchio, F. & Sacco, E. 2001: Thermo-mechanical modelling of a superelastic shape-memory wire under cyclic stretching-bending loadings, *International Journal of Solids and Structures*, Vol 38: (6123-6145).

11. Tanaka, K; Kobayashi, S. & Sato, Y. 1986:_Thermomechanics of transformation pseudoelasticity and shape memory effect in alloys, *International Journal of Plasticity*, Vol. 2: (59-72).

12. Shaw, J.A & Kyriakides, S. 1995: Thermomechanical aspects of NiTi, J. *Mech. Phys. Solids*, Vol. 43 (8): (1243-1281).

13. Huo, Y. & Müller, I. 1993: Nonequilibrium thermodynamics of pseudoelasticity, *Continuum Mechanics and Thermodynamics*, Vol 5: (163-204).

14 Khelfaoui, F; Thollet, G. & Guenin, G. 2002: Microstructural kinetics after plastic deformation of equiatomic Ti-Ni alloy during isothermal annealings, *Materials Science and Engineering*, A00 : (1-8).

15. Shaw, J.A. & Kyriakides, S. 1997. On the Nucleation and Propagation of Phase Transformation Fronts in a NiTi Alloys. *Acta Material*, 45(2): (683-700).

16 Shaw, J.A & Kyriakides, S. 1998: Initiation and propogation of localized deformation in elasto-plastic strips under uniaxial tension, International Journal of Plasticity, Vol. 13, No. 10, pp. 837-871.

17 Qidwai, M.A. & Lagoudas, D.C. 2000. On thermomechanics and transformation surfaces of polycrystalline NiTi shape memory alloy material, *International Journal of Plasticity*, 16: (1309-1343).

18. Tanaka, K; Kobayashi, S. & Sato, Y. 1986: Thermomechanics of transformation pseudoelasticity and shape memory effect in alloys, *International Journal of Plasticity*, Vol. 2: (59-72).

19. Gall, K; Sehitoglu, H; Anderson, R; Karaman, I; Chumlyakov, Y.I. & Kireeva, I. V. 2001. On the Mechanical Behaviour of Single crystal NiTi Shape Memory Alloys and Related Polycrystalline Phenomenon. *Materials Science and Engineering*, A317: (85-92).

20. Van Hambeeck, J. 1999. Non-medical Application of Shape Memory Alloys. *Materials and Science and Engineering*, A273-275: (134-148).

21. Linseis. Co. *Thermal analysis without a limit.* Online: http://www.linseis.net/html_en/thermal/dilatometer/pdf/L75_PT1600_ENG.pdf (02/10/05).

Bibliography List

Abel, E; Luo, H; Pridham, M. & Slade, A. 2004. Issues Concerning the Measurement of Transformation Temperatures of NiTi alloys. *Smarts Material Structure*, 13: (1110-1117).

Allafi, J.K; Ren, X. & Eggeler, G. 2001. The Mechanism of Multistage Martensitic Transformations in Aged Ni-rich NiTi Shape Memory Alloys. *Acta Material*, 50: (793–803).

Auricchoio, F. & Sacco, E. 2001. Thermo-mechanical Modelling of a Super Elastic Shape Memory Wire Under Cyclic Stretching-bending Loadings. *International Journal of solid and structures*, 38: (6123-6145).

Barnes, C. 1999. *Copper Applications in Innovative Technology Shape Memory and Superelastic Alloys. Available online* http://www.copper.org/innovations/1999/07/shape.html (11/09/05)

Barrett, R. & Gross, R.S. Super-active Shape-Memory Alloy Composites.1996. Auburn University. *Auburn. Smart Material Structure*, 5: (255-260).

Bekker, A. & Brinson, L. C. 1998. Phase Diagram Based Description of the Hysteresis Behaviour of Shape Memory Alloys. *Acta Material*, 46(10): (3649-3665).

Ben-Zeev, O. & Chopra, I. 1995. Advances in the Development of an Intelligent Helicopter Rotor Employing Smart Trailing-edge Flaps. *Smart Material Structure*, 5: (11-25).

Brocca, M; Brinson, L.C. & Bazant, Z.P. 2002. Three-dimensional Constitutive Model for Shape Memory Alloys Based on Microplane Model. *Journal of the Mechanics and Physics of solid*, 50: (1051-1077).

Chen, W.W; Wu, Q; Kang, J.H. & Winfree, N.A. 2001. Compressive Superelastic Behaviour of a NiTi Shape Memory Alloy at the Strain Rates of 0.001^{-1} – 750 s^{-1}. *International Journal of solid and structures*, 38: (8989-8998).

DeRoches, R; McCormick, J. & Delemont, M. 2004. Cyclic Properties of Superlastic Shape Memory Alloy wires and Bars. *Journal of Structural Engineering*, 130(1): (38-46).

Faciu, C. & Mih_ailescu-Suliciu, M. 2002. On Modelling Phase Propagation in SMAs by a Maxwellian Thermo-viscoelastic Approach. *International Journal of solid and structures,* 39: (3811-3830).

Furuichi, Y; Tobushi, H; Ikawa,T. & Matsui R. 2003. Proceedings of the I MECH E Part L. *Journal of Materials:Design and Applications* , 217 (2): (93-99).

Gall, K; Juntunen, K; Maier, H; Sehitoglu, J.H. & Chumlyakov, Y.I. 2002. Instrumented Micro-indentation of NiTi Shape Memory Alloys. *Acta Material*, 4(11): (3205-3217).

Ghomshei, M.M; Khajepour, A; Tabandeh, N. & Behdinan K. 2002. Finite Element Modeling of Shape Memory Alloy Composite Actuators: Theory and Experiment. *Journal of Intelligent Material system s and Structure*, 12: (773-761).

Huang, W. 1999. Yield Surfaces of Shape Memory Alloys and their Applications. *Acta Material*, 47(9): (2769-2776).

Khelfaoui, F; Thollet, G. & Guenin, G. 2002. Microstructural Evolution Kinetics After Plastic Deformation of Equiatomic TiNi Alloy During Isothermal Annealings. *Material Science and Engineering*, A00: (1-8).

Kuhn, G. & Jordan, L. 2002. Fatigue and Mechanical Properties of Nickel-Titanium Endodontic Instruments. *J Endod*, 28: (716-20).

Li, D. Y. & Chen, L.Q. 1997. Selective Variant growth of TiNi precipitate in a TiNi Alloy under Applied Stress. *Acta Material*, 45: (471-479).

Lim T.J. & McDowell D.L. 2002. *Cyclic* Thermo-mechanical Behaviour of a Polycrystalline Pseudo Elastic Shape Memory Alloy. *Journal of the Mechanics and Physics of Solids*, 50: (651 – 676).

Liu,Y; Xie, Z. L; Van Humbeeck, J. & Delaey, L. 1999. Effect of Texture Orientation on the Martensite Deformation of NiTi Shape Memory Alloy Sheet. *Acta Material*, 47(2): (645-660).

McKelvey, A. L. & Ritchie, R. O. 1998. *Fatigue-crack growth in the super elastic endovascular stent material nitinol.* Available online http://www.lbl.gov/Ritchie/Programs/NITI/MRSf98/ (08/08/05).

Ohta, T. 2001. Theory of Rubber-like Elasticity in Shape Memory Alloys. *Material Science and Engineering*, A312: (57-65).

Tobushi, H; Nakahara, T. & Shimeno, Y. 2000. Low-Cycle Fatigue of TiNi Shape Memory Alloy and Formulation of Fatigue Life. *Journal of Engineering Materials and Technology*, 122(2): (186-191).

Yoneyama, T; Doi, H; Kobayashi, E. & Hamanaka, H. 2000. Super-elastic Property of Ti-Ni alloy for Use in Dentistry. *Front Med Biol Eng*, 10: (97-103).

Takami, M; Fukui, K; Saitou, S; Sugiyama, I. & Terayama, K. 1992. Application of a Shape Memory Alloy to hand splinting. *Prosthet orthot Int*, 16: (57-63).

Shaw, J.A. & Kyriakides, S. 1997. On the Nucleation and Propagation of Phase Transformation Fronts in a NiTi Alloys. *Acta Material*, 45(2): (683-700).

Tylikowski, A. & Hetnars, R.B. 2001. Semi Active Control of a Shape Memory Alloy Hybrid Composite Rotating Shaft. *International Journal of solid and structures*, 38: (9347-935).

Park, C; Walz, C. & Chopra, I. 1995. Bending and Torsion Models of Beams with Induced-strain Actuators. *Smart Material Structure*, 5: (98-113).

Ren, X. & Otsuka, K. 1997.Origin of Rubber-like Behavior in Metal Alloys. *Nature*, 389: (579-582).

Rahman, M.A; Qiu, J. & Tani, J. 2001. Buckling and Post Buckling Characteristic of the Superelastic SMA Columns. *International Journal of solid and structures*, 38: (9253-9265).

Sehitoglu, H; Karaman, I; Zhang, X; Kim, H; Chumlyakov, Y; Maier, H.J. & Kireeva, I. 2001. Deformation of NiTiCu Shape Memory Single Crystals in Compression. *Metallurgical and Materials Transactions A*, 32 (3): (477-489).

Sun, Q. & Li, Z. 2002. Phase Transformation in Superelastic NiTi Polycrystalline Micro-tubes under Tension and Torsion from Localization to Homogeneous Deformation. *International Journal of solid and structures*, 39: (3797-3809).

Tobushi, H; Nakahara, T. & Shimeno, Y. 2000. Low-Cycle Fatigue of TiNi Shape Memory Alloy and Formulation of Fatigue Life. *Takiron Co., Ltd Journal of Engineering Materials and Technology*, 122(2): (186-191).

Uchil, J; Kumara, K. G. & Mahesh K.K. 2002. Effect of Thermal Cycling on R-phase Stability in a NiTi Shape Memory Alloy. *Material Science and Engineering*, A332: (25-28).

Xie, Z; Liu, Y. & Van Humbeeck, J.1998. Microstructure of NiTi Shape Memory Alloys due to Tension-compression Cyclic Deformation. *Acta Mater*, 46: (1989-2000).

Yi, S; Gao, S. & Shen, L. 2001. Fracture Toughening Mechanism of Shape Memory Alloy under Mixed Mode Loading due to Martensite Transformation. *Elsevier Science Ltd. International Journal of solid and structures*, 38: (4463-4476).

Appendix A

Load-Extension Behavior of NiTi SMA rods subjected to Thermo-Mechanical Cycling and Aging

This appendix shows selected load-extension plots of NiTi SMA specimens subjected to uniaxial tensile loading. The specimens were aged at temperatures ranging from 200 to 350°C. Each group of aged specimens were then thermo-mechanically cycled for a period of 10 cycles.

200°C Aging Temperature

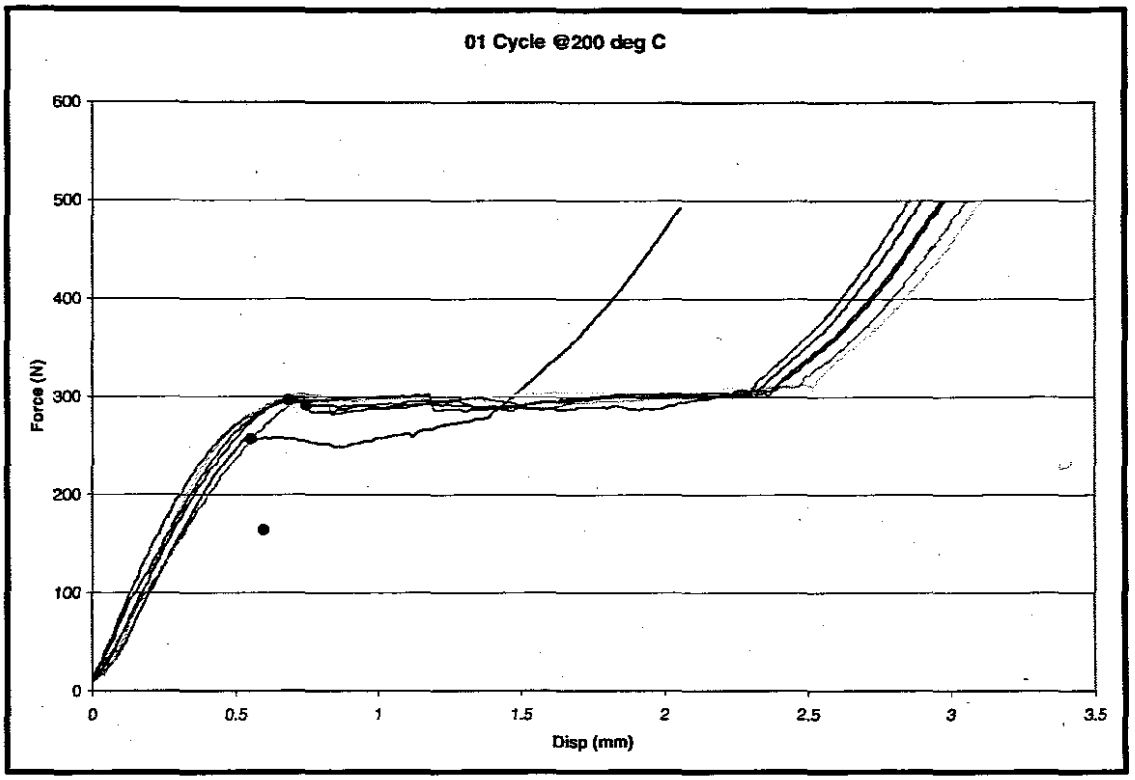

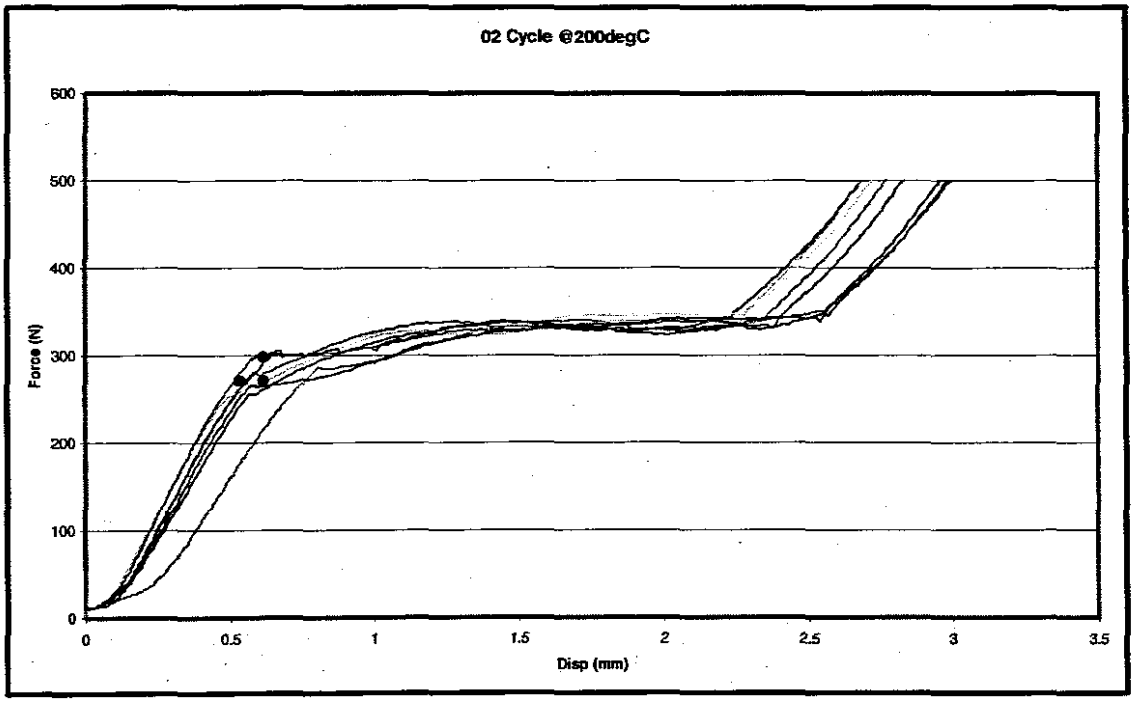

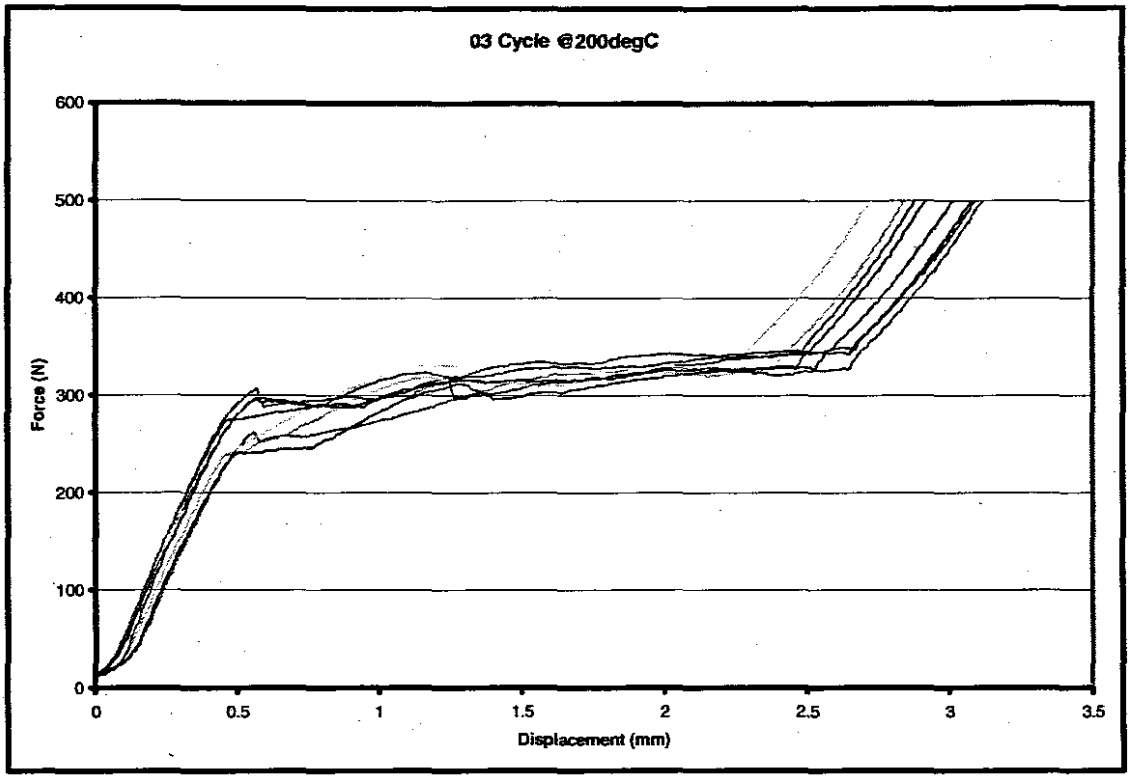
03 Cycle @200degC
Force (N)
600
500
400
300
200
100
0
0
0.5
1
1.5
2
2.5
3
3.5
Displacement (mm)

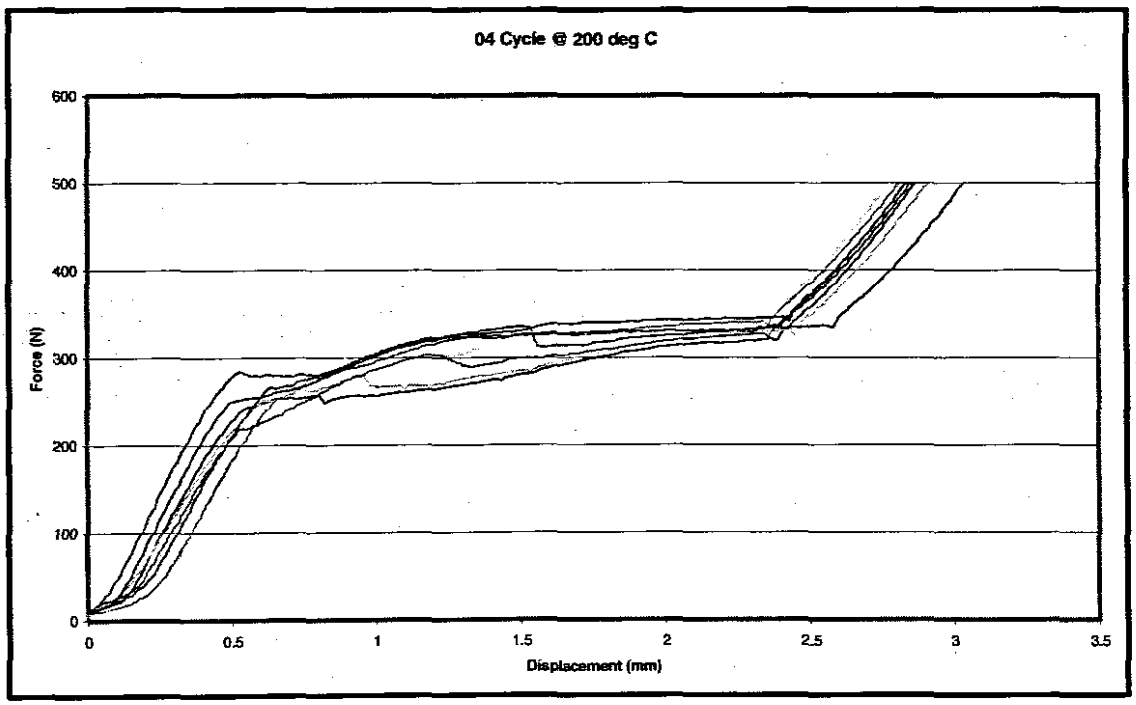
04 Cycle @ 200 deg C
Force (N)
600
500
400
300
200
100
0
0
0.5
1
1.5
2
2.5
3
3.5
Displacement (mm)

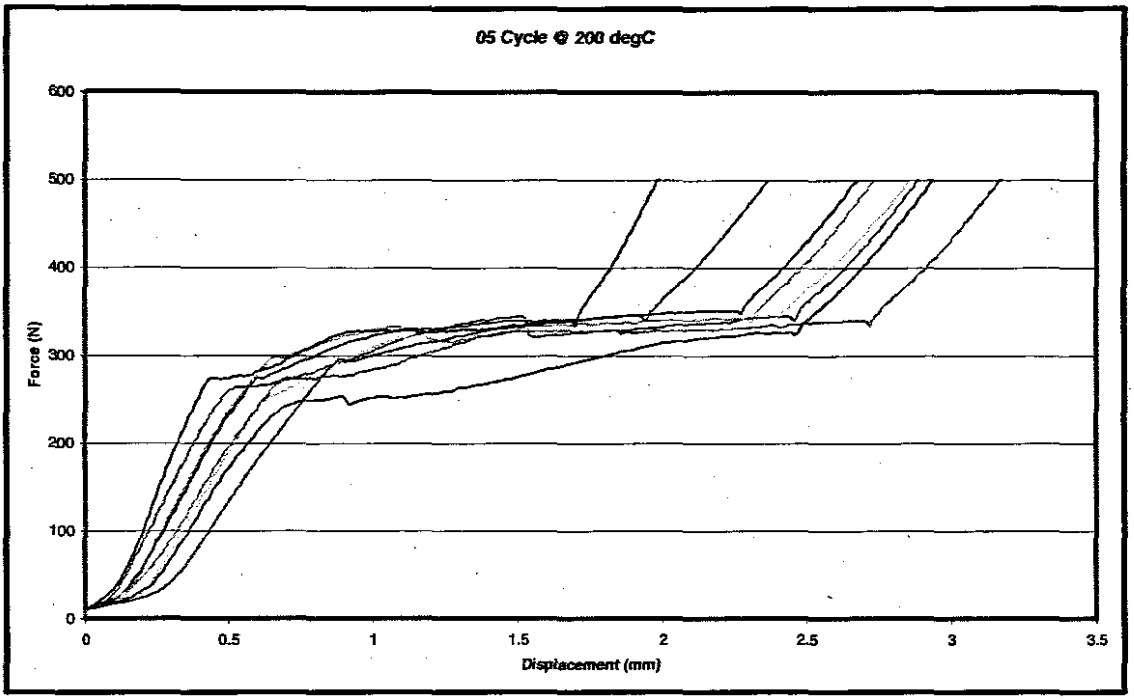
05 Cycle @ 200 degC
Force (N)
600
500
400
300
200
100
0
0
0.5
1
1.5
2
2.5
3
3.5
Displacement (mm)

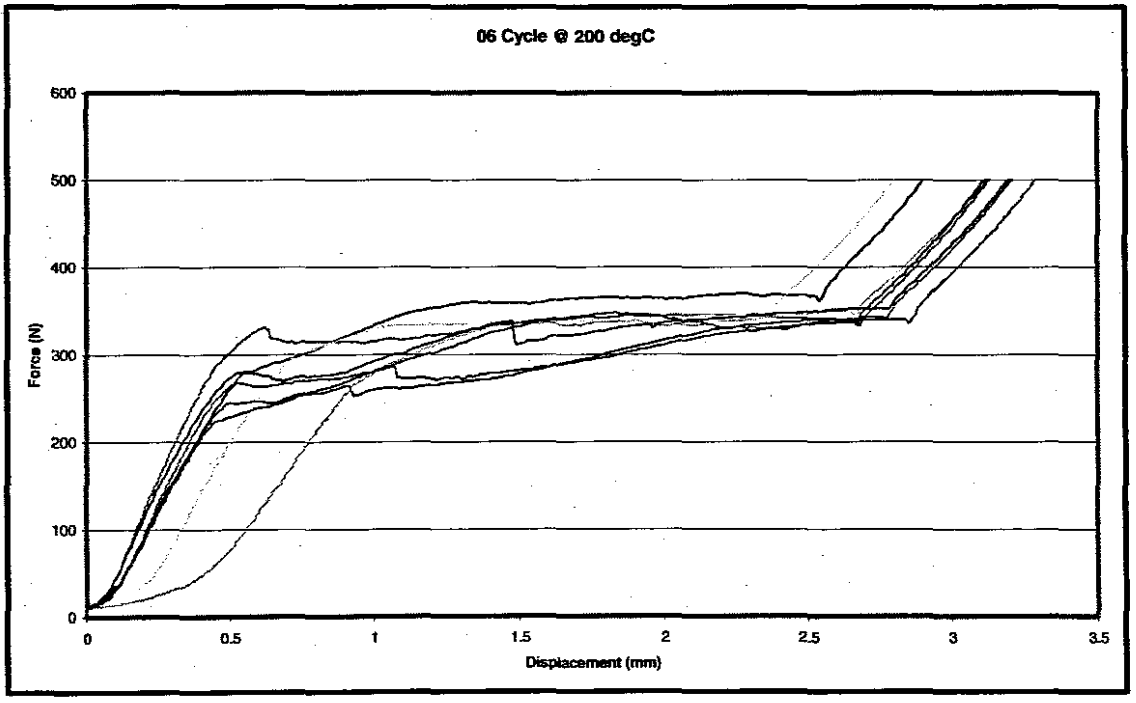
06 Cycle @ 200 degC
Force (N)
600
500
400
300
200
100
0
0
0.5
1
1.5
2
2.5
3
3.5
Displacement (mm)

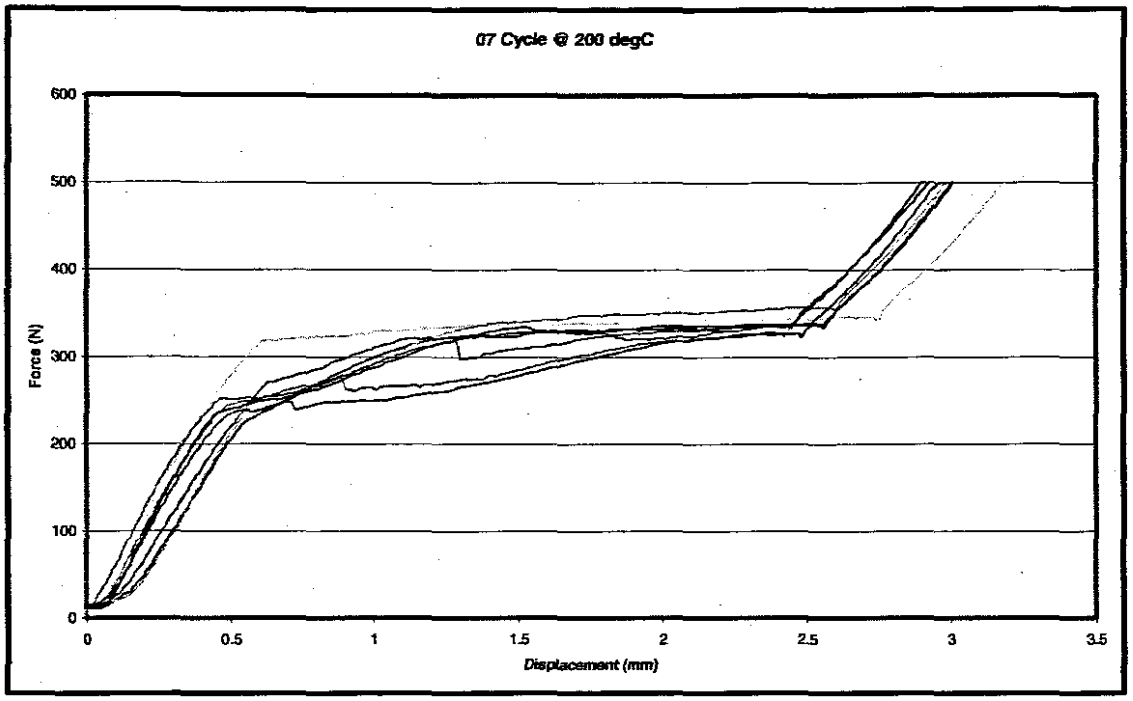
07 Cycle @ 200 degC
Force (N)
Displacement (mm)
0
100
200
300
400
500
600
0
0.5
1
1.5
2
2.5
3
3.5

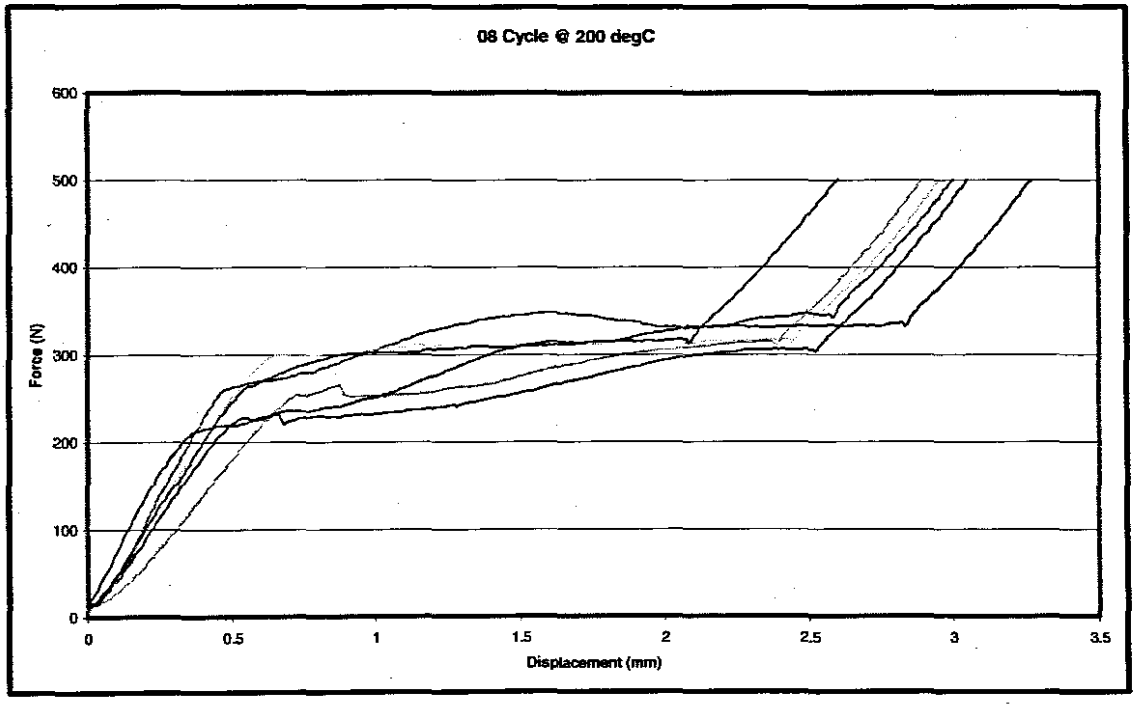
08 Cycle @ 200 degC
Force (N)
Displacement (mm)
0
100
200
300
400
500
600
0
0.5
1
1.5
2
2.5
3
3.5

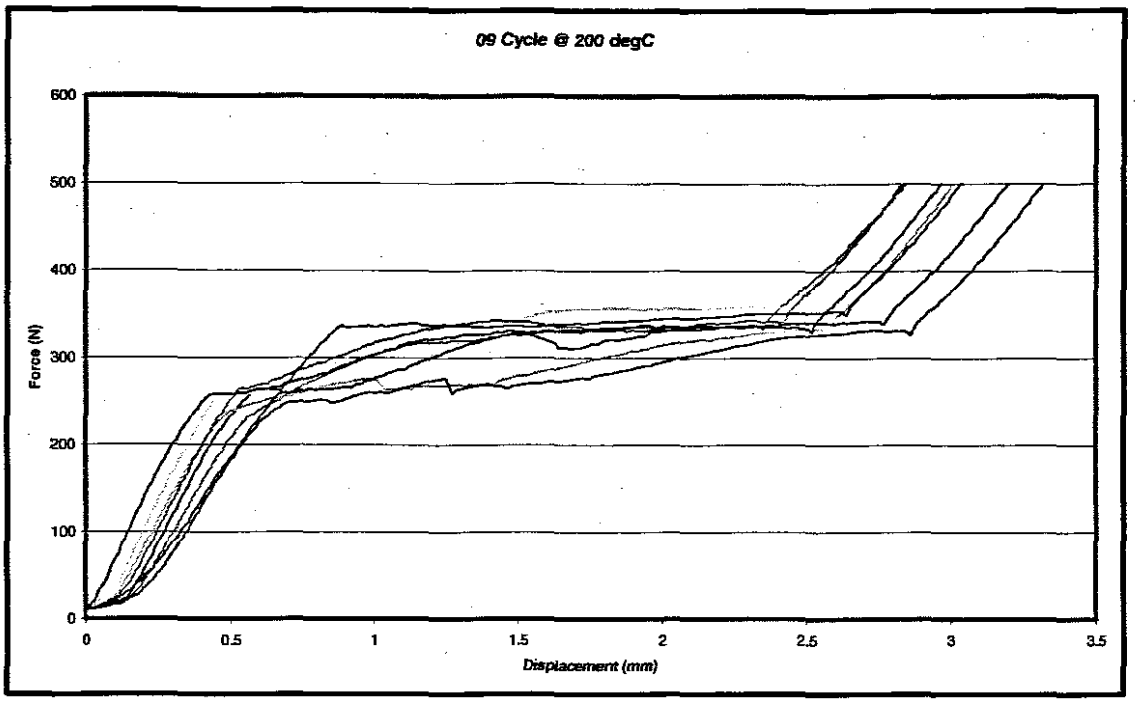
09 Cycle @ 200 degC
Force (N)
600
500
400
300
200
100
0
0
0.5
1
1.5
2
2.5
3
3.5
Displacement (mm)

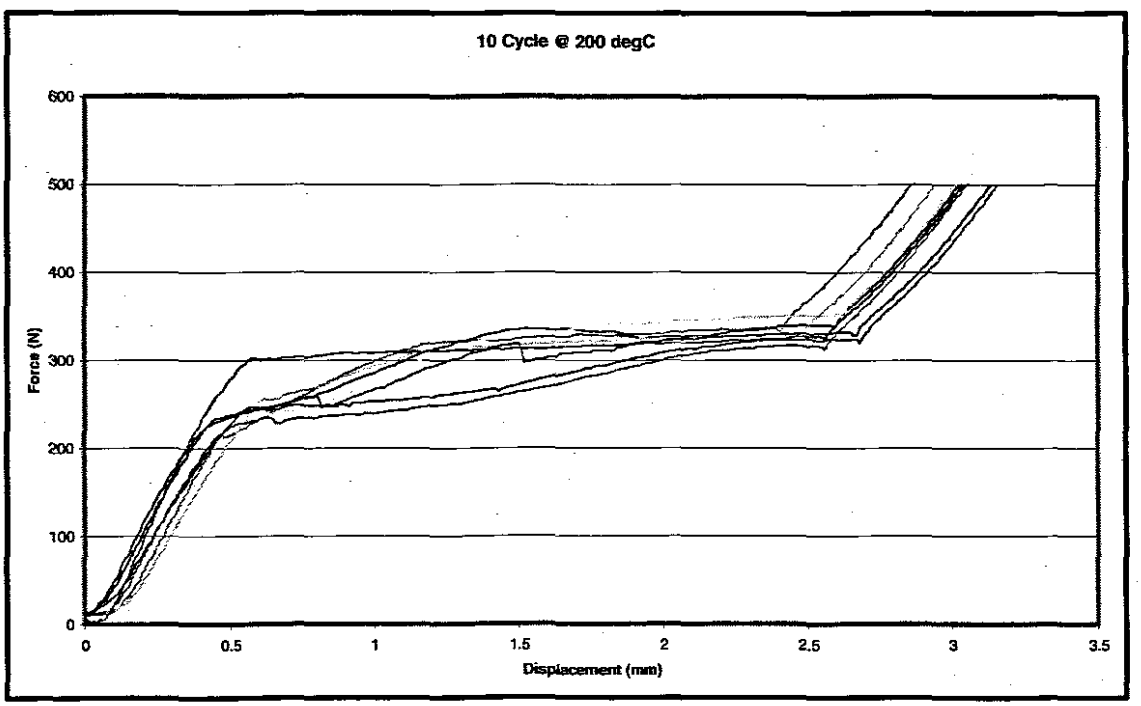
10 Cycle @ 200 degC
Force (N)
600
500
400
300
200
100
0
0
0.5
1
1.5
2
2.5
3
3.5
Displacement (mm)

250°C Aging Temperature

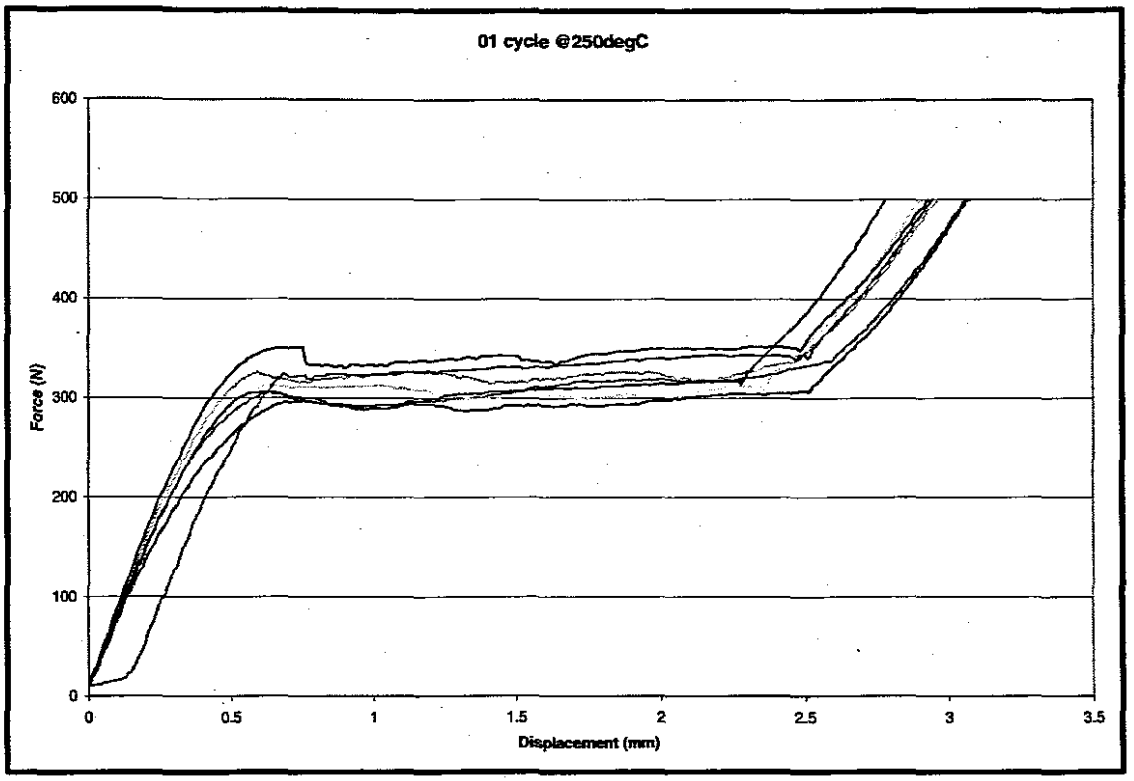

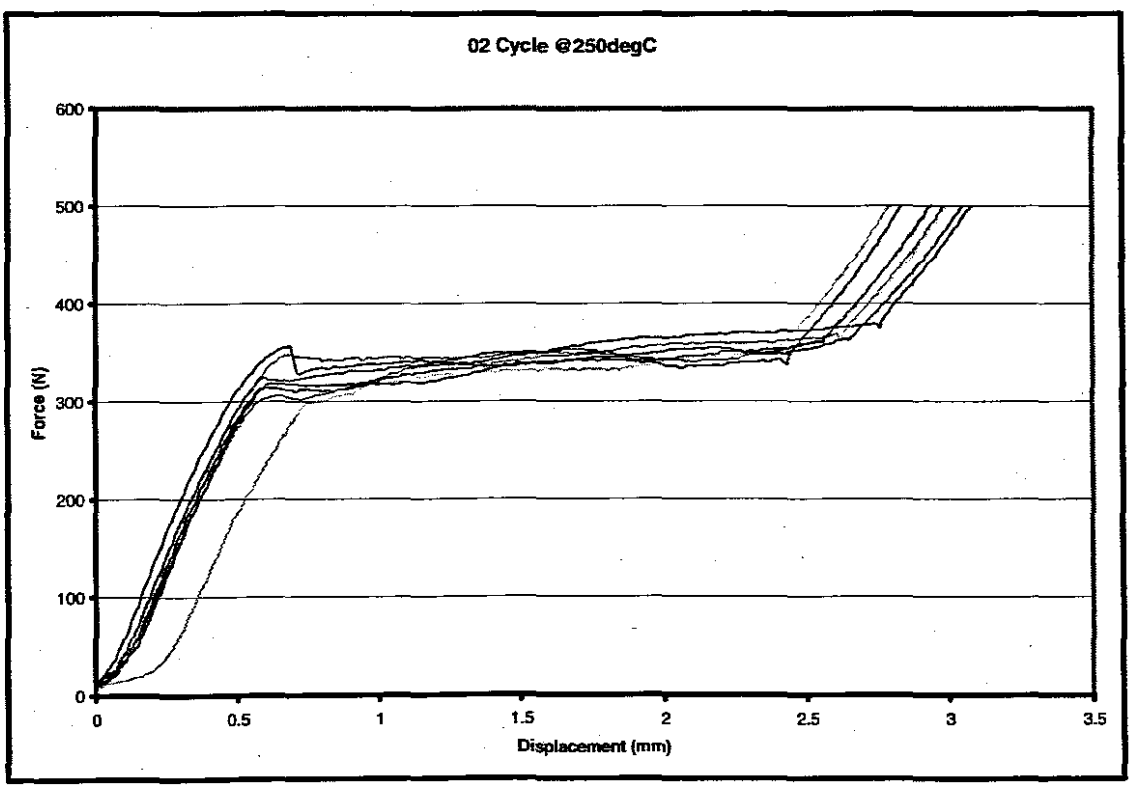

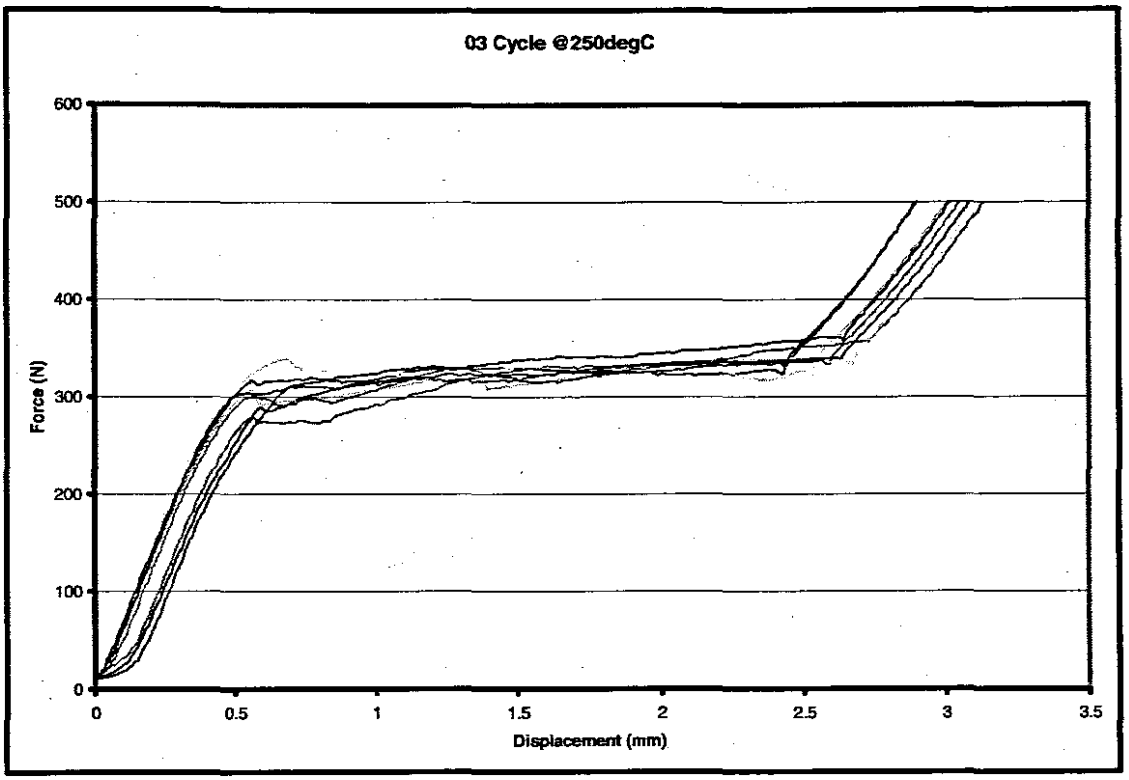
03 Cycle @250degC
Force (N)
600
500
400
300
200
100
0
0
0.5
1
1.5
2
2.5
3
3.5
Displacement (mm)

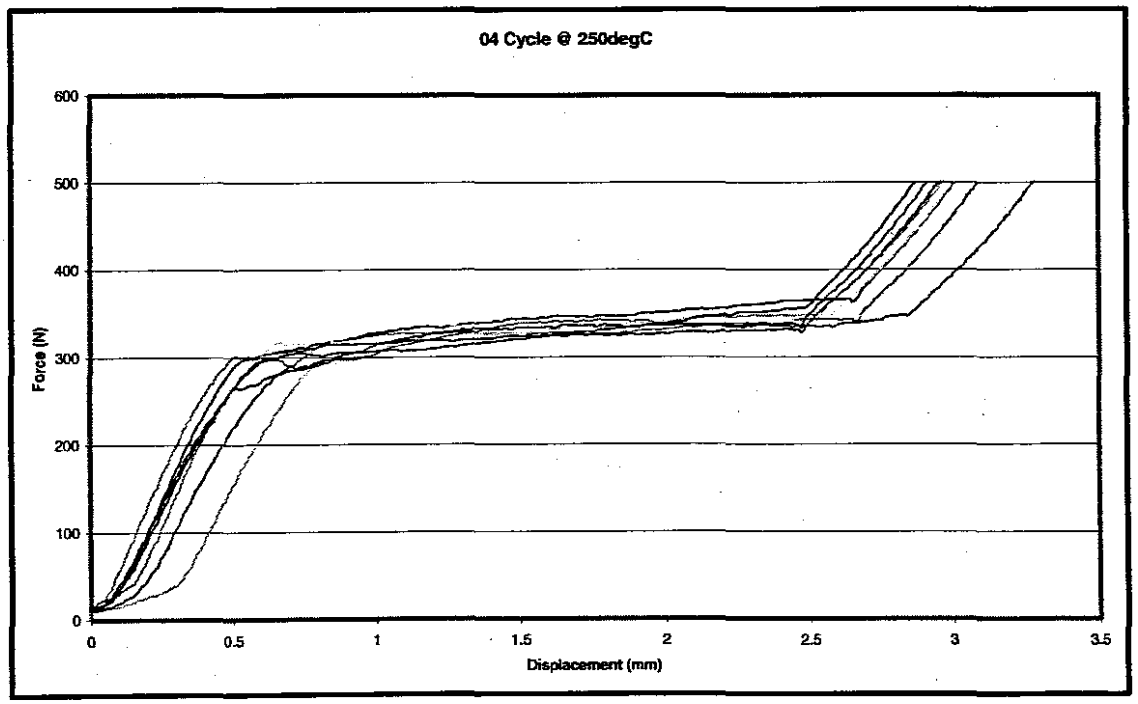
04 Cycle @ 250degC
Force (N)
600
500
400
300
200
100
0
0
0.5
1
1.5
2
2.5
3
3.5
Displacement (mm)

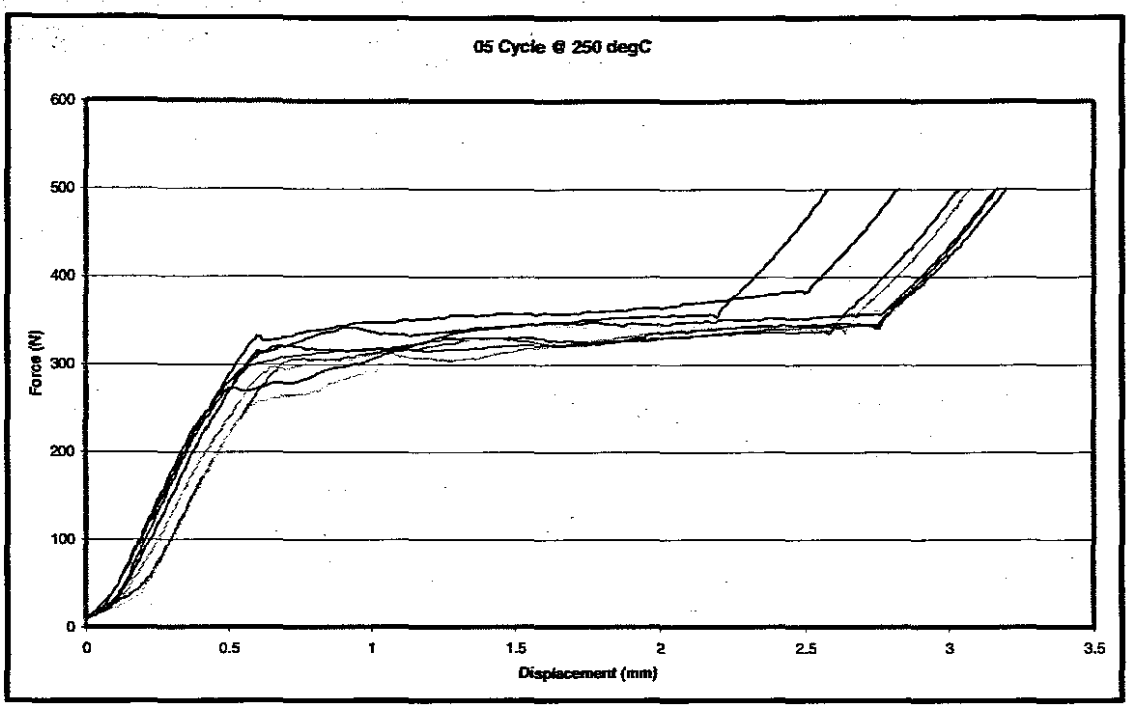
05 Cycle @ 250 degC
Force (N)
Displacement (mm)
0
100
200
300
400
500
600
0
0.5
1
1.5
2
2.5
3
3.5

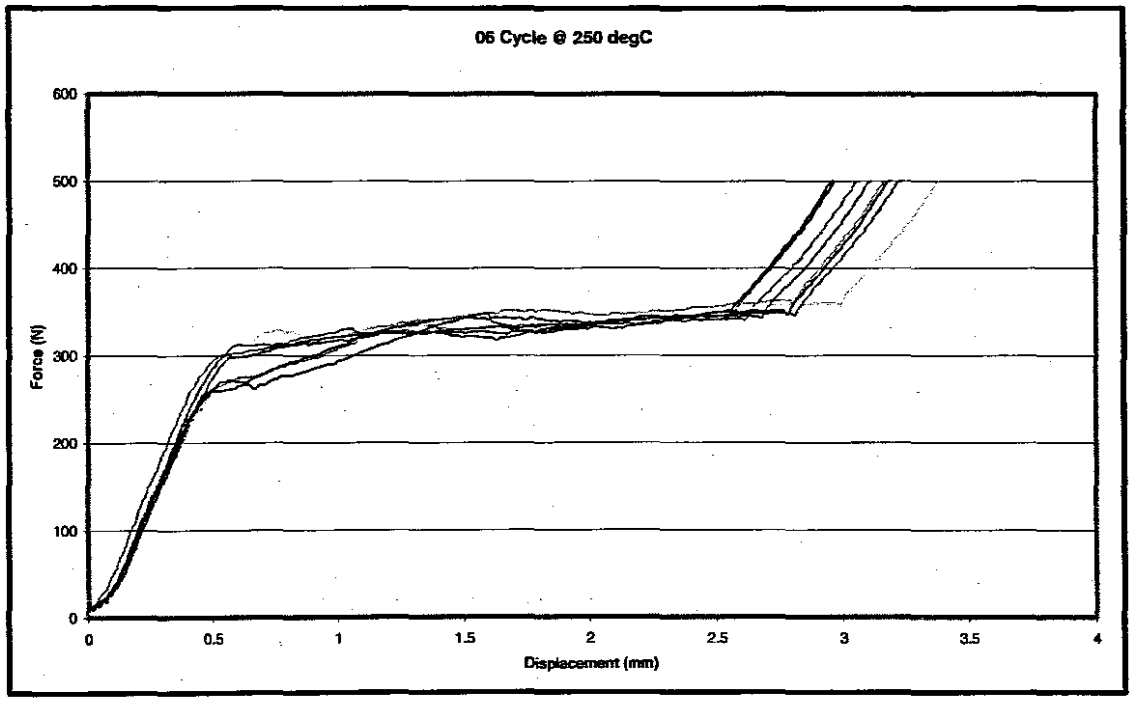
06 Cycle @ 250 degC
Force (N)
Displacement (mm)
0
100
200
300
400
500
600
0
0.5
1
1.5
2
2.5
3
3.5
4

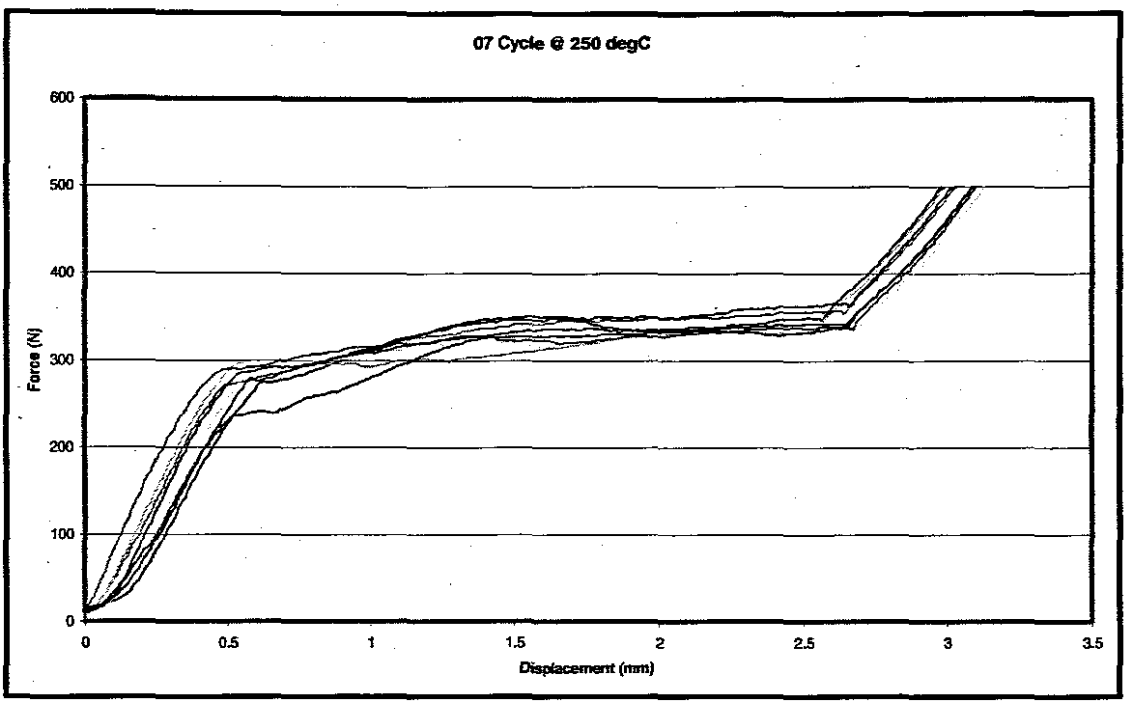
07 Cycle @ 250 degC
Force (N)
600
500
400
300
200
100
0
0
0.5
1
1.5
2
2.5
3
3.5
Displacement (mm)

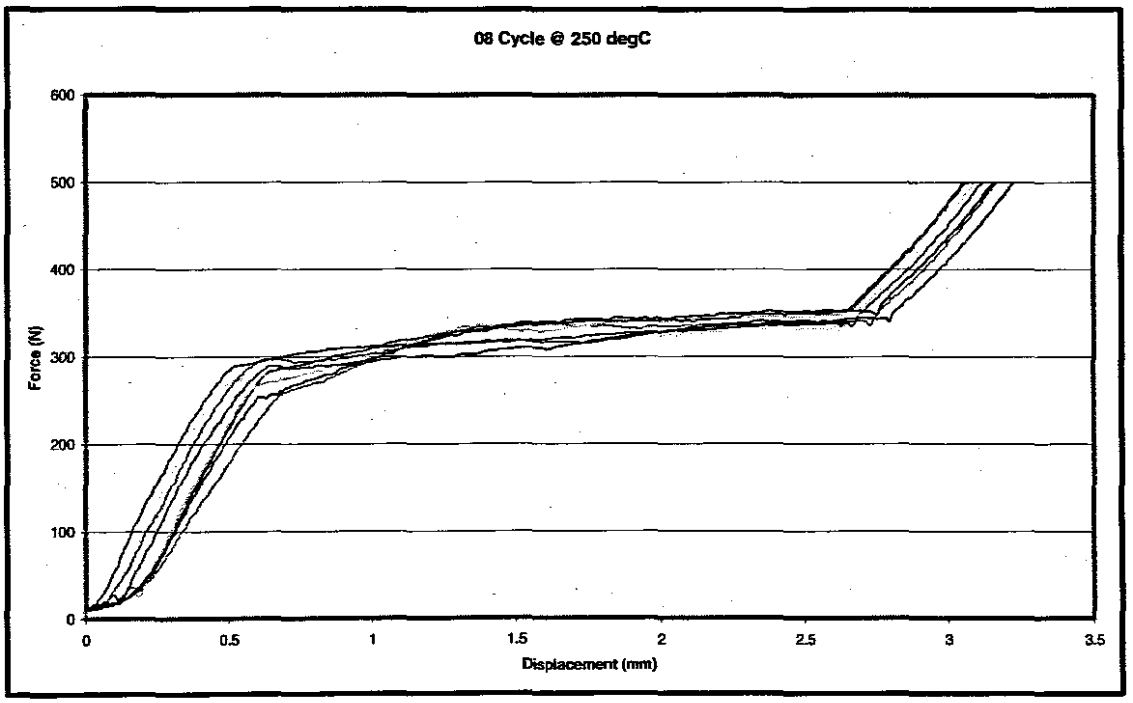
08 Cycle @ 250 degC
Force (N)
600
500
400
300
200
100
0
0
0.5
1
1.5
2
2.5
3
3.5
Displacement (mm)

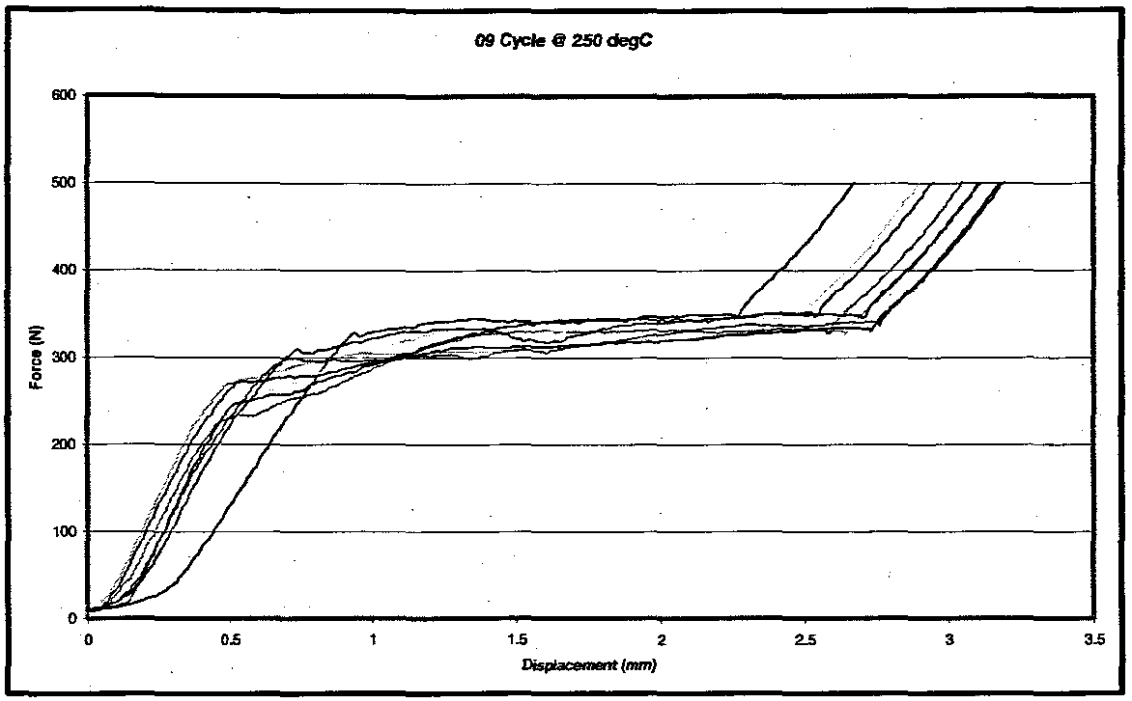
09 Cycle @ 250 degC
Force (N)
600
500
400
300
200
100
0
0
0.5
1
1.5
2
2.5
3
3.5
Displacement (mm)

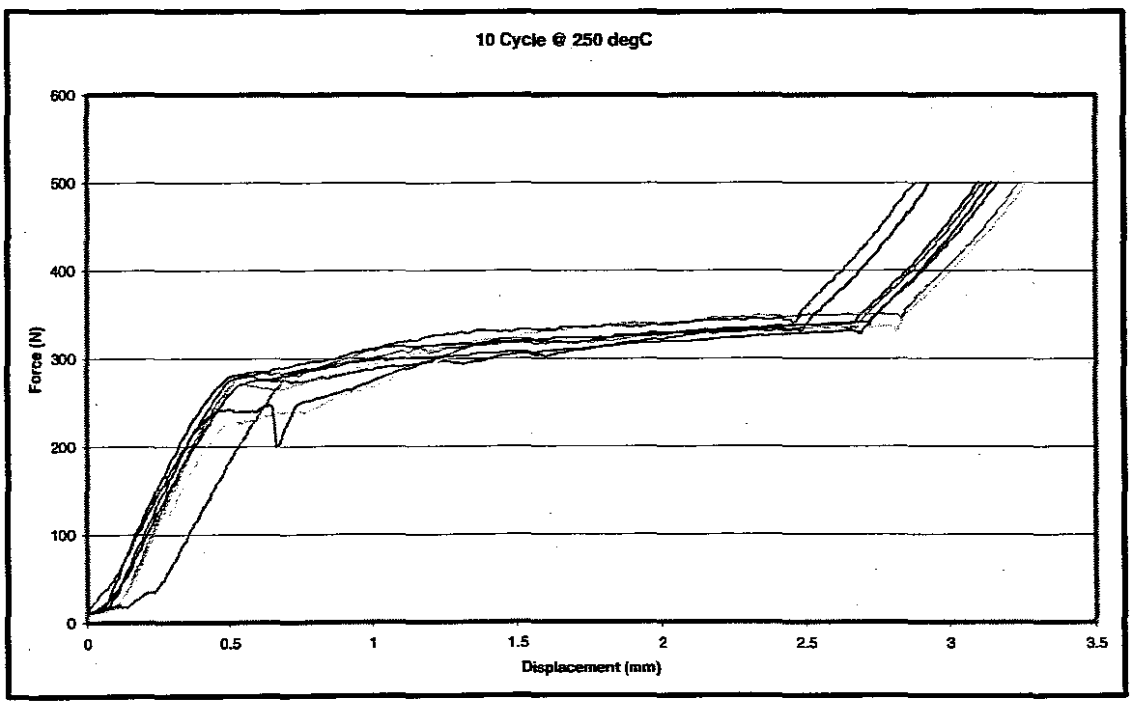
10 Cycle @ 250 degC
Force (N)
600
500
400
300
200
100
0
0
0.5
1
1.5
2
2.5
3
3.5
Displacement (mm)

300°C Aging Temperature

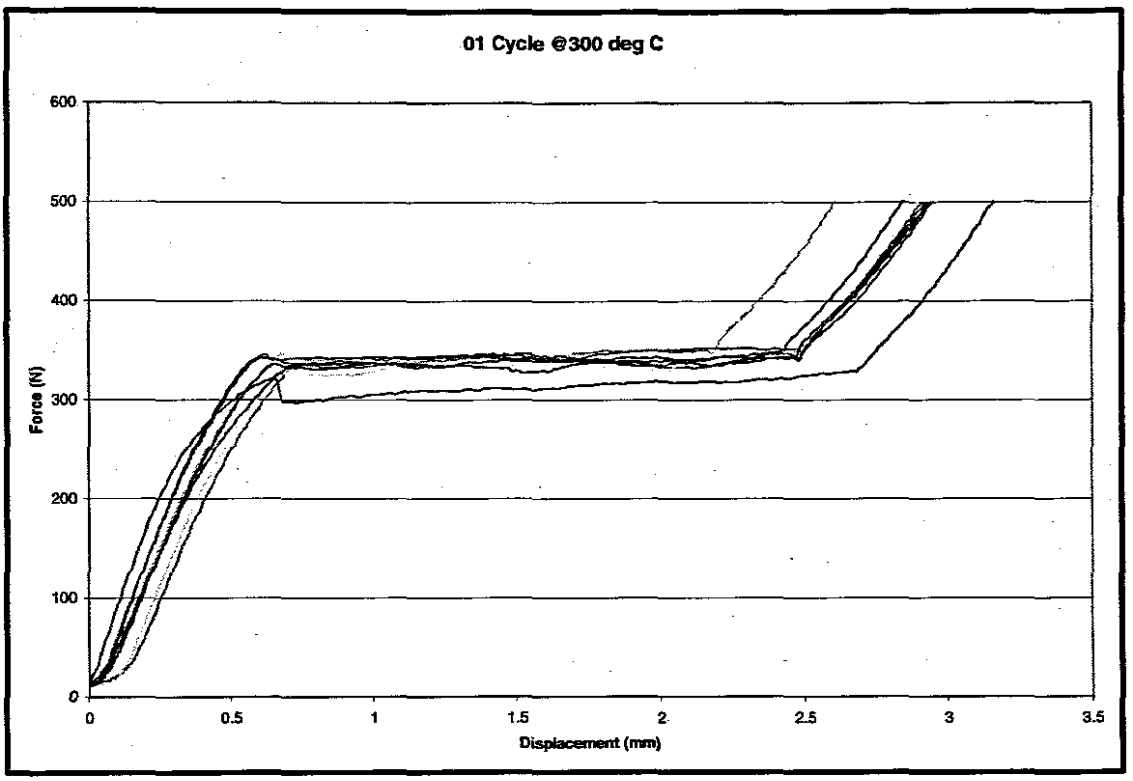

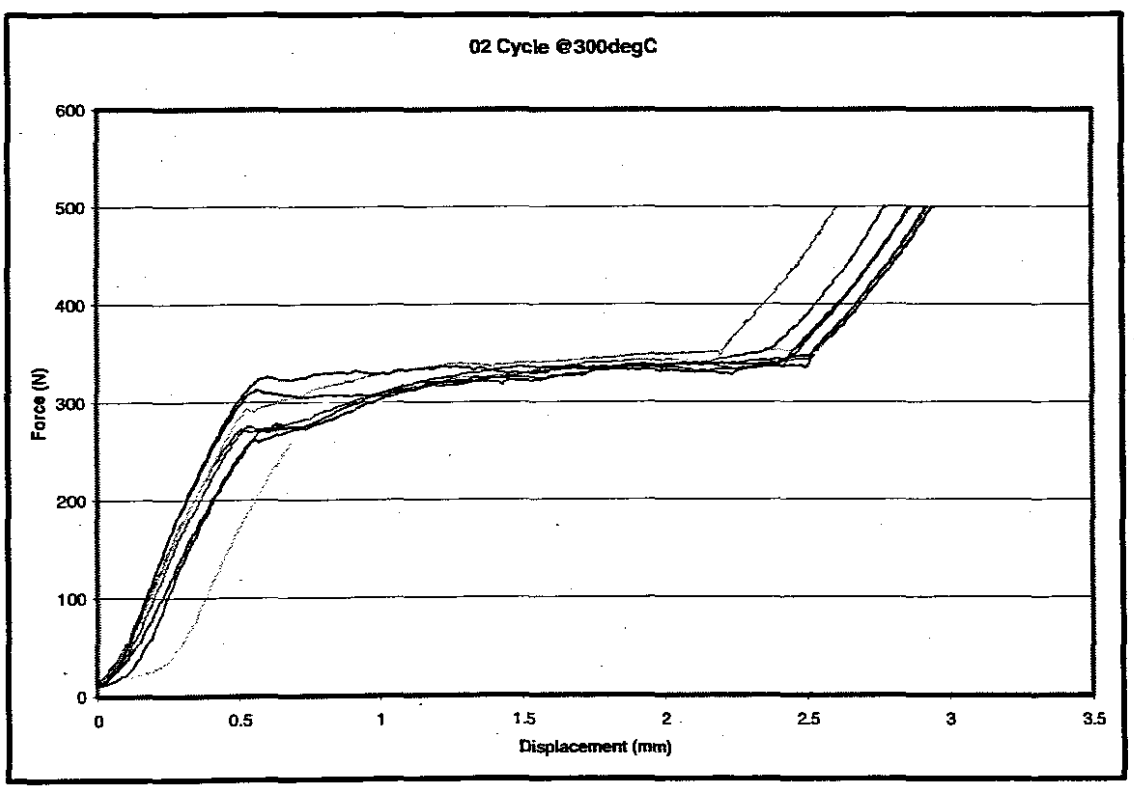

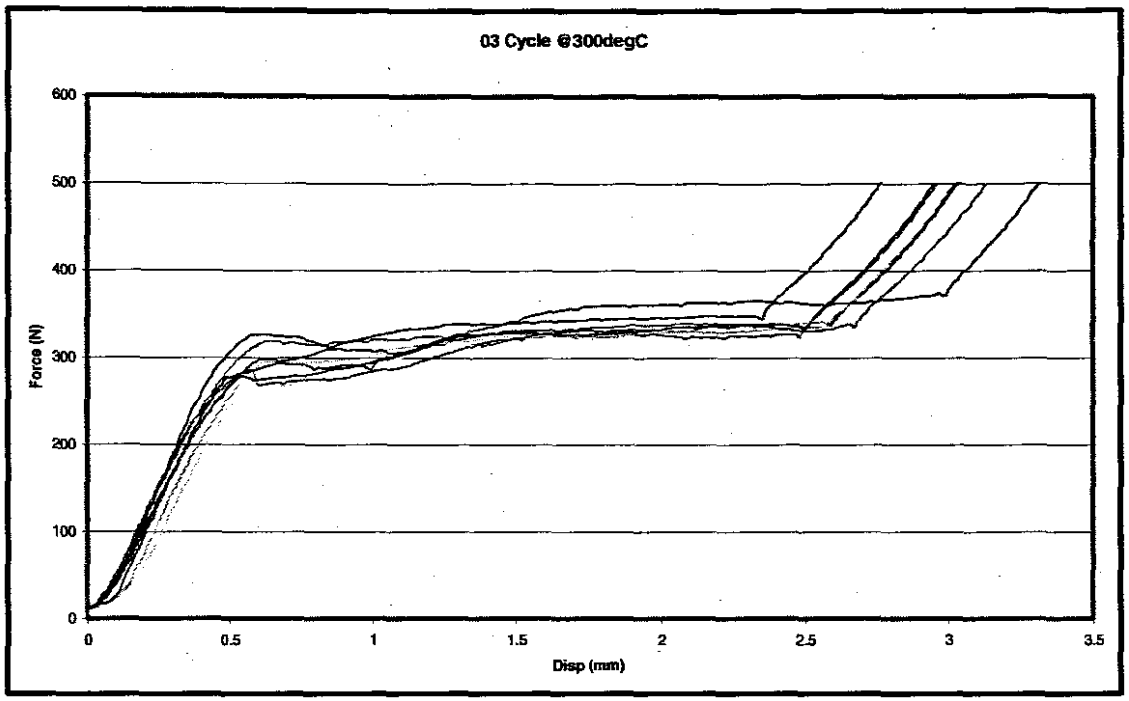
03 Cycle @300degC
Force (N)
600
500
400
300
200
100
0
0
0.5
1
1.5
2
2.5
3
3.5
Disp (mm)

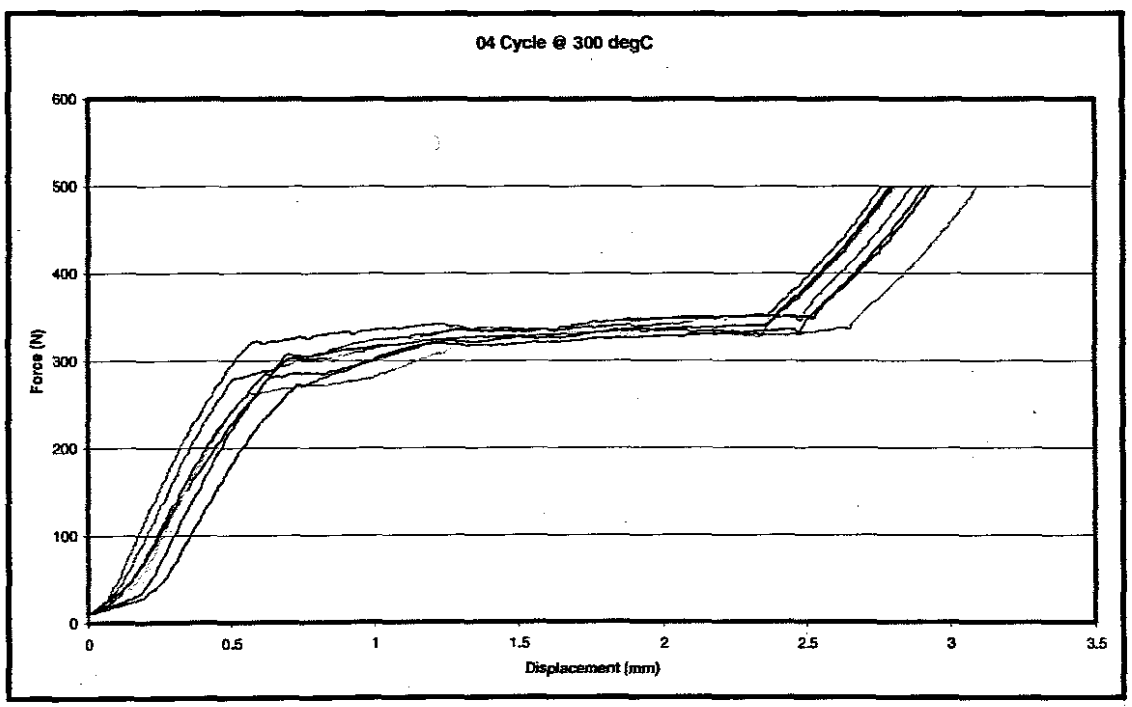
04 Cycle @ 300 degC
Force (N)
600
500
400
300
200
100
0
0
0.5
1
1.5
2
2.5
3
3.5
Displacement (mm)

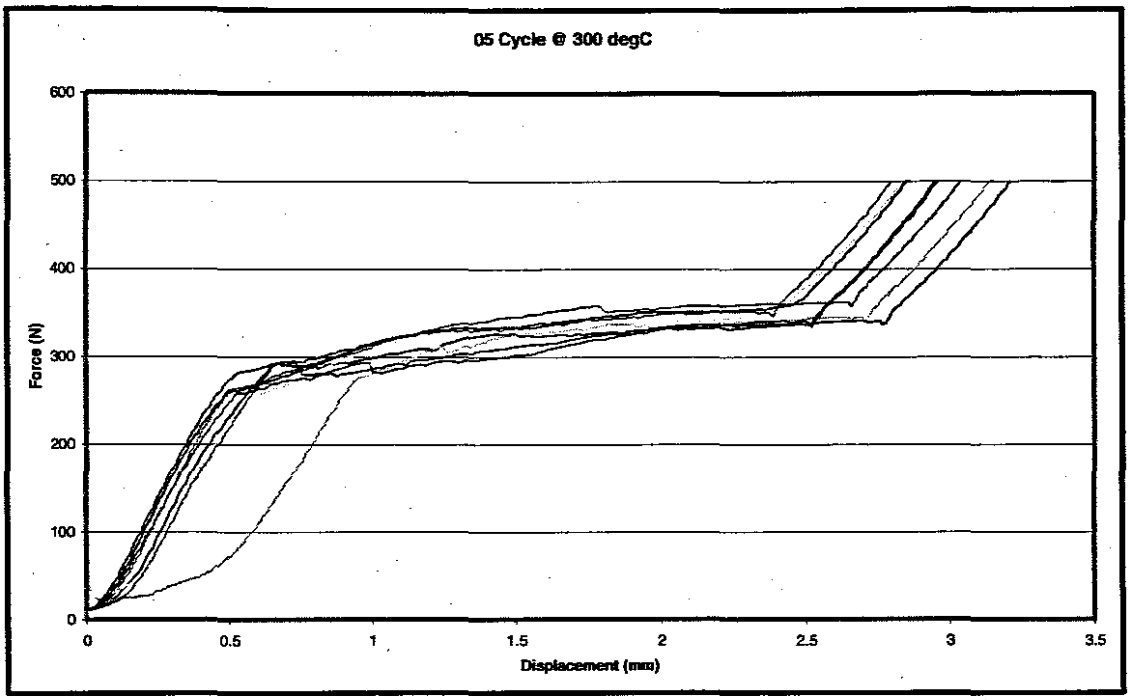
05 Cycle @ 300 degC
Force (N)
600
500
400
300
200
100
0
0
0.5
1
1.5
2
2.5
3
3.5
Displacement (mm)

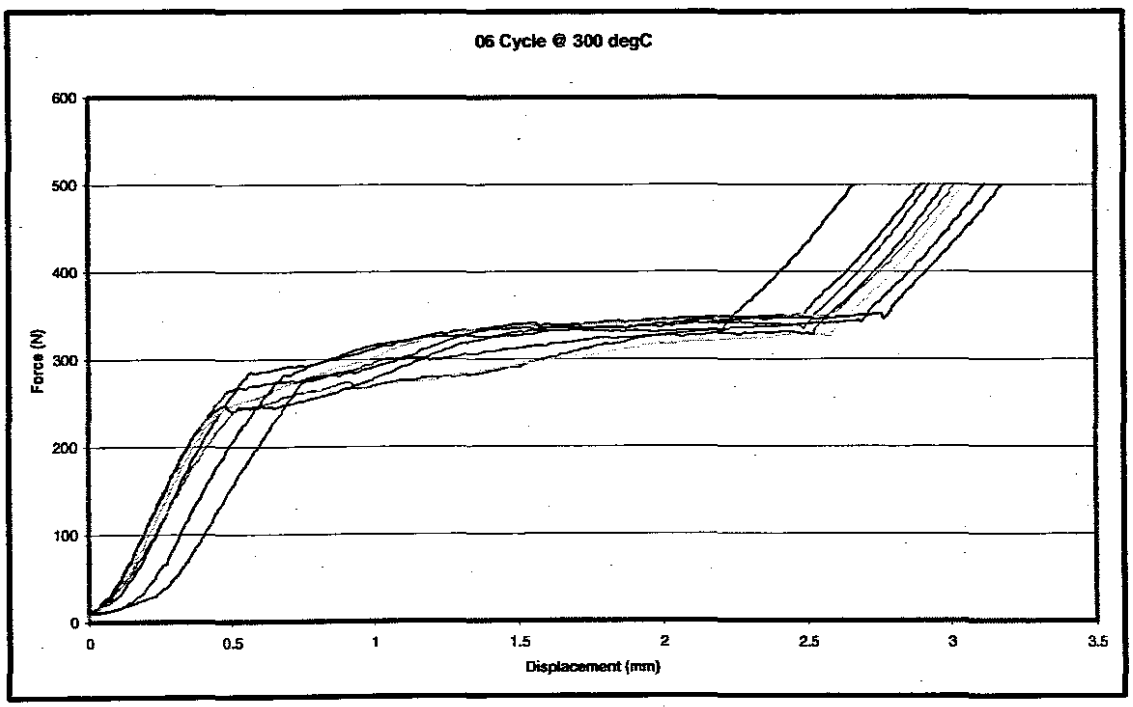
06 Cycle @ 300 degC
Force (N)
600
500
400
300
200
100
0
0
0.5
1
1.5
2
2.5
3
3.5
Displacement (mm)

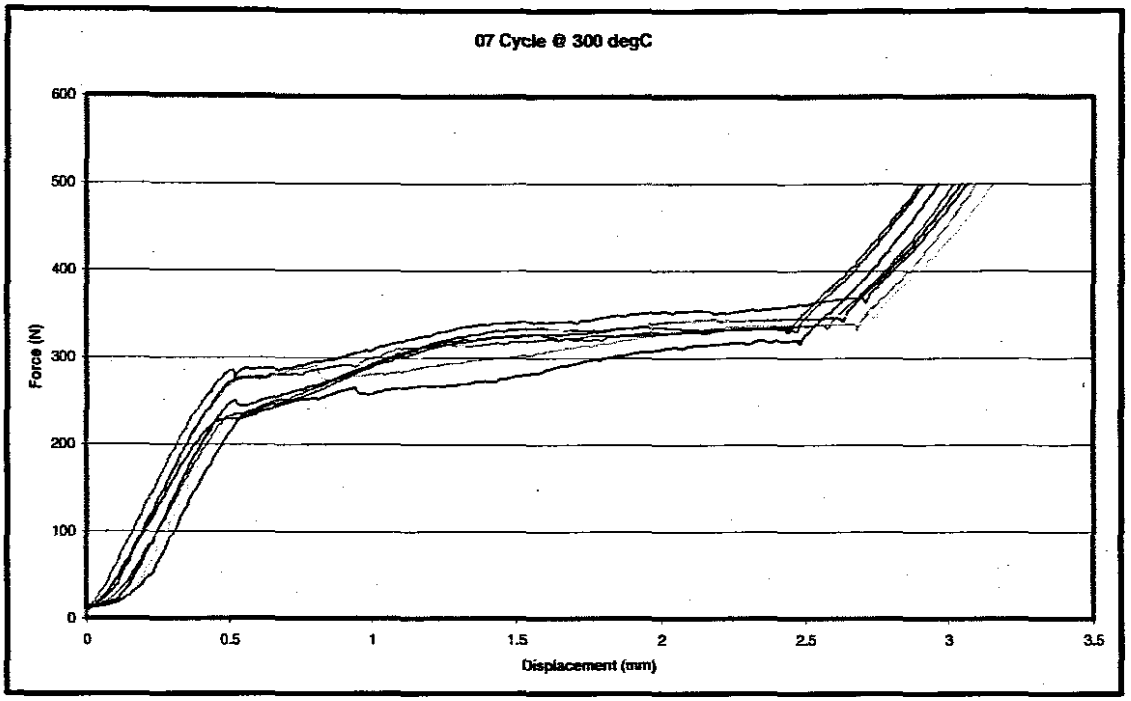
07 Cycle @ 300 degC
Force (N)
600
500
400
300
200
100
0
0
0.5
1
1.5
2
2.5
3
3.5
Displacement (mm)

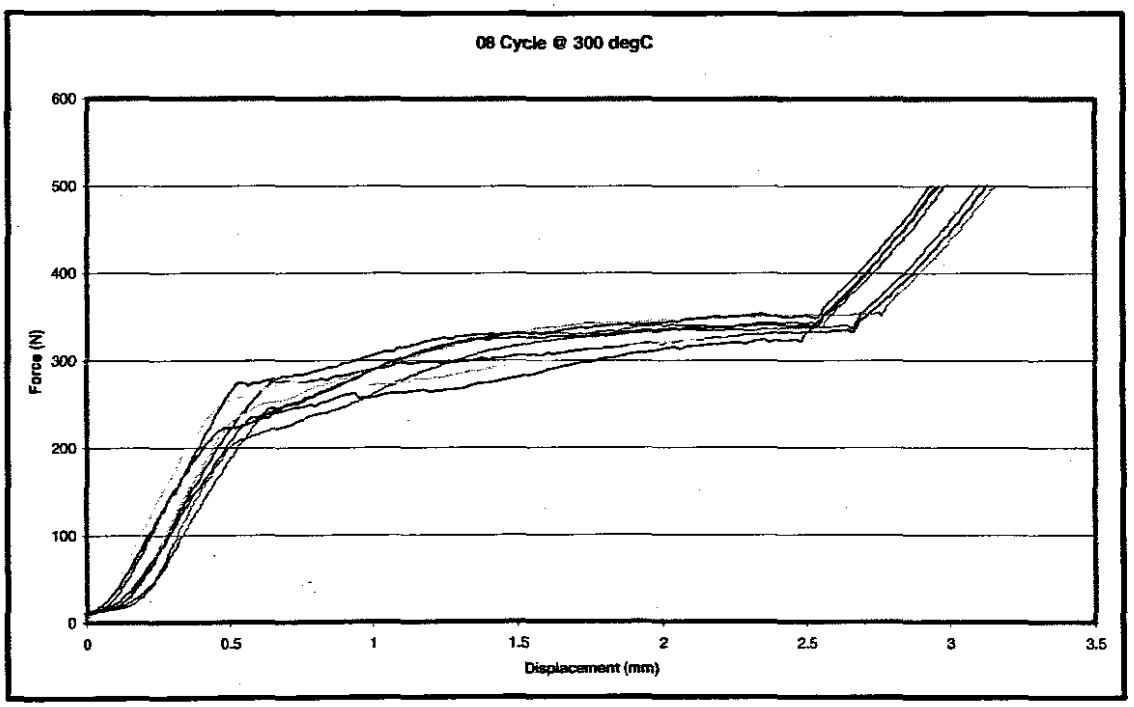
08 Cycle @ 300 degC
Force (N)
600
500
400
300
200
100
0
0
0.5
1
1.5
2
2.5
3
3.5
Displacement (mm)

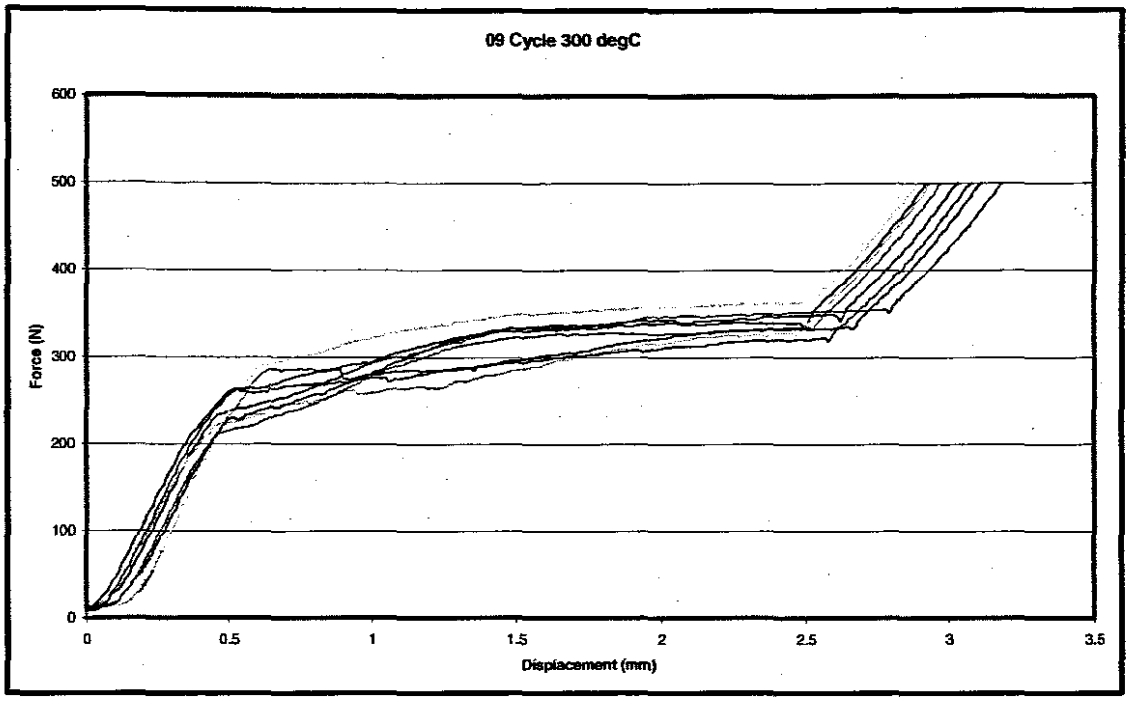
09 Cycle 300 degC
Force (N)
600
500
400
300
200
100
0
0
0.5
1
1.5
2
2.5
3
3.5
Displacement (mm)

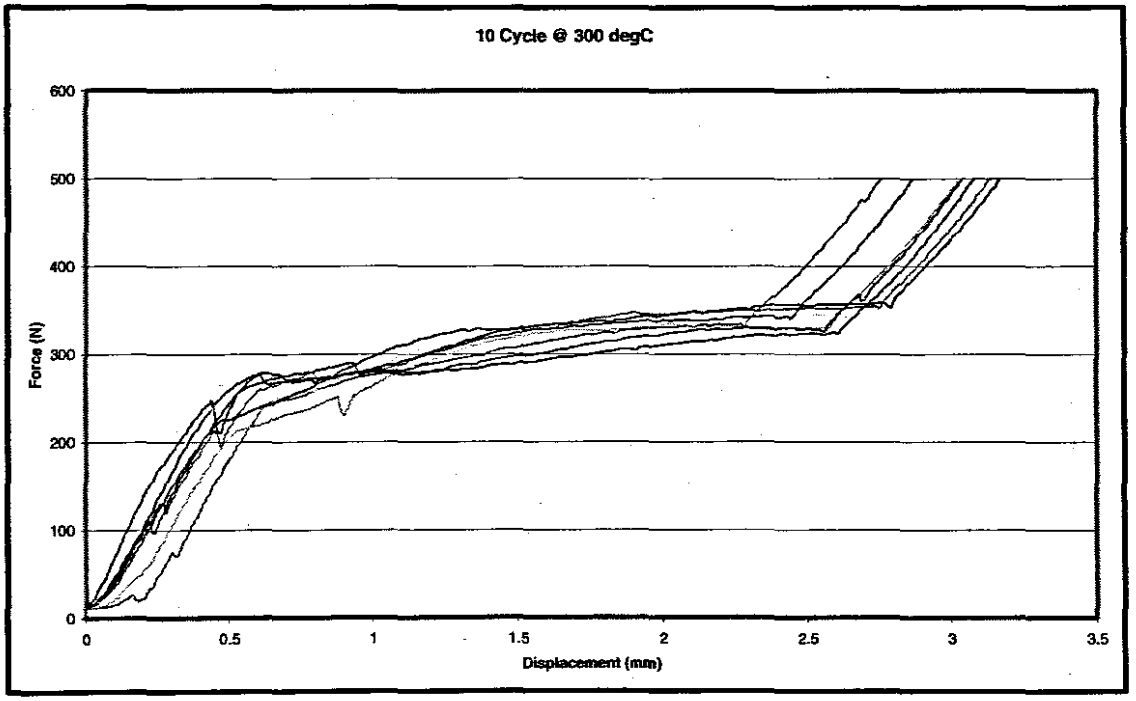
10 Cycle @ 300 degC
Force (N)
600
500
400
300
200
100
0
0
0.5
1
1.5
2
2.5
3
3.5
Displacement (mm)

350°C Aging Temperature

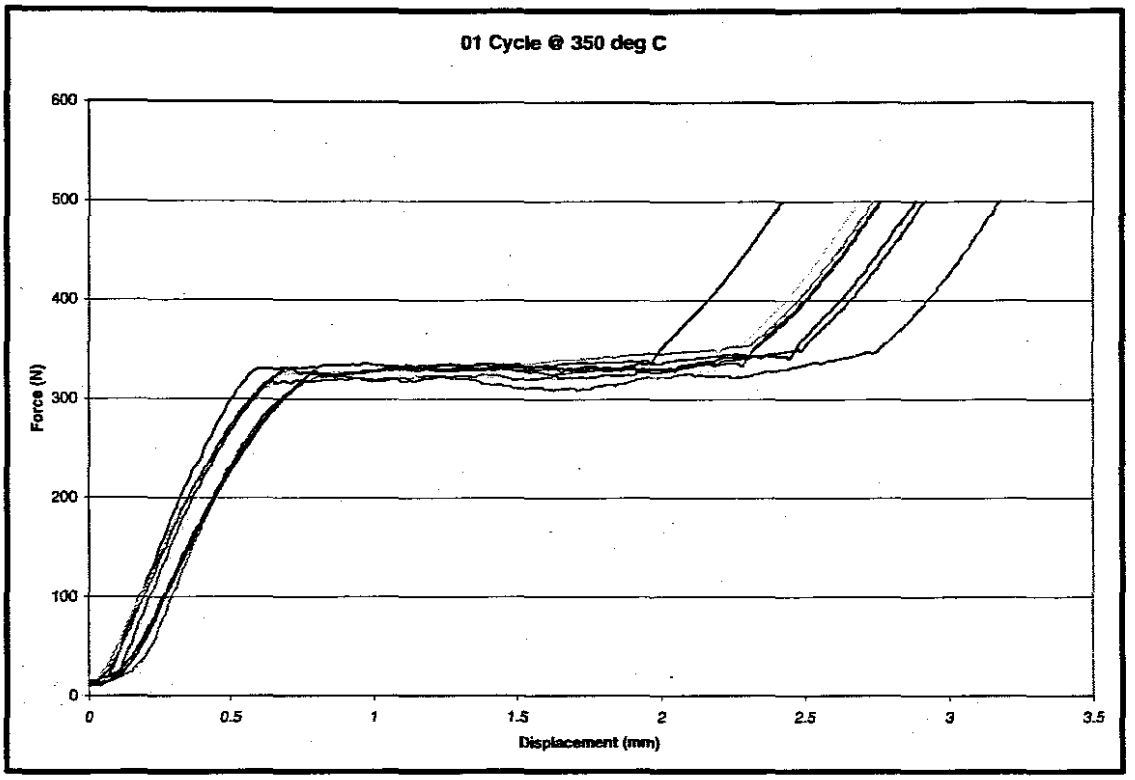

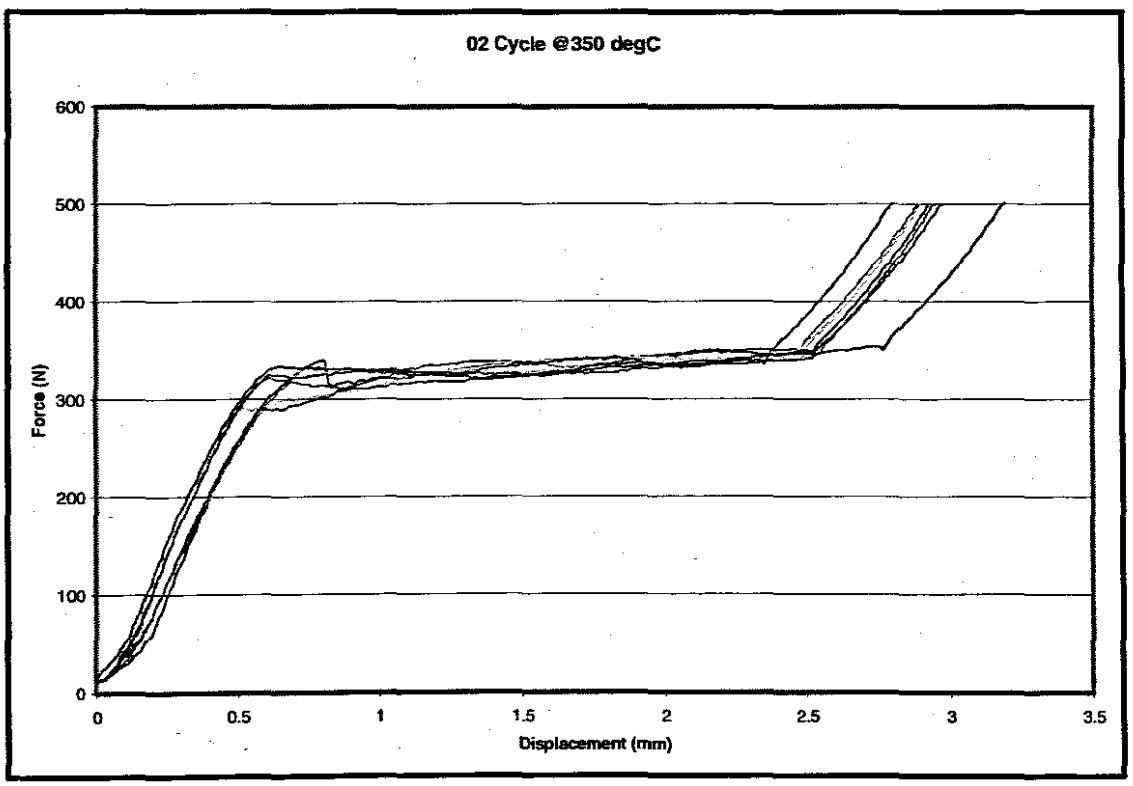

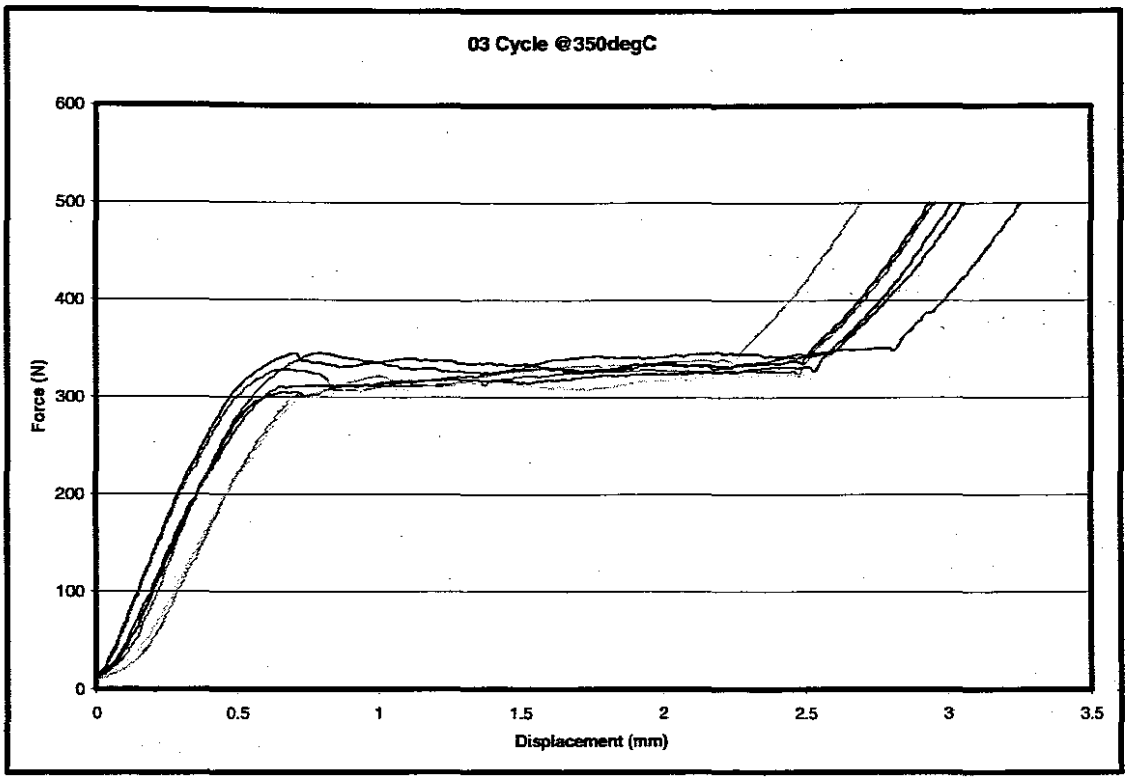
03 Cycle @350degC
Force (N)
Displacement (mm)
0
100
200
300
400
500
600
0
0.5
1
1.5
2
2.5
3
3.5

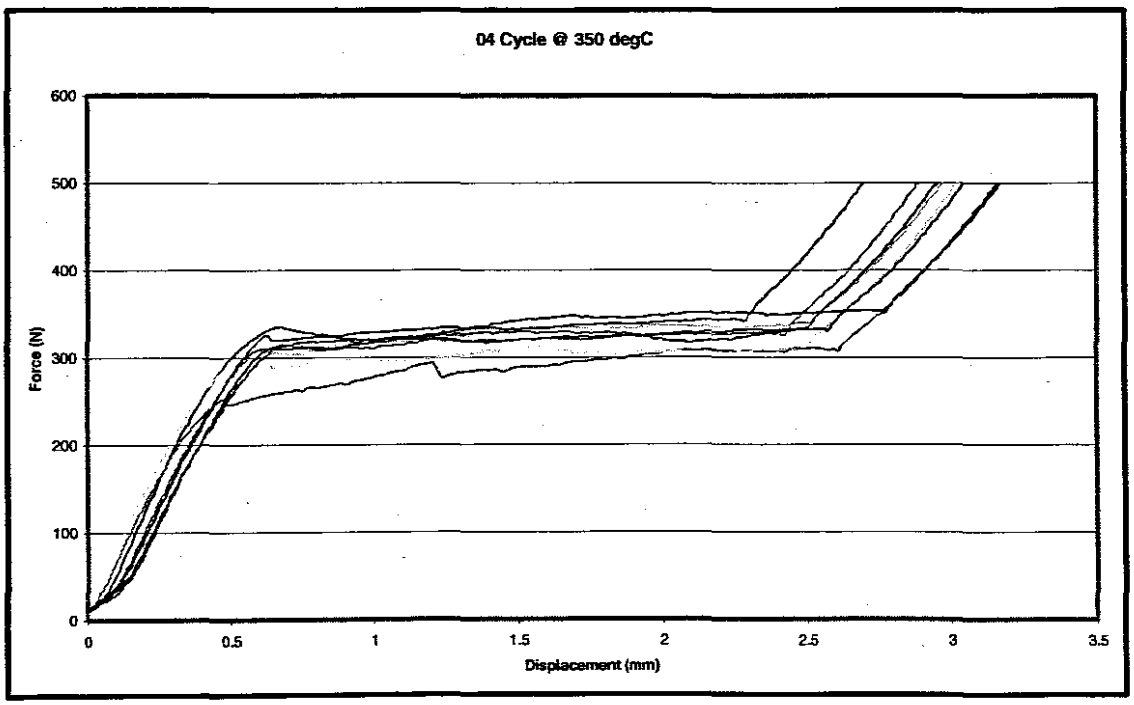
04 Cycle @ 350 degC
Force (N)
Displacement (mm)
0
100
200
300
400
500
600
0
0.5
1
1.5
2
2.5
3
3.5

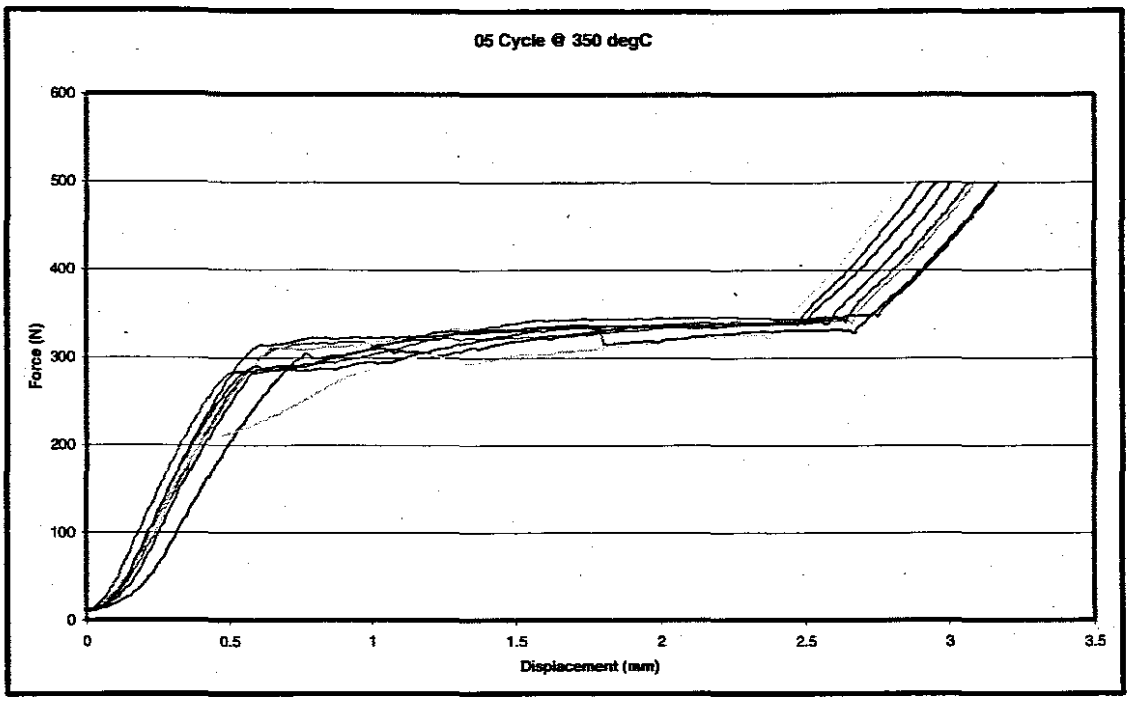
05 Cycle @ 350 degC
Force (N)
600
500
400
300
200
100
0
0
0.5
1
1.5
2
2.5
3
3.5
Displacement (mm)

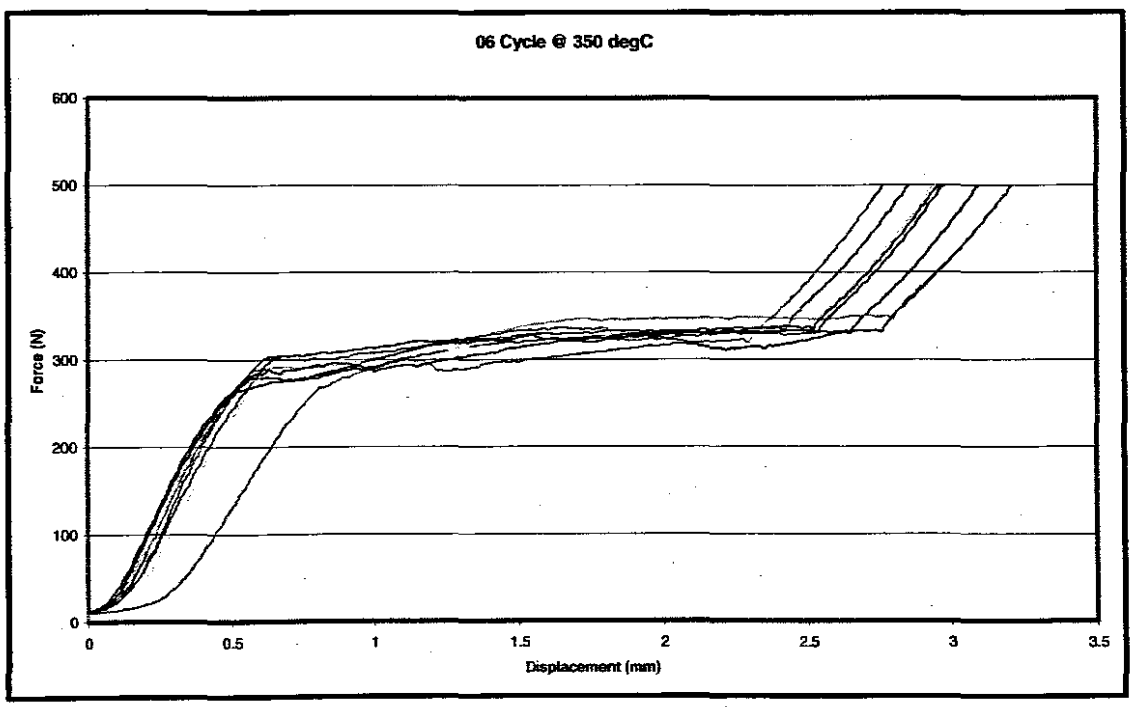
06 Cycle @ 350 degC
Force (N)
600
500
400
300
200
100
0
0
0.5
1
1.5
2
2.5
3
3.5
Displacement (mm)

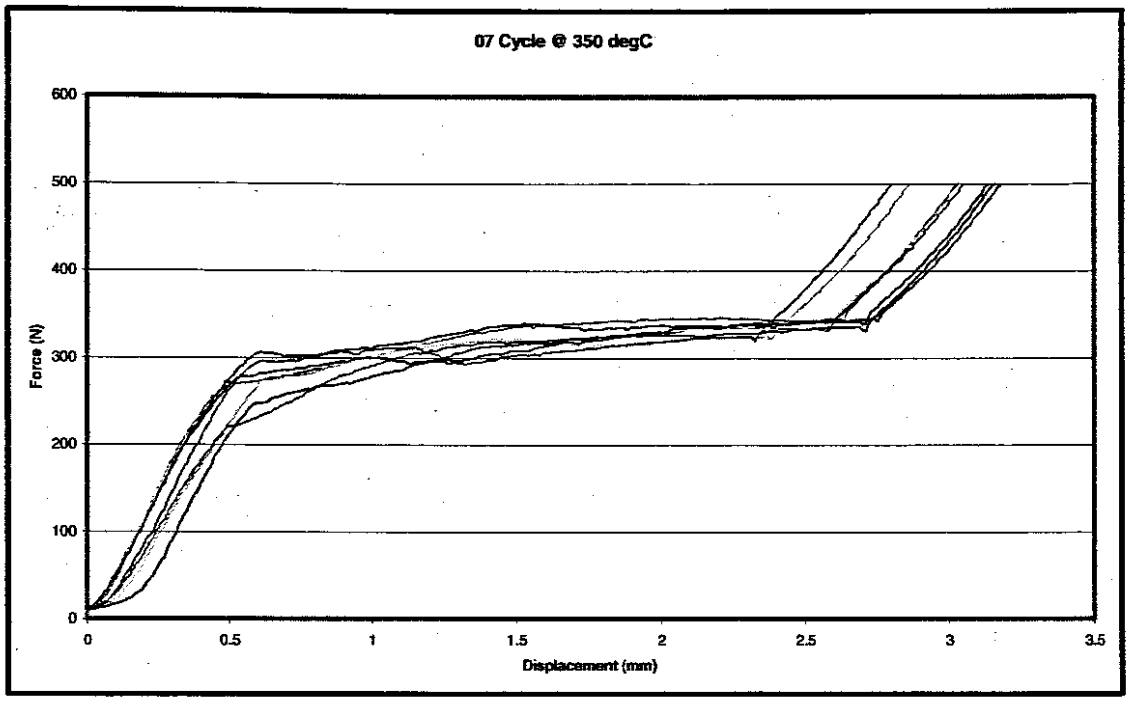
07 Cycle @ 350 degC
Force (N)
600
500
400
300
200
100
0
0
0.5
1
1.5
2
2.5
3
3.5
Displacement (mm)

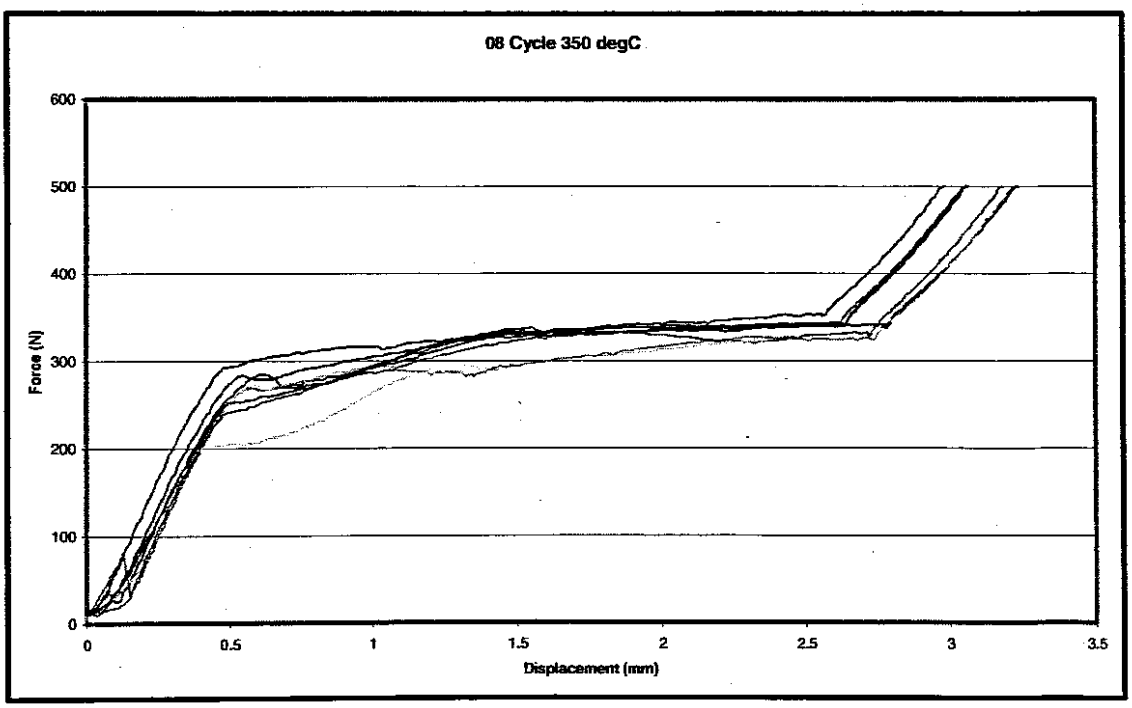
08 Cycle 350 degC
Force (N)
600
500
400
300
200
100
0
0
0.5
1
1.5
2
2.5
3
3.5
Displacement (mm)

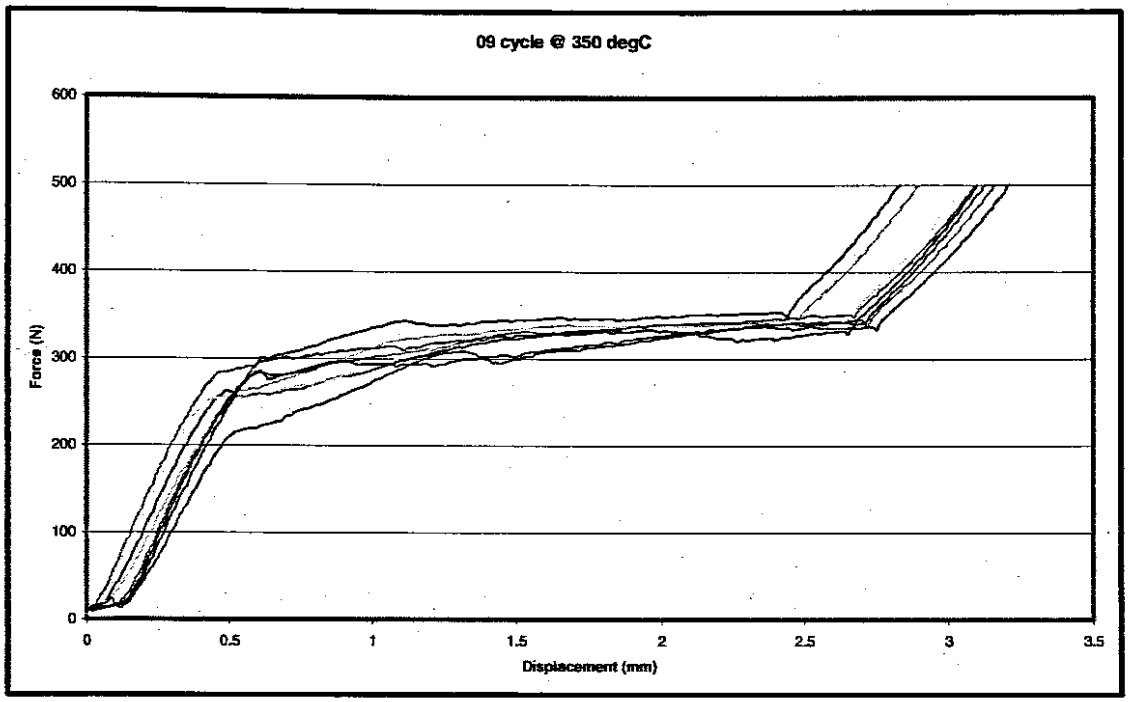
09 cycle @ 350 degC
Force (N)
600
500
400
300
200
100
0
0
0.5
1
1.5
2
2.5
3
3.5
Displacement (mm)

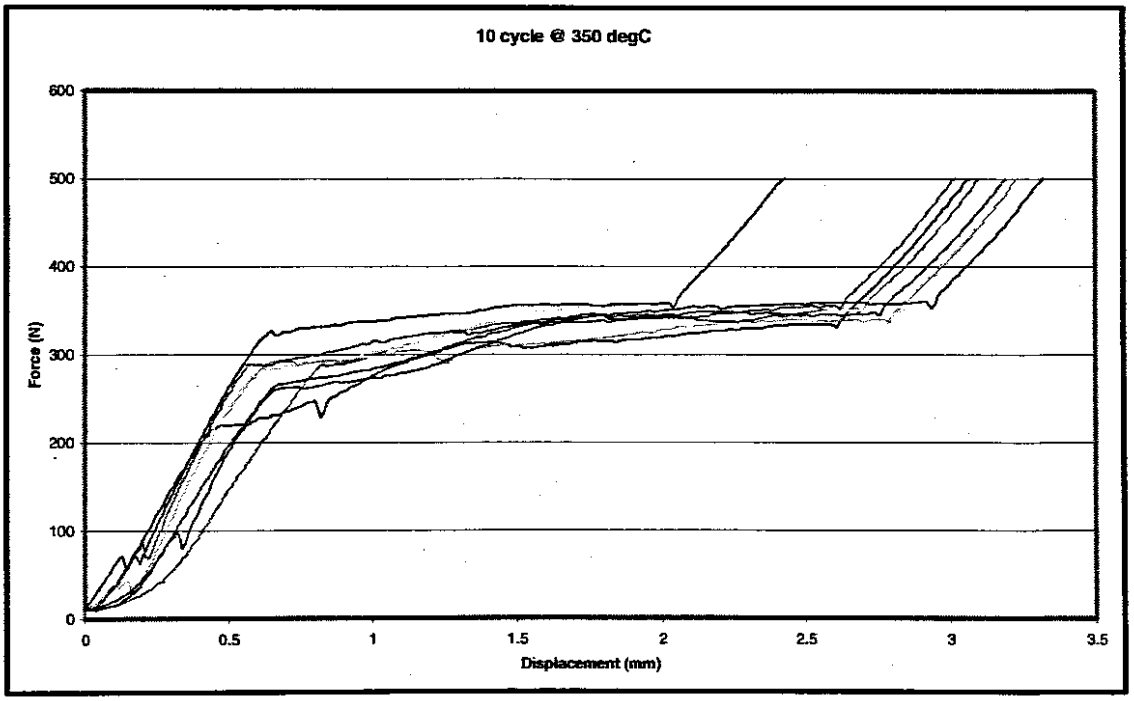
10 cycle @ 350 degC
Force (N)
600
500
400
300
200
100
0
0
0.5
1
1.5
2
2.5
3
3.5
Displacement (mm)

Appendix B

Initial and Second Yield Load Data for each specimen

This appendix shows all initial and second yield load data for each specimen. It also shows the average for each aging temperature. This data has abstracted from Load – Displacements graph at Appendix A.

Initial Yield Load

	200 degC									
No Cycle	**1**	**2**	**3**	**4**	**5**	**6**	**7**	**8**	**9**	**10**
	300.5	300.8	306	283	273	279	252	300	258	231
	295.5	301.5	298	250	279	281	240	262	258	230
	295.5	281	298	264	273	267	237	267	264	240
	295	265	277	279	264	244	249	212	240	255
	300	259	258	255	274	228	271	228	264	237
	296	285	236	244	273	302	228	254	234	225
	260	253	239	252	256	267	237		240	213
		297	240	218	244					303
Average	**292**	**280**	**269**	**256**	**267**	**267**	**245**	**254**	**251**	**242**

	250 degC									
No Cycle	**1**	**2**	**3**	**4**	**5**	**6**	**7**	**8**	**9**	**10**
	351	356	338	300	330	313	297	290	325	280
	322	348	315	299	314	325	290	296	305	276
	224	323	303	317	317	300	286	289	300	281
	312	318	300	300	297	300	272	268	270	270
	305	318	300	293	297	297	290	289	270	270
	304	303	292	264	310	270	277	267	261	236
	294	298	276	295	273	265	278	256	247	230
		317	312	316	258	258	236	258	230	283
Average	**302**	**323**	**305**	**298**	**300**	**291**	**278**	**277**	**276**	**266**

	300 degC									
No Cycle	**1**	**2**	**3**	**4**	**5**	**6**	**7**	**8**	**9**	**10**
	344	324	326	321	282	284	281	275	291	210
	345	312	318	307	262	265	286	248	285	213
	343	291	294	304	262	259	279	223	263	278
	335	274	298	279	261	243	247	222	263	278
	335	272	284	285	262	243	229	235	235	268
	335	270	277	283	293	282	229	245	228	237
	334	260	280	268	293	278	225	207	223	229
	325	300	275	272	273	246	232	279	212	242
Average	**337**	**288**	**294**	**290**	**274**	**263**	**251**	**242**	**250**	**244**

	350 degC									
No Cycle	**1**	**2**	**3**	**4**	**5**	**6**	**7**	**8**	**9**	**10**
	330	333	342	334	314	303	306	292	283	320
	330	332	345	324	313	301	298	283	300	292
	329	324	327	309	313	300	296	283	287	291
	315	332	310	310	310	292	282	270	287	288
	326	336	306	310	288	282	276	270	262	290
	326	293	300	292	285	283	274	252	262	266
	323	288	300	254	285	265	221	241	254	260
	329	332		313	211	268	248		216	222
Average	**326**	**321**	**319**	**306**	**290**	**287**	**275**	**270**	**269**	**279**

Second Yield Load

	200 degC									
No Cycle	1	2	3	4	5	6	7	8	9	10
	303	341	329	338	337	346	345	337	331	324
	303	333	346	330	326	350	336	306	341	332
	313	340	347	325	342	341	336	315	327	315
	310	333	329	325	347	341	355	311	352	327
	310	342	332	345	341	336	327	346	334	342
	303	348	341	337	352	345	327	315	342	348
	308	348	328	336	343	338	338		360	327
		334	327	334	337	356	337		336	331
Average	**307**	**340**	**335**	**334**	**341**	**344**	**338**	**322**	**340**	**331**

	250 degC									
No Cycle	**1**	**2**	**3**	**4**	**5**	**6**	**7**	**8**	**9**	**10**
	311	379	360	349	341	356	340	342	340	337
	318	350	336	340	341	356	340	341	336	348
	341	355	342	360	360	350	340	352	331	343
	348	370	336	335	360	360	340	340	332	331
	348	355	363	333	340	348	340	340	347	338
	318	355	338	336	370	345	370	335	350	331
	310	341	336	347	355	350	355	350	345	334
		345	320	357	340	345	348	352	345	341
Average	**328**	**356**	**341**	**345**	**351**	**351**	**347**	**344**	**341**	**338**

	300 degC									
No Cycle	**1**	**2**	**3**	**4**	**5**	**6**	**7**	**8**	**9**	**10**
	332	338	371	338	340	331	368	354	352	354
	345	347	337	335	340	347	348	339	332	358
	345	354	332	353	340	340	337	339	320	328
	346	345	336	350	340	340	339	330	345	330
	350	345	336	350	360	347	339	322	332	341
	350	350	325	341	354	330	318	344	324	331
	354	349	335	353	358	352	333	348	361	344
	350	350	345	335	350	343	333	345	338	328
Average	**347**	**347**	**340**	**344**	**348**	**341**	**339**	**340**	**338**	**339**

	350 degC									
No Cycle	**1**	**2**	**3**	**4**	**5**	**6**	**7**	**8**	**9**	**10**
	348	351	348	312	354	348	347	341	334	358
	348	350	321	353	330	332	332	331	336	349
	349	350	327	333	330	332	340	325	343	338
	333	349	321	312	348	332	342	325	341	345
	327	341	340	342	348	336	335	342	351	350
	355	348	350	333	340	336	335	342	342	338
	336	344	340	330	340	336	330	342	347	352
	343	348	348	342	340	328	330	351	351	354
Average	**342**	**348**	**337**	**332**	**341**	**335**	**336**	**337**	**343**	**348**

Appendix C

Results of Thermal Analyses performed on NiTi SMA using a Dilatometer

This appendix shows selected plots of the change in length of NiTi SMA specimens as a function of an increase in temperature. Specimens were subjected to aging temperatures ranging from 200 to 350°C.

10mm length of the first 0-50mm sample of NiTi Rod aged at 200°C

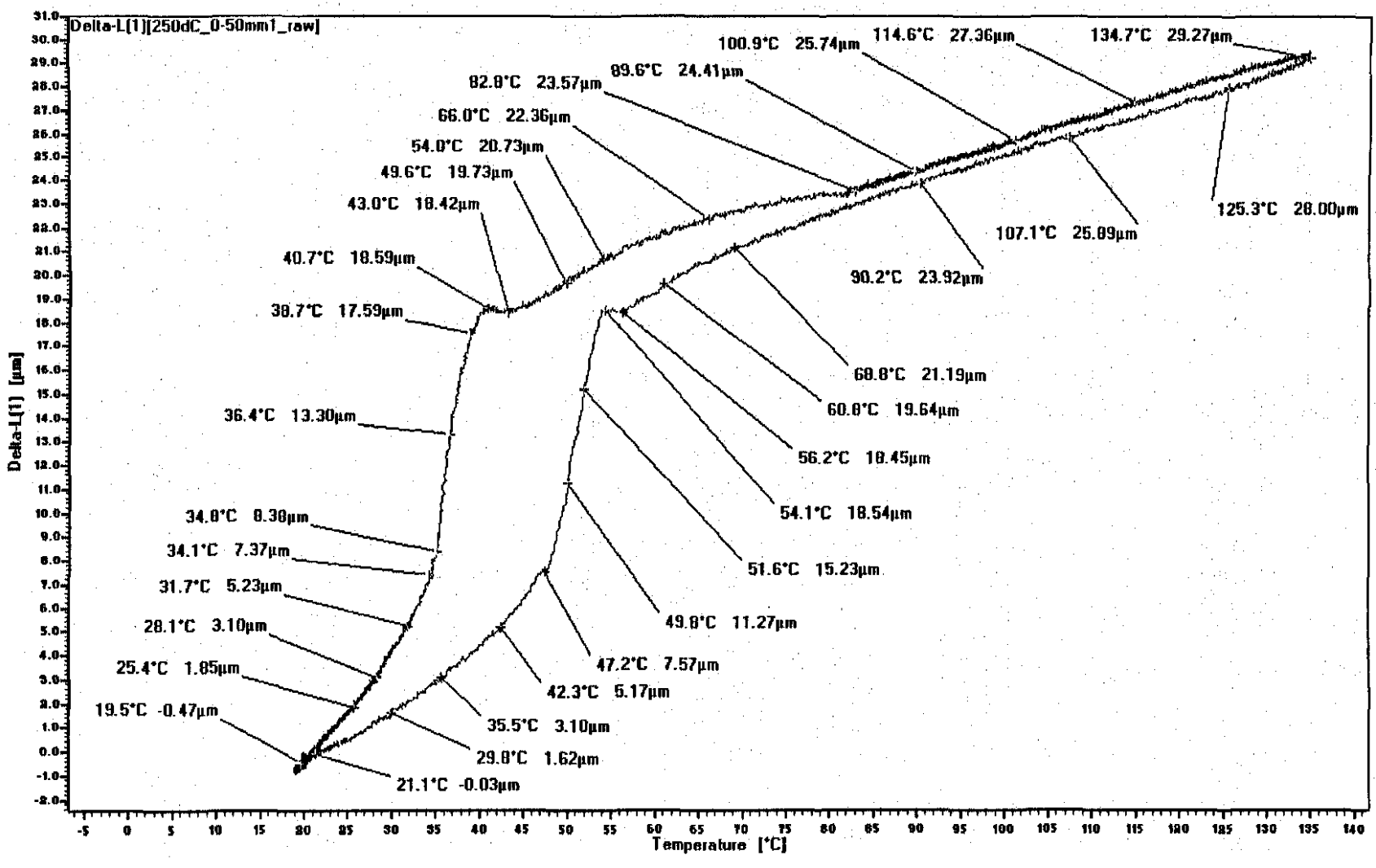

10mm length of the fifth 0-50mm sample of NiTi Rod aged at 200°C

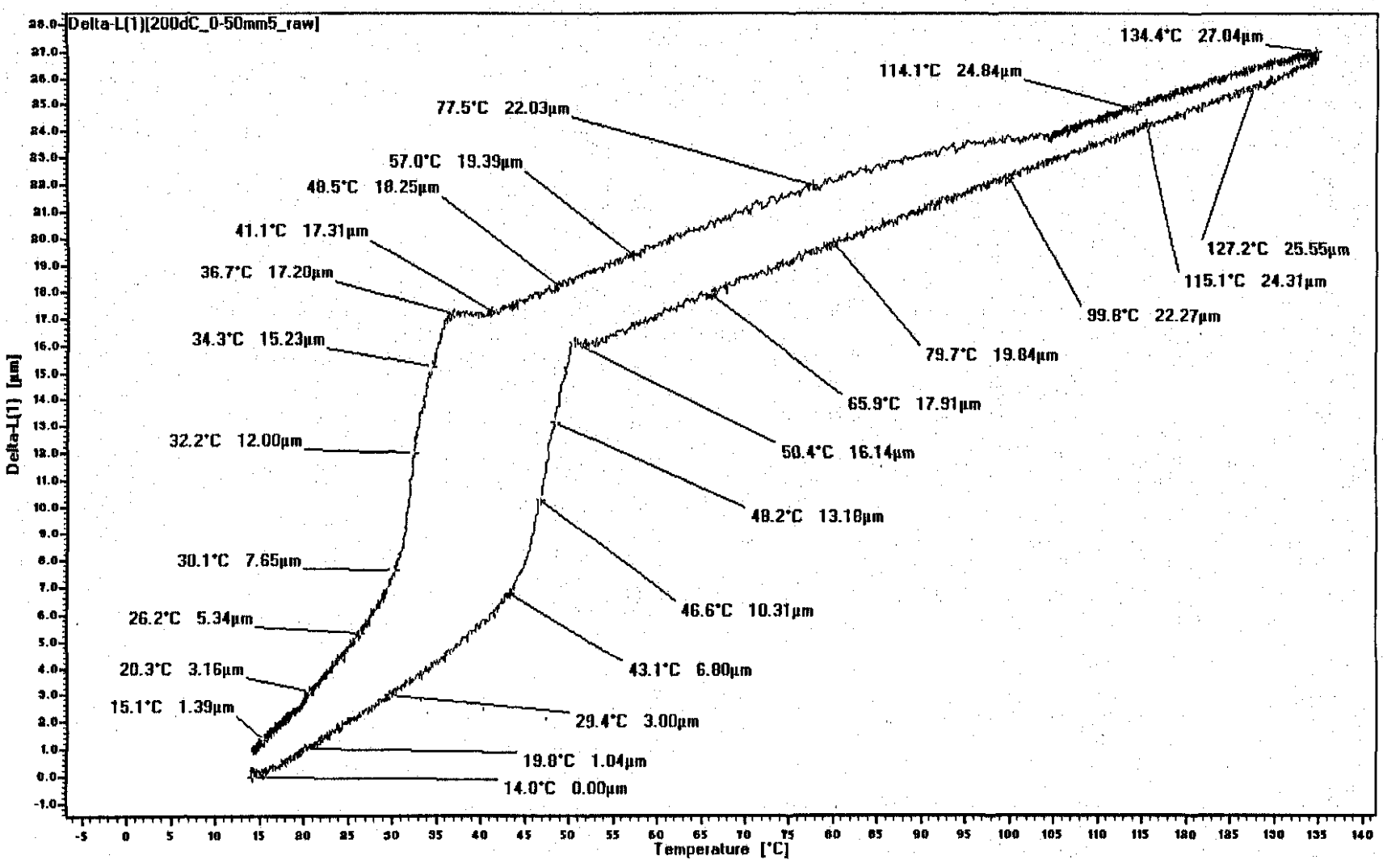

10mm length of first 50-100mm sample of NiTi Rod aged at 200°C

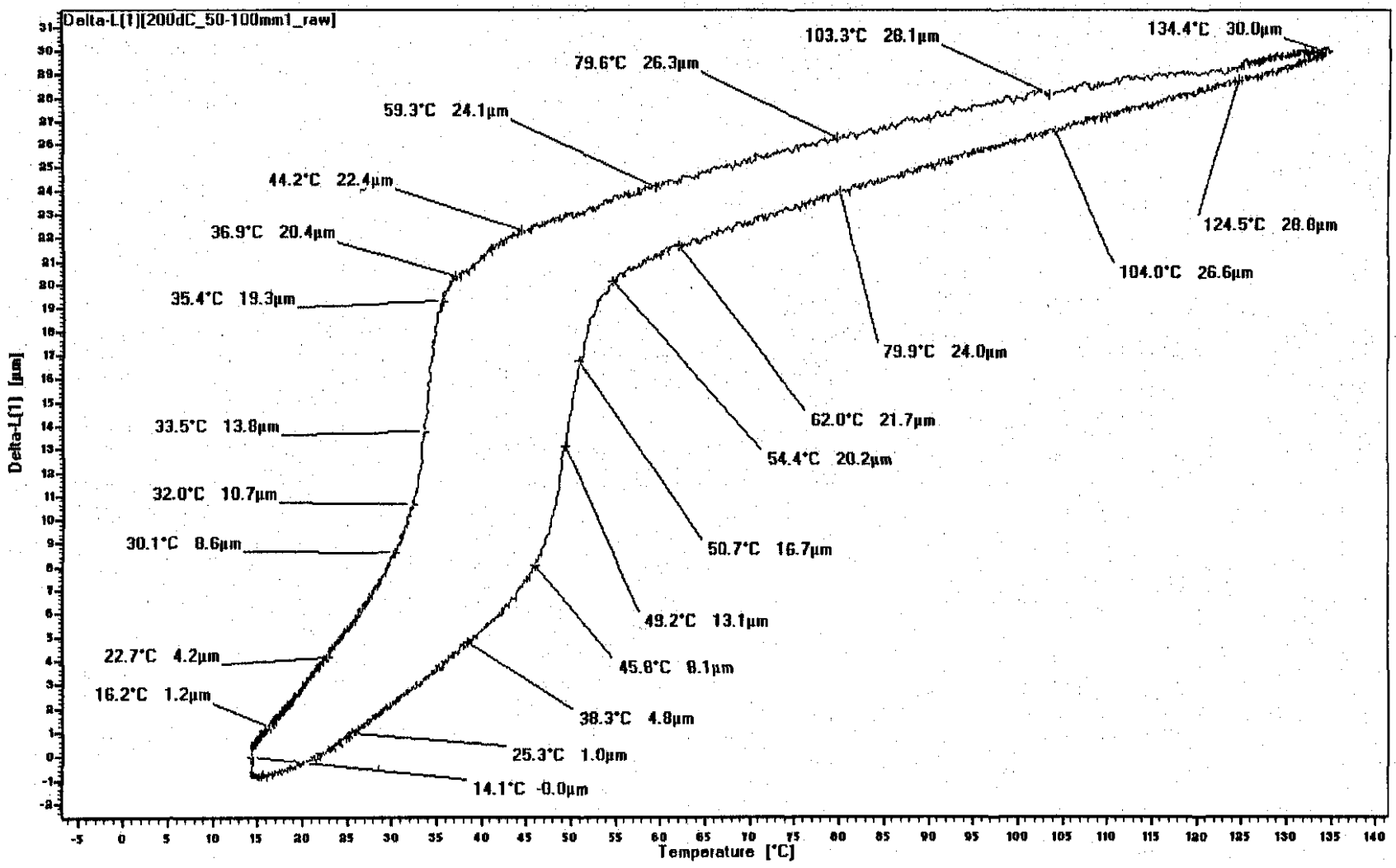

10mm length of the fifth 50-100mm sample of NiTi Rod aged at 200°C

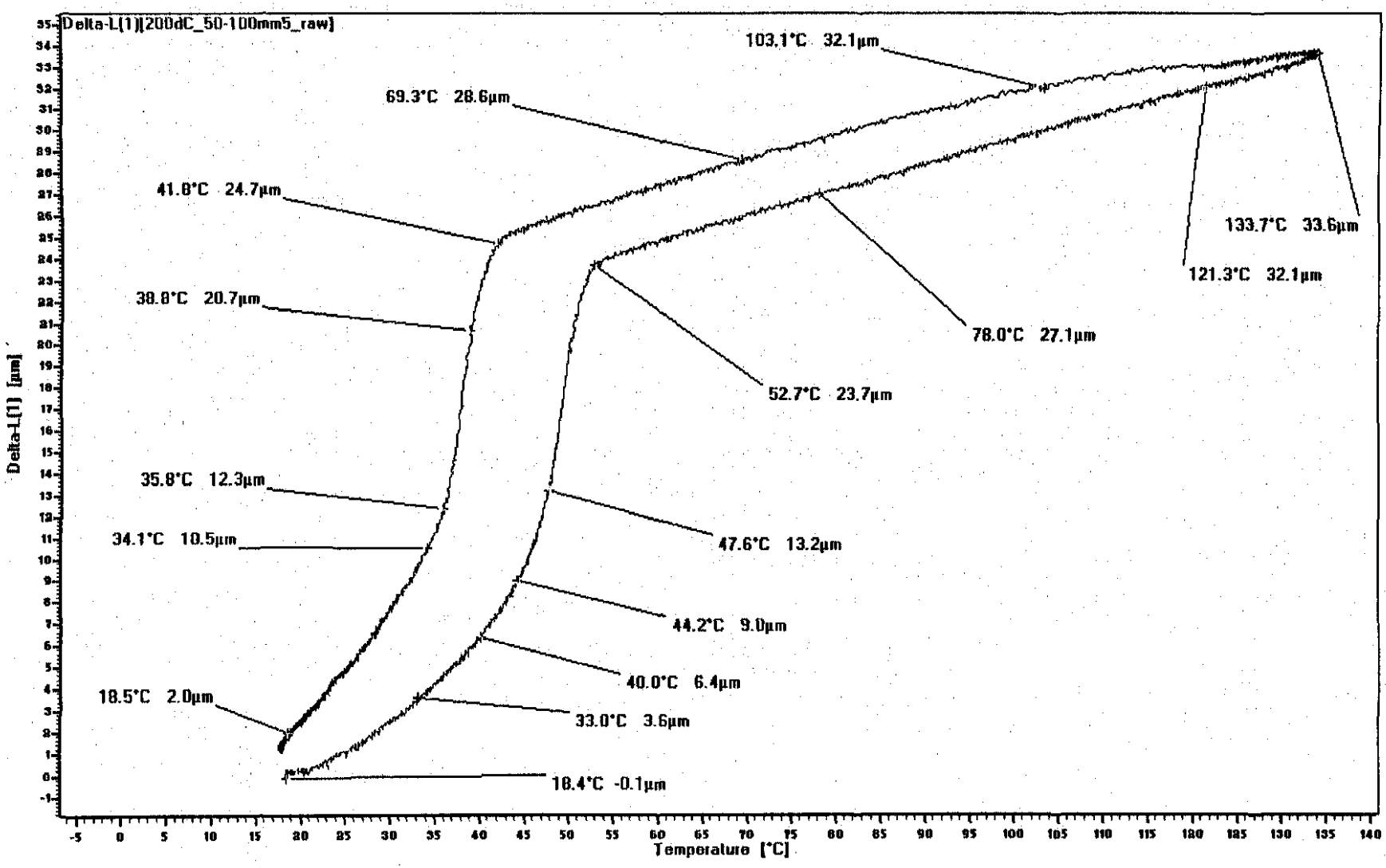

10mm length of the third 200-250mm sample of NiTi Rod aged at 200°C

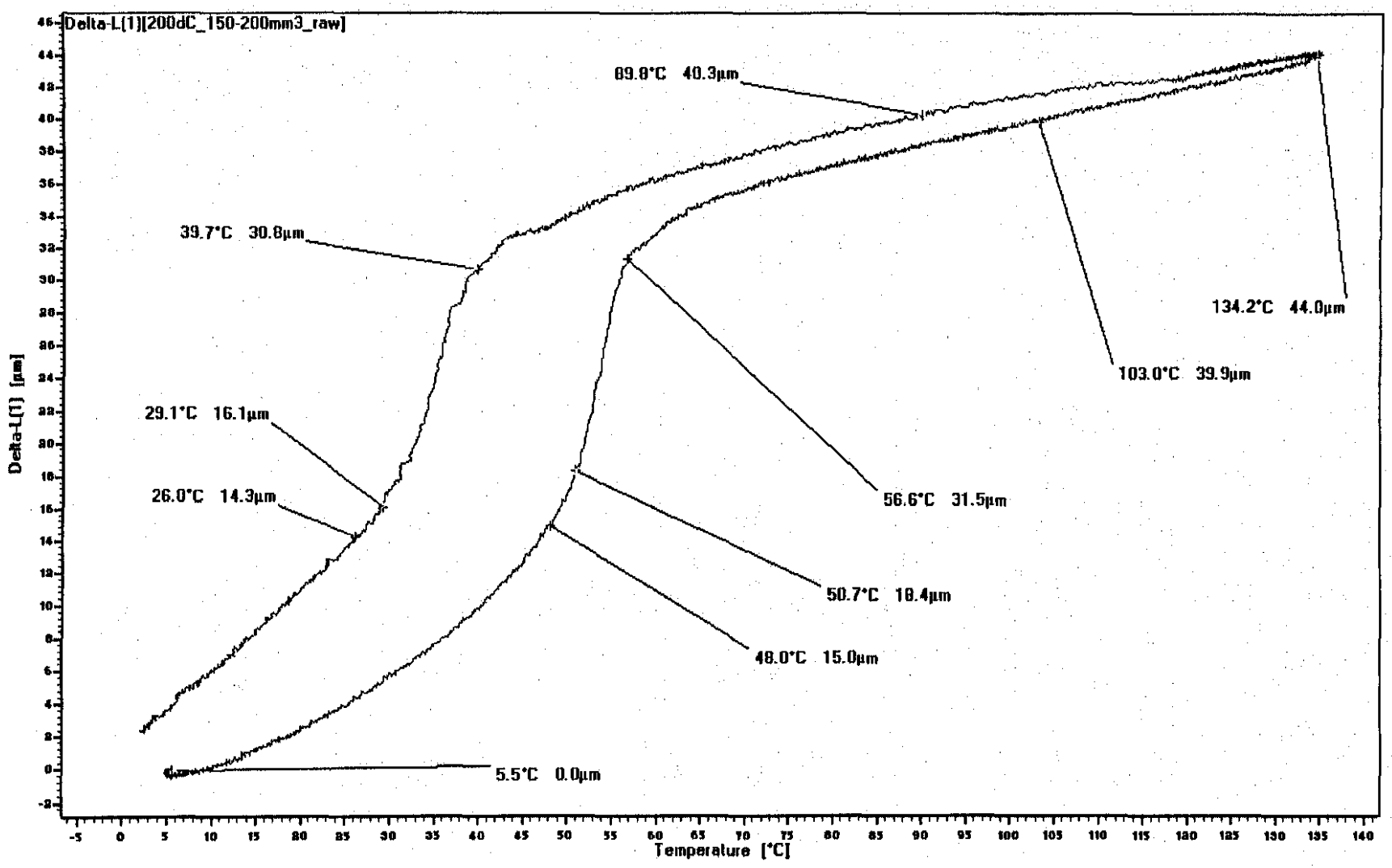

10mm length of the fifth 200-250mm sample of NiTi Rod aged at 200°C

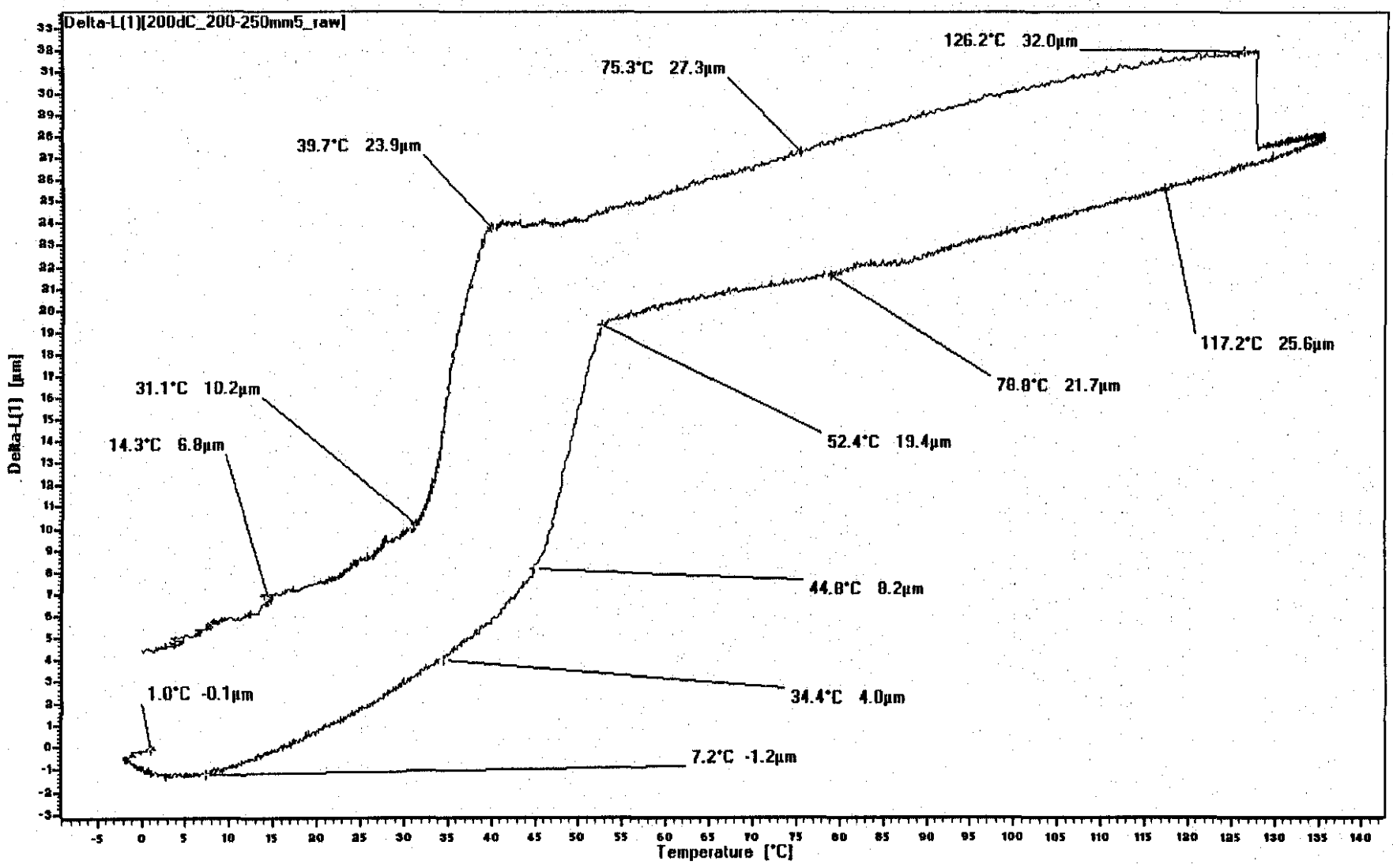

10mm length of the forth 250-300mm sample of NiTi Rod aged at 200°C

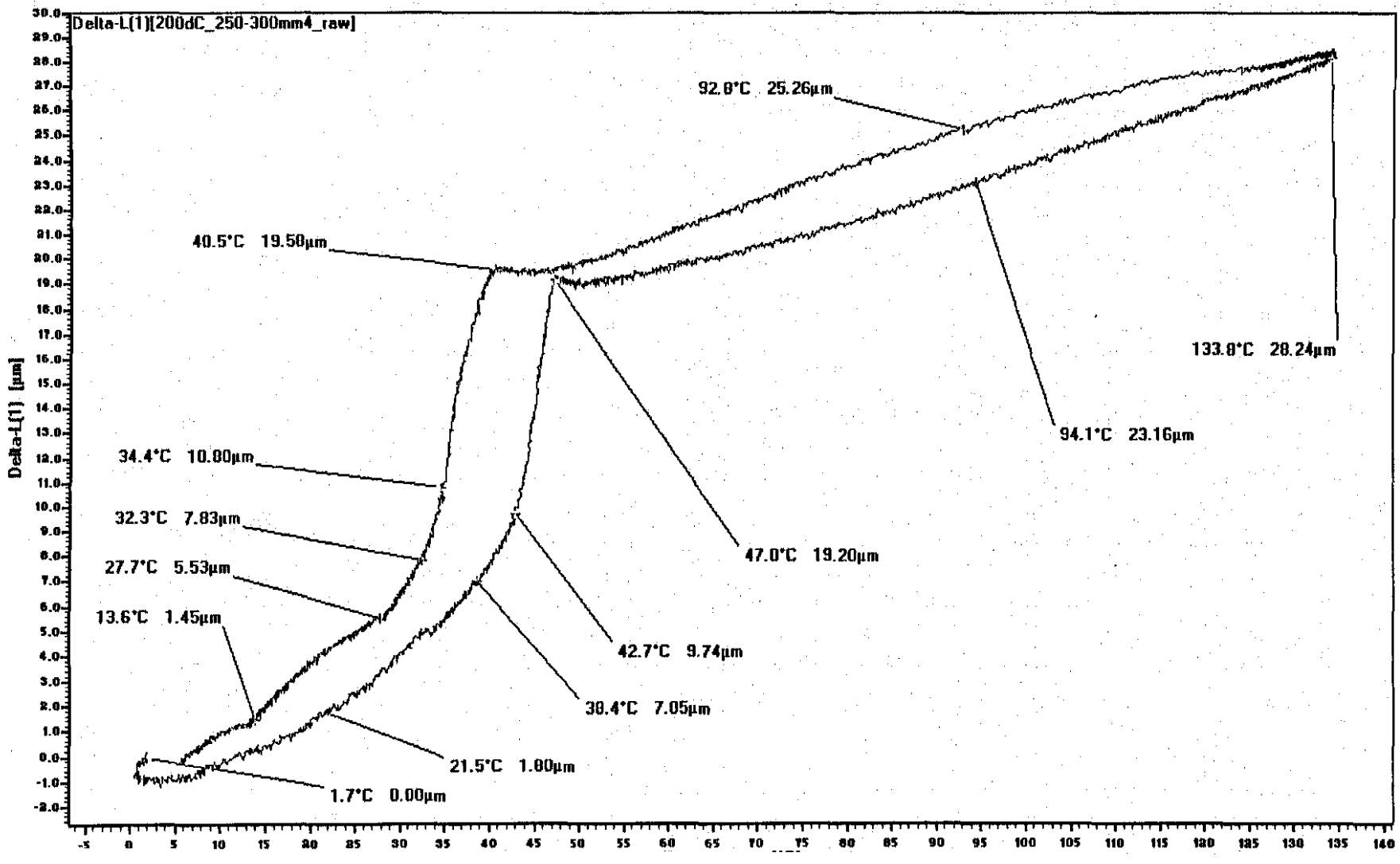

10mm length of the forth 100-150mm sample of NiTi Rod aged at 250°C

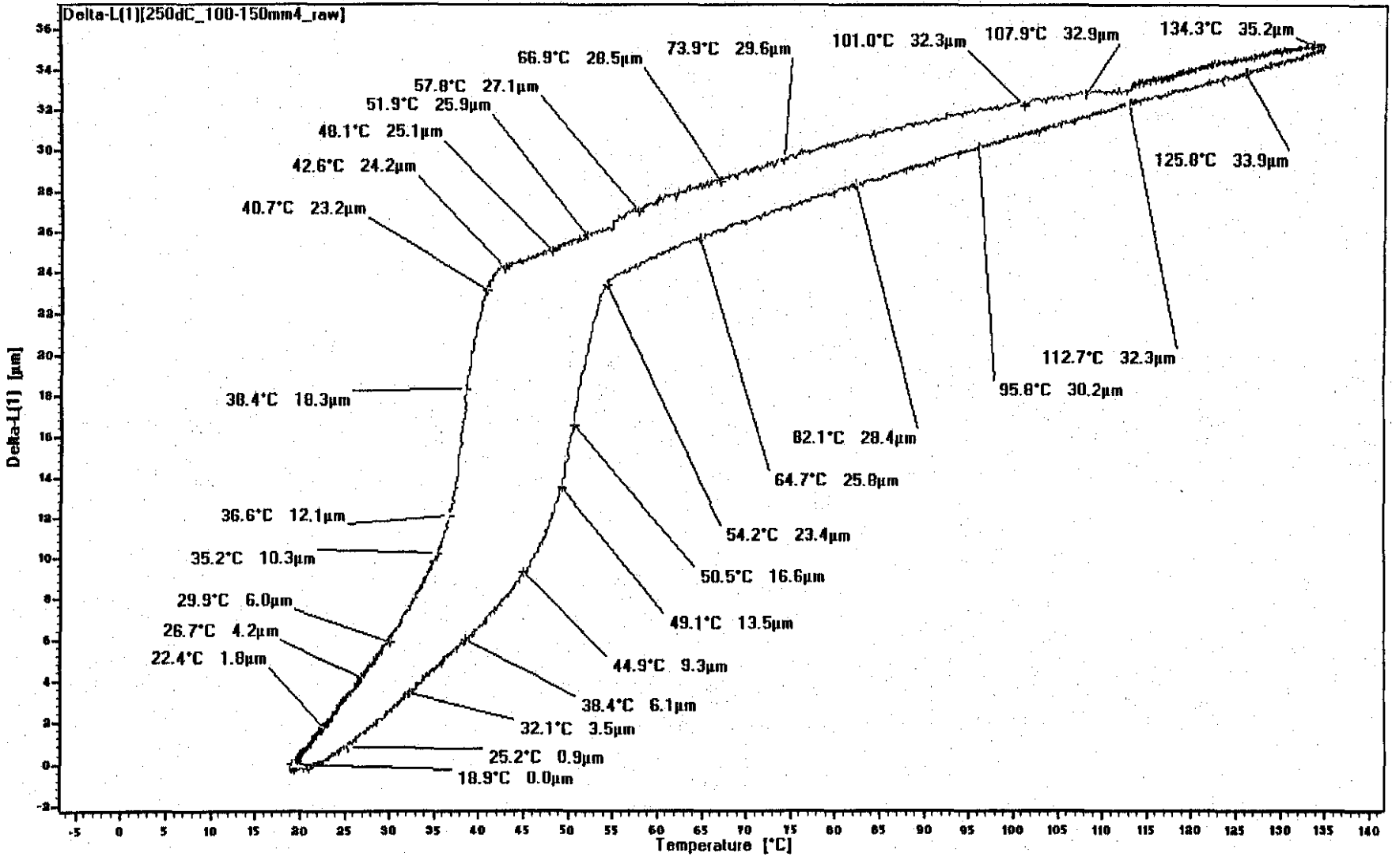

10mm length of the fifth 250-300mm sample of NiTi Rod aged at 250°C

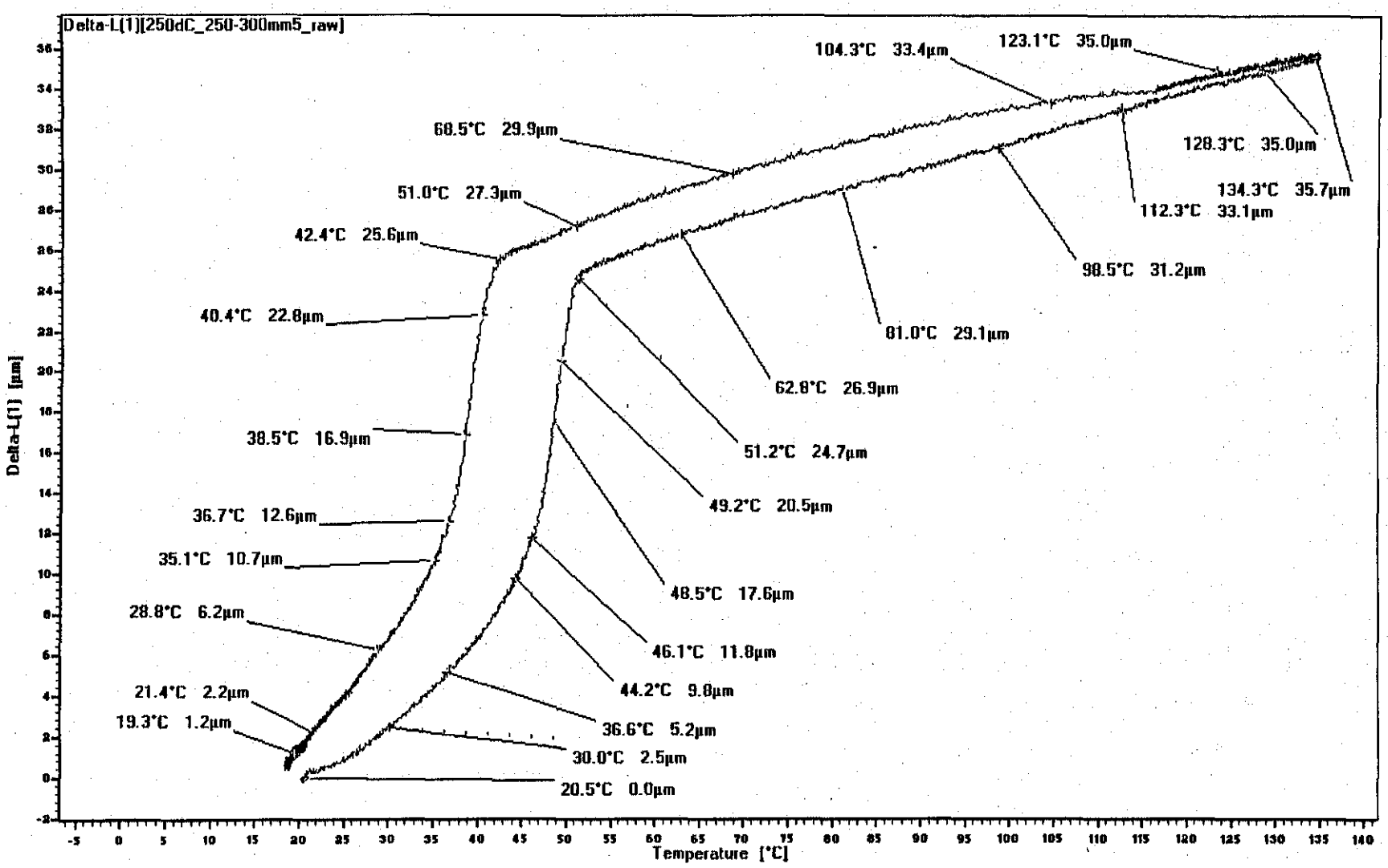

10mm length of the fifth 100-150mm sample of NiTi Rod aged at 300°C

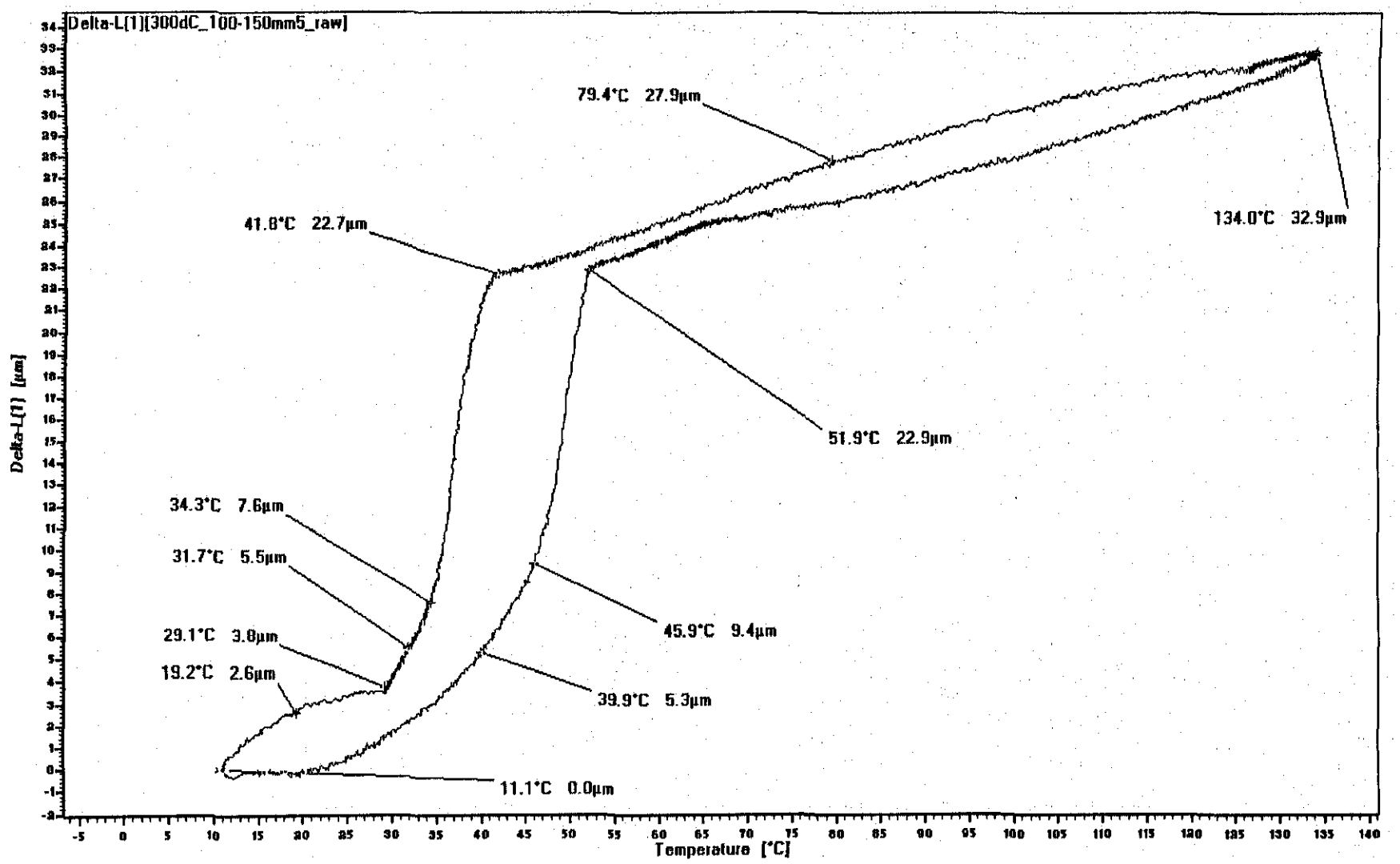

10mm length of the forth 150-200mm sample of NiTi Rod aged at 300°C

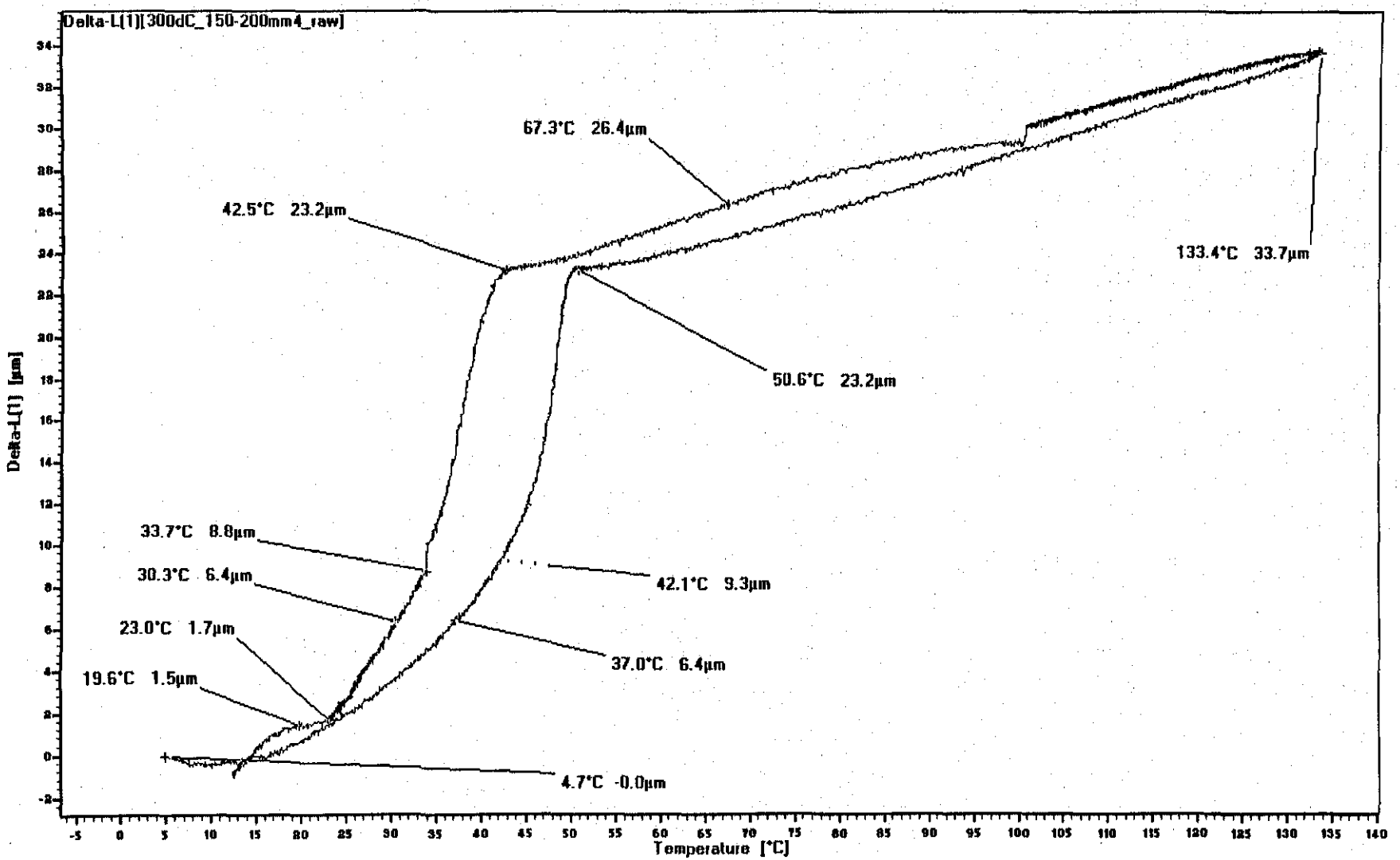

10mm length of the third 250-300mm sample of NiTi Rod aged at 300°C

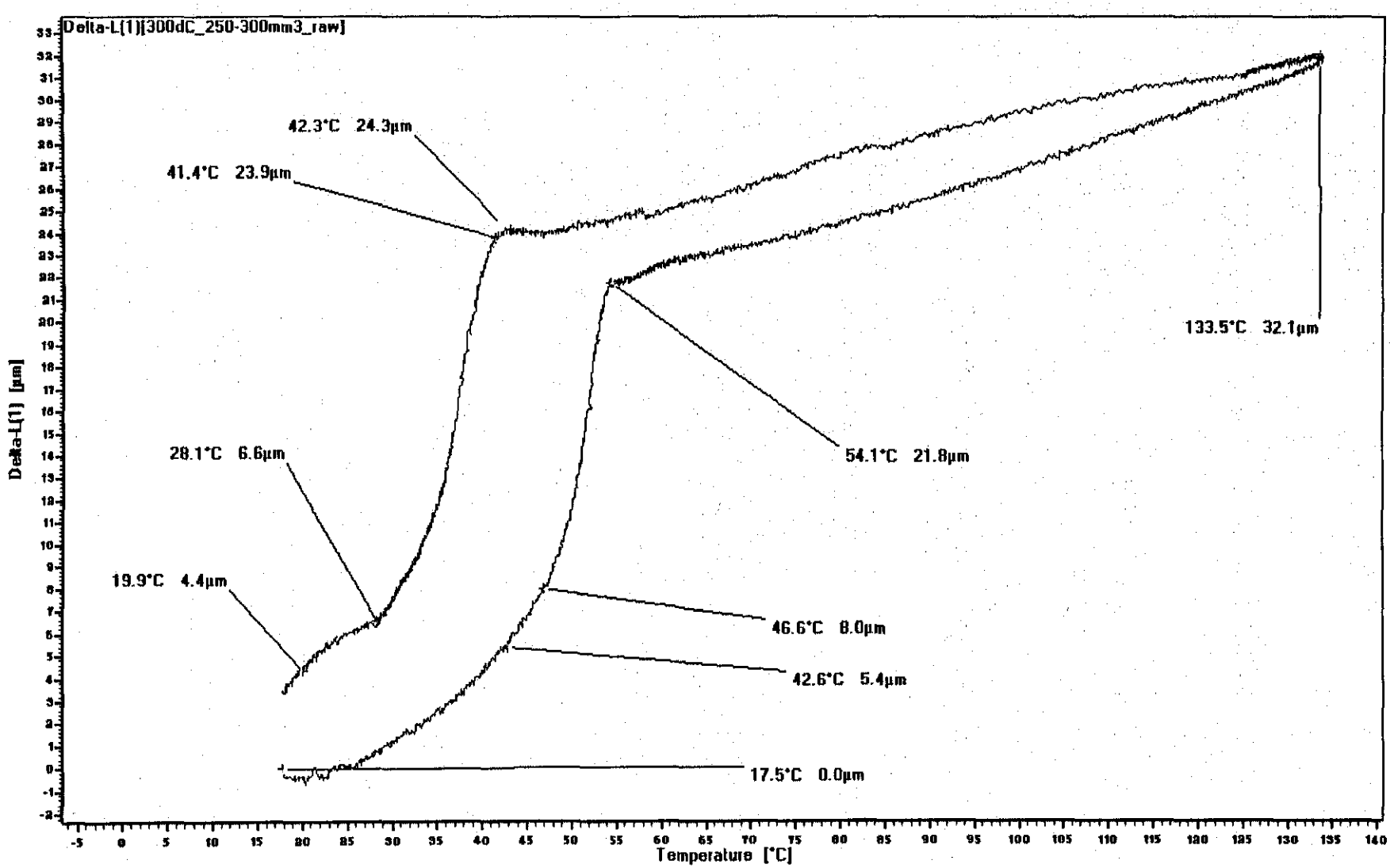

10mm length of the third 0-50mm sample of NiTi Rod aged at 350°C

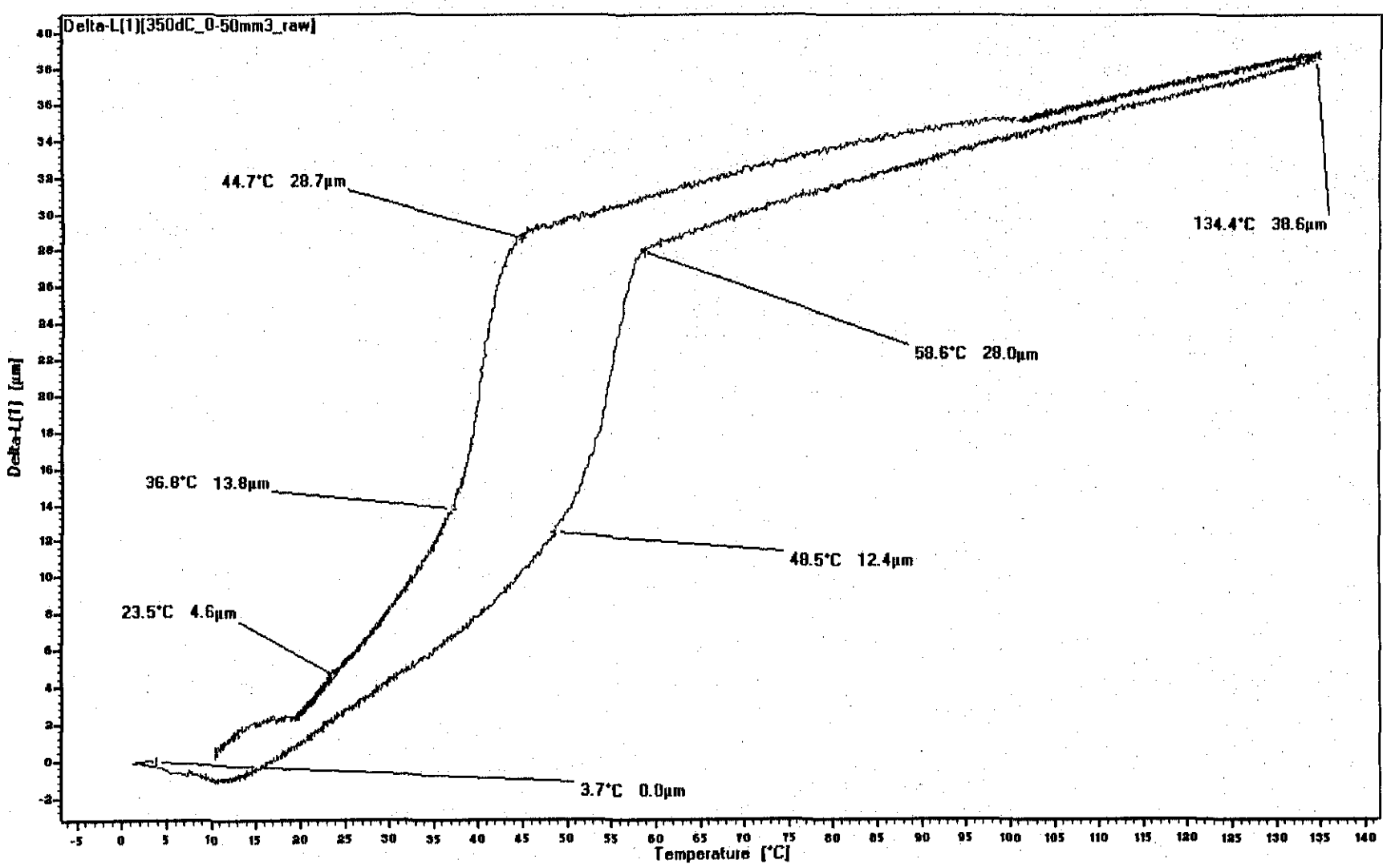

10mm length of the forth 100-150mm sample of NiTi Rod aged at 350°C

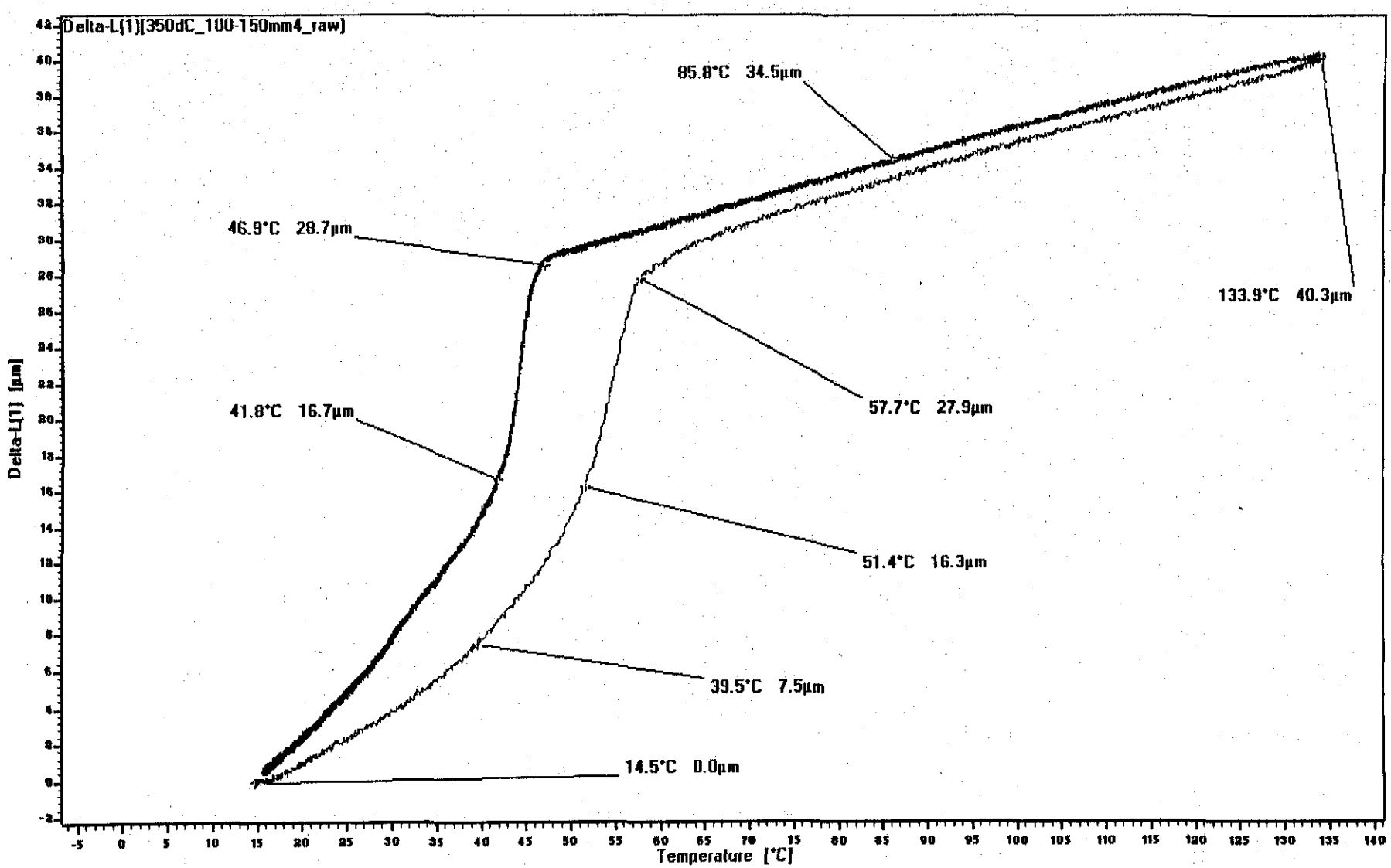

10mm length of the fifth 200-250mm sample of NiTi Rod aged at 350°C

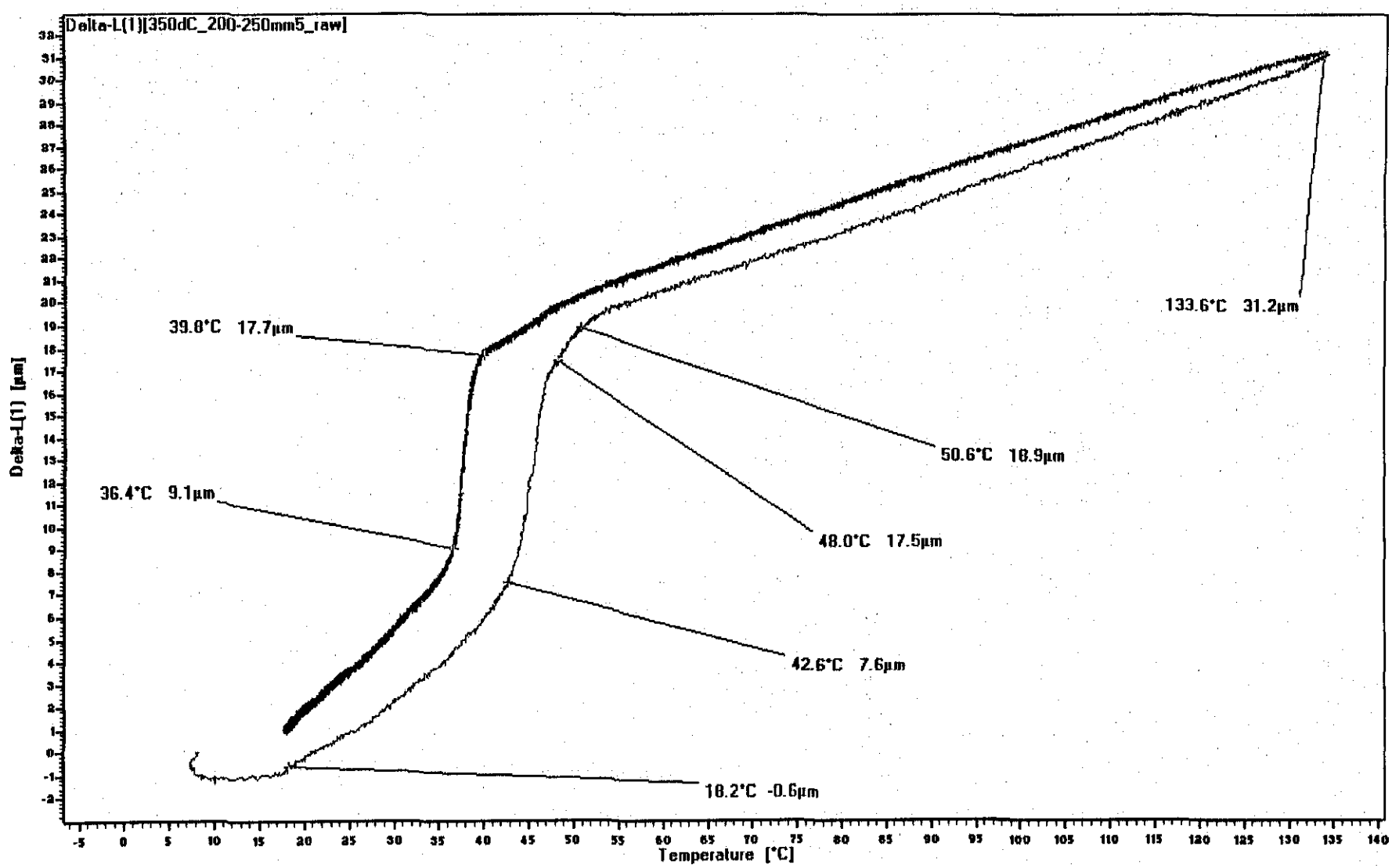

10mm length of the second 250-300mm sample of NiTi Rod aged at 350°C

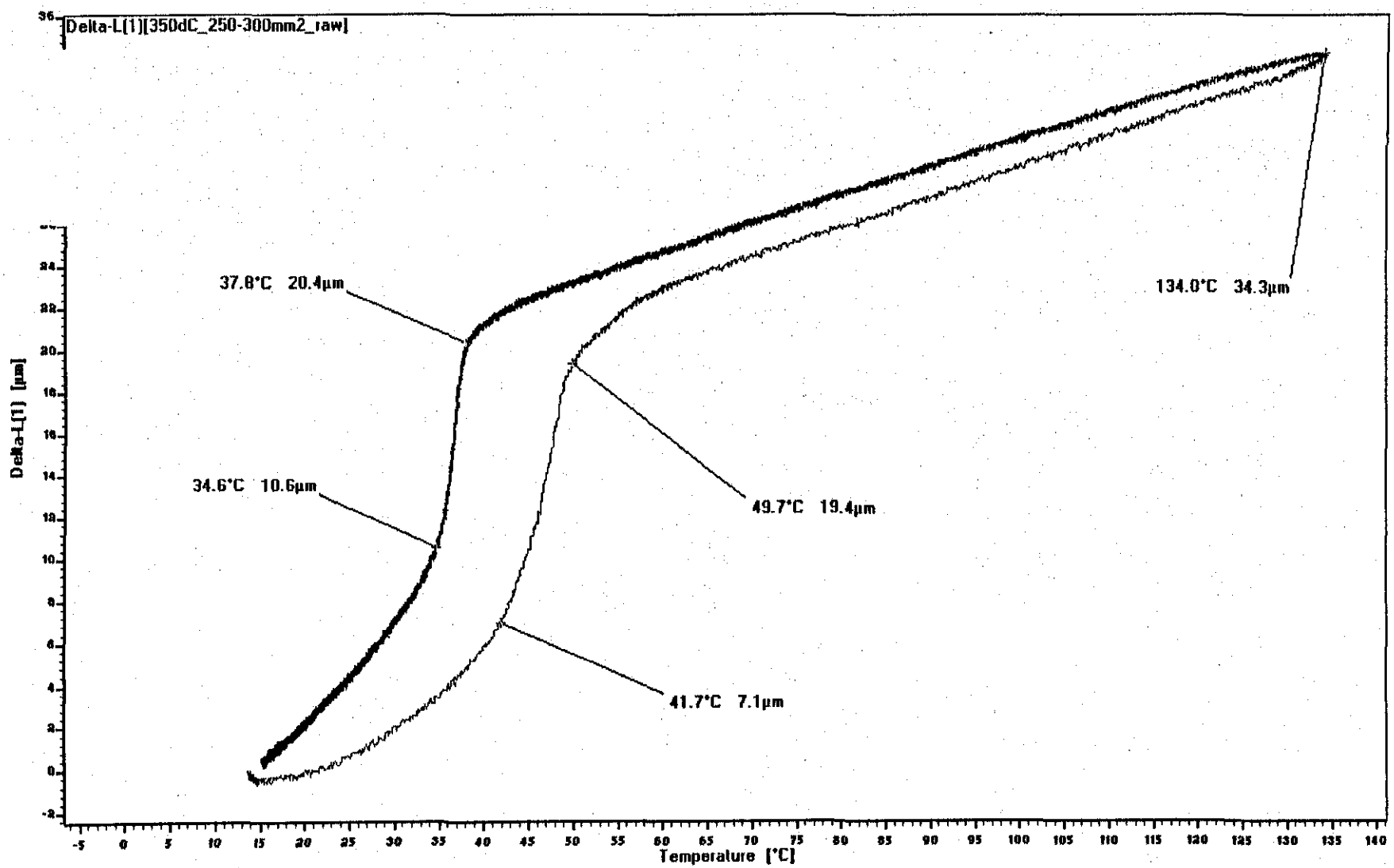

10mm length of the third 250-300mm sample of NiTi Rod aged at 350°C

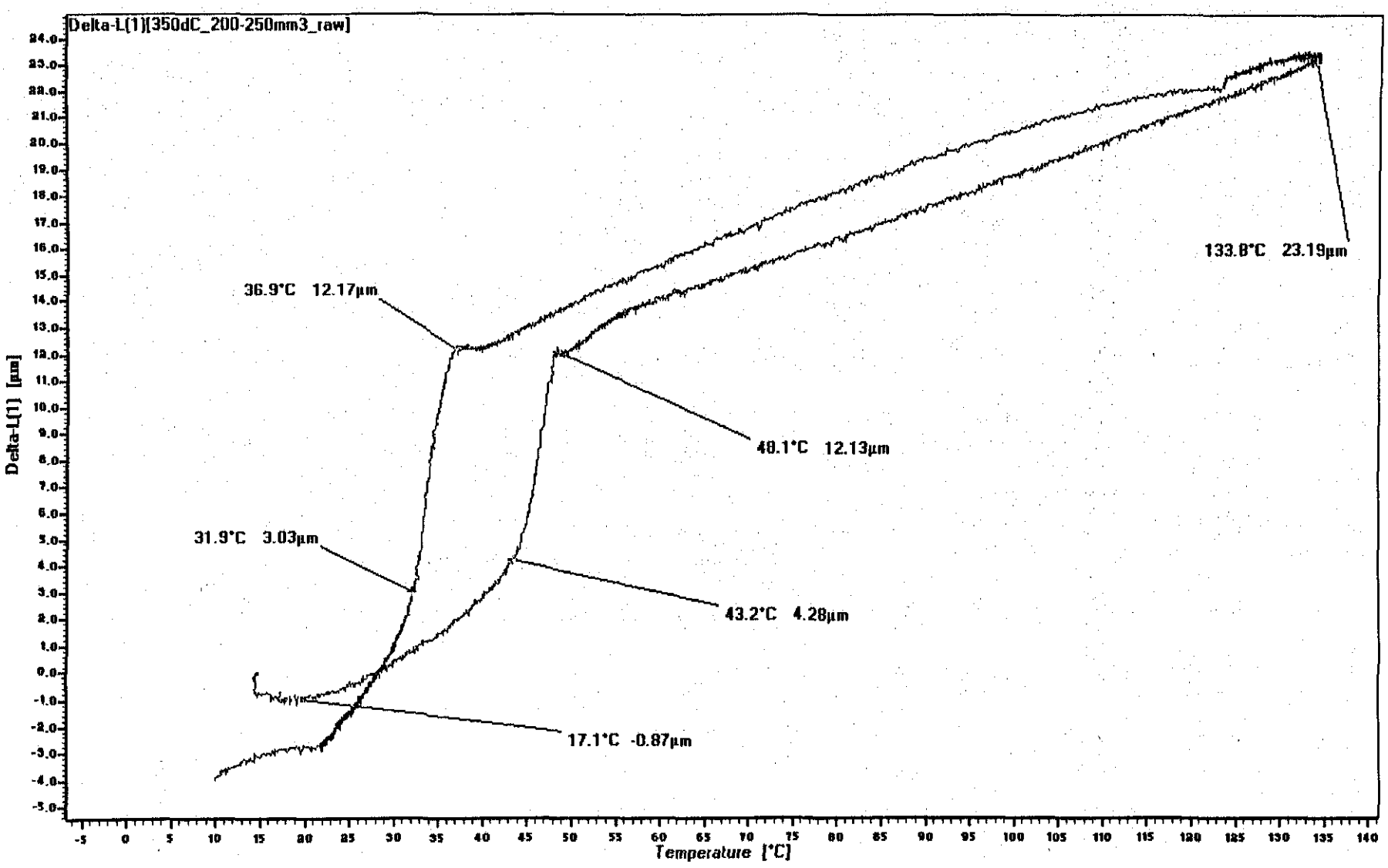

Appendix D

Summary of Results of Thermal Analyses performed on NiTi SMA using a Dilatometer

This appendix shows transformation temperature for each section on the specimen for each aged. Is also a summary of Appendix B.

Performance of 200°C aged specimen on the Dilatometer

200 degC	A_s		A_f		M_s		M_f	
	Temp.	% ΔL	Temp.	% ΔL	Temp.	% ΔL	Temp.	% ΔL
200 degC 0-50mm1	47	0.075	54	0.18	40	0.185	34	0.083
200 degC 0-50mm2	43.5	0.0614	50	0.149	40	0.1499	34	0.061
200 degC 0-50mm3	42.5	0.06	48	0.15	38	0.16	33	0.0734
200 degC 0-50mm4	45	0.072	52	0.17	37.5	0.17	32	0.078
200 degC 0-50mm5	43	0.07	50	0.16	37	0.172	30	0.076
200 degC 50-100mm1	45	0.081	53	0.19	37	0.09	32	0.101
200 degC 50-100mm2	46	0.102	54	0.21	38	0.22	32	0.1
200 degC 50-100mm3	46	0.08	54	0.22	40	0.23	33	0.09
200 degC 50-100mm4	45	0.086	49	0.21	39	0.29	34	0.11
200 degC 50-100mm5	45	0.1	52	0.23	41	0.24	35	0.12
200 degC 100-150mm1	49	0.11	56	0.25	42	0.25	37	0.12
200 degC 100-150mm2	45	0.11	55	0.26	41	0.29	35	0.14
200 degC 100-150mm3	45	0.08	55	0.21	39	0.22	30	0.07
200 degC 100-150mm4	42	0.15	53	0.32	41	0.33	31	0.15
200 degC 100-150mm5	43	0.14	52	0.3	40	0.31	33	0.14
200 degC 150-200mm1	48	0.1	55	0.24	32	0.26	22	0.083
200 degC 150-200mm2	43	0.15	50	0.28	42	0.29	36	0.18
200 degC 150-200mm3	48	0.18	56	0.31	39	0.3	29	0.16
200 degC 150-200mm4	48	0.15	55	0.32	43	0.35	37	0.24
200 degC 150-200mm5	48	0.13	54	0.26	43	0.27	36	0.13
200 degC 200-250mm1	44	0.09	52	0.2	42	0.2	32	0.08
200 degC 200-250mm3	43	0.1	49	0.2	40	0.21	32	0.11
200 degC 200-250mm4	45	0.08	53	0.16	40	0.16	32	0.07
200 degC 250-300mm1	40	0.09	48	0.2	40	0.19	31	0.08
200 degC 250-300mm3	40	0.05	47	0.16	39	0.17	32	0.07
200 degC 250-300mm4	42	0.1	47	0.19	40	0.2	32	0.08
average	**44.65**	**0.10**	**52.04**	**0.22**	**39.63**	**0.23**	**32.54**	**0.11**
min	**40.00**	**0.05**	**47.00**	**0.15**	**32.00**	**0.09**	**22.00**	**0.06**
max	**49.00**	**0.18**	**56.00**	**0.32**	**43.00**	**0.35**	**37.00**	**0.24**
Variances range	**9.00**	**0.13**	**9.00**	**0.17**	**11.00**	**0.26**	**15.00**	**0.18**
stdev	**2.44**	**0.03**	**2.82**	**0.05**	**2.28**	**0.06**	**3.01**	**0.04**

Performance of 250°C aged specimen on the Dilatometer

250 degC	A_s		A_f		M_s		M_f	
	Temp.	% ΔL	Temp.	% ΔL	Temp.	% ΔL	Temp.	% ΔL
250 degC 0-50mm1	47	0.08	53	0.19	40	0.19	35	0.09
250 degC 0-50mm2	47	0.083	55	0.21	39	0.24	33	0.11
250 degC 0-50mm3	44	0.06	52	0.14	39	0.17	33	0.07
250 degC 0-50mm4	45	0.07	52	0.16	39	0.17	33	0.07
250 degC 0-50mm5	45	0.08	54	0.19	39	0.24	32	0.11
250 degC 50-100mm1	46	0.09	53	0.21	39	0.23	33	0.11
250 degC 50-100mm2	46	0.11	53	0.24	41	0.24	34	0.1
250 degC 50-100mm3	47	0.1	53	0.22	40	0.23	34	0.1
250 degC 50-100mm4	43	0.1	50	0.18	39	0.19	34	0.08
250 degC 50-100mm5	43	0.1	49	0.2	40	0.21	34	0.09
250 degC 100-150mm1	46	0.1	52	0.24	41	0.25	35	0.12
250 degC 100-150mm2	47	0.09	55	0.22	41	0.23	35	0.11
250 degC 100-150mm3	45	0.12	55	0.25	42	0.26	35	0.12
250 degC 100-150mm4	46	0.12	54	0.23	41	0.23	35	0.1
250 degC 150-200mm1	45	0.09	54	0.19	44	0.19	38	0.08
250 degC 150-200mm2	44	0.11	52	0.24	44	0.25	37	0.13
250 degC 150-200mm3	46	0.11	55	0.25	44	0.25	38	0.1
250 degC 150-200mm4	47	0.09	55	0.24	44	0.24	37	0.083
250 degC 150-200mm5	47	0.08	55	0.21	44	0.21	38	0.09
250 degC 200-250mm1	46	0.16	53	0.33	40	0.34	34	0.2
250 degC 200-250mm2	46	0.17	55	0.31	40	0.31	31	0.15
250 degC 200-250mm3	45	0.16	55	0.3	40	0.31	30	0.16
250 degC 200-250mm4	46	0.17	54	0.35	36	0.36	27	0.17
250 degC 200-250mm5	47	0.13	55	0.27	40	0.27	33	0.13
250 degC 250-300mm1	46	0.07	56	0.81	40	0.18	32	0.08
250 degC 250-300mm2	47	0.14	54	0.23	40	0.24	35	0.12
250 degC 250-300mm3	46	0.11	53	0.25	41	0.26	35	0.11
250 degC 250-300mm4	46	0.1	55	0.23	42	0.24	34	0.11
250 degC 250-300mm5	45	0.1	50	0.25	42	0.26	35	0.1
average	**45.72**	**0.11**	**53.48**	**0.25**	**40.72**	**0.24**	**34.10**	**0.11**
min	**43**	**0.06**	**49**	**0.14**	**36**	**0.17**	**27**	**0.07**
max	**47**	**0.17**	**56**	**0.81**	**44**	**0.36**	**38**	**0.2**
Variances range	**4.00**	**0.11**	**7.00**	**0.67**	**8.00**	**0.19**	**11.00**	**0.13**
Stdev	**1.16**	**0.03**	**1.74**	**0.12**	**1.93**	**0.05**	**2.40**	**0.03**

Performance of 300°C aged specimen on the Dilatometer

300 degC	A_s		A_f		M_s		M_f	
	Temp.	% ΔL	Temp.	% ΔL	Temp.	% ΔL	Temp.	% ΔL
300 degC 0-50mm2	42	0.08	49	0.16	39	0.17	34	0.07
300 degC 0-50mm5	42	0.08	51	0.16	39	0.19	33	0.1
300 degC 50-100mm1	42	0.07368	50	0.15789	39	0.16842	35	0.07895
300 degC 50-100mm2	42	0.07368	49	0.16842	39	0.17895	34	0.08421
300 degC 50-100mm3	45	0.06316	51	0.16842	38	0.17895	32	0.07368
300 degC 50-100mm4	41	0.07143	46	0.19388	38	0.20408	32	0.09184
300 degC 100-150mm1	44	0.08	50	0.22	44	0.24	38	0.1
300 degC 100-150mm2	46	0.09	56	0.21	41	0.21	38	0.11
300 degC 100-150mm3	46	0.09474	55	0.21053	38	0.23158	33	0.11579
300 degC 100-150mm4	47	0.09	50	0.22	41	0.21	33	0.08
300 degC 100-150mm5	47	0.1	52	0.23	42	0.23	34	0.08
300 degC 150-200mm1	47	0.09804	52	0.2451	44	0.2549	37	0.10784
300 degC 150-200mm2	48	0.09615	53	0.24038	45	0.25	41	0.125
300 degC 150-200mm3	46	0.07	52	0.16	38	0.16	34	0.07
300 degC 150-200mm4	46	0.1	52	0.24	43	0.23	39	0.11
300 degC 150-200mm5	48	0.12	53	0.25	37	0.24	32	0.12
300 degC 200-250mm1	48	0.09524	56	0.24762	42	0.25714	38	0.13333
300 degC 200-250mm2	49	0.16	56	0.31	41	0.3	35	0.18
300 degC 200-250mm3	46	0.12	55	0.25		0.25	34	0.12
300 degC 200-250mm4	47	0.09524	56	0.21905	42	0.20952	34	0.09524
300 degC 200-250mm5	49	0.1	59	0.22	41	0.25	36	0.12
300 degC 250-300mm1	47	0.06364	58	0.16364	39	0.16364	33	0.07273
300 degC 250-300mm2	47	0.1	55	0.23	41	0.24	35	0.11
300 degC 250-300mm3	46	0.07619	54	0.2	41	0.22857	35	0.10476
300 degC 250-300mm4	46	0.1	56	0.23	41	0.22	34	0.09
average	**45.76**	**0.09**	**53.04**	**0.21**	**40.54**	**0.22**	**34.92**	**0.10**
min	**41.00**	**0.06**	**46.00**	**0.16**	**37.00**	**0.16**	**32.00**	**0.07**
max	**49.00**	**0.16**	**59.00**	**0.31**	**45.00**	**0.30**	**41.00**	**0.18**
Variances range	**8.00**	**0.10**	**13.00**	**0.15**	**8.00**	**0.14**	**9.00**	**0.11**
stdev	**2.31**	**0.02**	**3.16**	**0.04**	**2.17**	**0.04**	**2.36**	**0.02**

Performance of 350°C aged specimen on the Dilatometer

350 degC	A_s		A_f		M_s		M_f	
	Temp.	% ΔL	Temp.	% ΔL	Temp.	% ΔL	Temp.	% ΔL
350 degC 0-50mm1	51	0.150	60	0.310	43	0.320	35	0.170
350 degC 0-50mm2	47	0.120	57	0.250	45	0.250	37	0.120
350 degC 0-50mm4	48	0.120	58	0.240	45	0.240	38	0.110
350 degC 50-100mm1	48	0.064	59	0.173	46	0.182	36	0.073
350 degC 50-100mm2	47	0.120	58	0.270	46	0.280	38	0.160
350 degC 50-100mm3	47	0.116	54	0.284	46	0.295	39	0.137
350 degC 50-100mm4	47	0.086	56	0.200	45	0.238	38	0.114
350 degC 50-100mm5	48	0.100	55	0.280	47	0.290	38	0.150
350 degC 100-150mm1	48	0.076	57	0.207	42	0.239	33	0.109
350 degC 100-150mm2	47	0.152	56	0.272	43	0.283	35	0.141
350 degC 100-150mm3	46	0.118	52	0.224	47	0.235	40	0.165
350 degC 100-150mm4	50	0.130	58	0.270	46	0.280	40	0.150
350 degC 100-150mm5	48	0.134	57	0.258	44	0.258	38	0.144
350 degC 150-200mm1	48	0.100	55	0.236	40	0.245	32	0.091
350 degC 150-200mm2	48	0.110	57	0.270	42	0.280	34	0.120
350 degC 150-200mm3	44	0.090	52	0.210	38	0.200	33	0.090
350 degC 150-200mm4	44	0.074	51	0.168	38	0.179	32	0.074
350 degC 150-200mm5	46	0.112	54	0.276	45	0.286	40	0.163
350 degC 200-250mm1	43	0.075	54	0.204	35	0.226	31	0.108
350 degC 200-250mm2	40	0.050	48	0.140	38	0.130	32	0.040
350 degC 200-250mm3	43	0.042	48	0.126	37	0.126	32	0.032
350 degC 200-250mm4	41	0.076	48	0.181	37	0.190	31	0.086
350 degC 200-250mm5	42	0.067	49	0.171	40	0.162	36	0.086
350 degC 250-300mm2	42	0.066	49	0.179	38	0.189	34	0.094
350 degC 250-300mm3	44	0.051	48	0.122	37	0.122	32	0.031
Average	**45.88**	**0.10**	**53.68**	**0.22**	**42.00**	**0.23**	**35.36**	**0.11**
min	**40.00**	**0.04**	**48.00**	**0.12**	**35.00**	**0.12**	**31.00**	**0.03**
max	**51.00**	**0.15**	**60.00**	**0.31**	**47.00**	**0.32**	**40.00**	**0.17**
Variances range	**11.00**	**0.11**	**12.00**	**0.19**	**12.00**	**0.20**	**9.00**	**0.14**
stdev	**2.8624**	**0.03127**	**3.90512**	**0.05328**	**3.82971**	**0.05664**	**3.06703**	**0.04107**

Performance non aged specimen on the Dilatometer

No aging	A_s		A_f		M_s		M_f	
	Temp.	% ΔL	Temp.	% ΔL	Temp.	% ΔL	Temp.	% ΔL
no aging 0-50mm1	47.00	0.12	53.00	0.24	38.00	0.23	30.00	0.09
no aging 0-50mm2	45.00	0.06	55.00	0.21	41.00	0.22	36.00	0.11
no aging 0-50mm3	45.00	0.09	54.00	0.22	41.00	0.23	31.00	0.09
no aging 0-50mm4	33.00	0.04	50.00	0.21	41.00	0.21	37.00	0.12
no aging 0-50mm5	47.00	0.10	56.00	0.24	39.00	0.25	32.00	0.11
no aging 50-100mm1	42.00	0.05	53.00	0.22	36.00	0.22	30.00	0.09
no aging 50-100mm2	48.00	0.09	55.00	0.20	38.00	0.22	31.00	0.09
no aging 50-100mm3	46.00	0.10	54.00	0.22	38.00	0.22	32.00	0.09
no aging 50-100mm4	43.00	0.07	49.00	0.18	42.00	0.18	37.00	0.08
no aging 50-100mm5	46.00	0.07	53.00	0.22	39.00	0.24	33.00	0.11
no aging 100-150mm1	45.00	0.09	55.00	0.21	44.00	0.20	38.00	0.09
no aging 100-150mm2	46.00	0.10	55.00	0.26	40.00	0.29	33.00	0.14
no aging 100-150mm3	45.00	0.11	51.00	0.25	45.00	0.26	40.00	0.14
no aging 100-150mm4	48.00	0.12	57.00	0.26	46.00	0.28	40.00	0.17
no aging 100-150mm5	48.00	0.09	56.00	0.26	45.00	0.27	36.00	0.13
no aging 150-200mm1	48.00	0.08	56.00	0.24	39.00	0.25	33.00	0.08
no aging 150-200mm2	49.00	0.07	56.00	0.23	41.00	0.24	33.00	0.11
no aging 150-200mm3	49.00	0.07	56.00	0.21	47.00	0.22	40.00	0.12
no aging 150-200mm4	47.00	0.09	58.00	0.20	47.00	0.21	41.00	0.11
no aging 150-200mm5	47.00	0.14	53.00	0.27	45.00	0.28	40.00	0.15
no aging 200-250mm1	46.00	0.16	54.00	0.31	40.00	0.32	34.00	0.20
no aging 200-250mm3	49.00	0.11	57.00	0.24	42.00	0.24	35.00	0.12
no aging 200-250mm4	47.00	0.11	56.00	0.26	41.00	0.29	34.00	0.15
no aging 200-250mm5	49.00	0.13	58.00	0.27	43.00	0.28	35.00	0.13
no aging 250-300mm1	43.00	0.09	52.00	0.25	45.00	0.26	40.00	0.15
no aging 250-300mm3	47.00	0.15	54.00	0.27	46.00	0.28	40.00	0.16
no aging 250-300mm4	48.00	0.13	57.00	0.29	41.00	0.29	35.00	0.13
no aging 250-300mm5	48.00	0.12	58.00	0.25	45.00	0.26	40.00	0.14
average	**46.07**	**0.10**	**54.74**	**0.24**	**42.11**	**0.25**	**35.78**	**0.12**
min	**33.00**	**0.04**	**49.00**	**0.18**	**36.00**	**0.18**	**30.00**	**0.08**
max	**49.00**	**0.16**	**58.00**	**0.31**	**47.00**	**0.32**	**41.00**	**0.20**
Variances range	**16.00**	**0.11**	**9.00**	**0.13**	**11.00**	**0.14**	**11.00**	**0.12**
stdev	**3.17792**	**0.02883**	**2.3421**	**0.02968**	**3.085**	**0.03305**	**3.54264**	**0.0299**